博士論文

A Study of Air-Sea Carbon Dioxide Exchange in the Greenland Sea, the Barents Sea and the Southern Ocean

グリーンランド海、バレンツ海および南大洋における大気-海洋間の二酸化炭素交換に関する研究

by

Shin-ichiro Nakaoka

中岡 慎一郎

Thesis Presented for the Degree of Doctor of Science,

Graduate School of Science, Tohoku University

東北大学大学院理学研究科

平成 18 年

Acknowledgements

I am most grateful to Prof. T. Nakazawa for his continuous supports, precious advices and encouragement. I also wish to express my gratitude to Prof. S. Aoki for valuable advice and helpful discussions. I deeply appreciate Prof. H. Yoshikawa-Inoue, Hokkaido University, for providing useful advices and various supports. I wish to thank Dr. G. Hashida, National Institute of Polar Research, for providing the various data and helpful advises. I also wish to thank Dr. M. Ishii, Meteorological Research Institute, for providing the various data and valuable comments. I am deeply grateful to Dr. S. Morimoto, National Institute of Polar Research, for providing atmospheric CO_2 data in Ny-Ålesund and in Syowa Station. I also wish to thank Dr. B. Tilbrook, Commonwealth Scientific and Research Organization Division of Oceanography, for providing their various data. I would like to thank Dr. T. Watai for technical advices. I am very grateful Dr. K. Higuchi, Meteorological Service of Canada, for helpful comments and suggestions. I greatly appreciate Dr. K. Kawamura, Tohoku University, for his encouragement and valuable comments. I wish thank Dr. S. Ishidoya, Tohoku University, for his encouragement and helpful comments. I am also grateful to all members belonged to our laboratory for their continuous encouragement, valuable supports and discussions.

Abstract

In order to elucidate the seasonal and interannual variations of oceanic CO_2 uptake in the Greenland Sea and the Barents Sea, pCO_2^{sea} was measured between 1992 and 2001. Monthly relationships between pCO_2^{sea} and SST were derived, and then pCO_2^{sea} and air-sea CO_2 flux were calculated for the two seas using SST data from the NCEP/NCAR reanalysis. The pCO_2^{sea} values were normalized to the year 1995 by assuming that pCO_2^{sea} increased at the same growth rate (1.5 μatm yr^{-1}) as pCO_2^{air} did for the period of 1992 to 2001. The annual net air-sea CO_2 flux for 1995 was evaluated to be 52 gC m^{-2} yr^{-1} for the Greenland Sea and 46 gC m^{-2} yr^{-1} for the Barents Sea. The CO_2 flux into the ocean reached the maximum in winter and the minimum in summer. The seasonal variation of oceanic CO_2 uptake was affected much stronger by wind speed and ΔpCO_2 than by sea ice coverage. The annual CO_2 uptake by these seas (70°-80°N, 20°W-40°E) in 1995 was estimated to be 0.050 GtC yr^{-1}.

The interannual variation of the annual CO_2 uptake was positively correlated with the North Atlantic Oscillation Index through wind speed and negatively with ΔpCO_2 and sea ice coverage. This study also indicated that wind speed and sea ice coverage play a major role for the interannual variation of oceanic CO_2 uptake in this area, while ΔpCO_2 has a minor effect.

We also observed pCO_2^{sea}, DIC, and $\delta^{13}C$ in the Southern Ocean during the summer from 2001 through 2003. The pCO_2^{sea} values measured on the Umitaka-Maru cruise from January to February 2003 showed a negative correlation with SST. We derived the pCO_2^{sea}–SST relationship based on the results from this cruise, and calculated pCO_2^{sea} and air-sea CO_2 flux in this ocean using the obtained relationship and the SST data from NCEP/NCAR reanalysis. The results showed that the pCO_2^{sea} value was low (< 345 μatm) in the Australian side and high (>360 μatm) in the Antarctic side.

The average oceanic CO_2 uptake for the two months of January and February was estimated to be 0.012 GtC $month^{-1}$ for the Indian and western Pacific sectors (110°-150°E) and 0.14 GtC $month^{-1}$ for the whole Southern Ocean.

It was found that the physical process is much more essential than the biological process for the CO_2 uptake in the Southern Ocean even in summer, while the biological process is important in the Greenland Sea and the Barents Sea, by comparing the values of air-sea CO_2 flux for the respective seas.

From the results obtained by multi-ship observations with 4 research vessels in the Southern Ocean in summer, we found that the values of pCO_2^{sea} off the coast of the Antarctic Continent (66°S) varied temporally by 100 μatm for 5 months, mainly due to seawater upwelling from deep layers and biological activities limited by iron supply. The total CO_2 uptake by the ocean for 5 months amounted to 0.037 GtC yr^{-1} for the western Pacific Sector (140°-150°E) and 1.4 GtC yr^{-1} for the whole Southern Ocean. We also found that nDIC decreased with time from December 2001 to March 2002 in the upper layer of 100-200 m, depending on latitude, due to biological activities during summer, while it increased temporally but slightly in the layer below 100-200 m due to re-mineralization of organic matter.

The increase rates of pCO_2^{sea} for the area covered by this study, except for SSIZ, were estimated to be 1.5-2.2 μatm yr^{-1} by comparing the difference of pCO_2^{sea} measured by 10-year JARE cruises, which is larger than that of pCO_2^{sea} (1.4 μatm yr^{-1}). For SSIZ, we estimated the pCO_2^{sea} increase rate to be 2.6 μatm yr^{-1} based on our result of DIC increase rate of 1.2 mol kg^{-1} yr^{-1}. A significant difference of $\delta^{13}C$ for 10 years was not detected.

Table of Contents

Chapter 1

Introduction 1

Chapter 2

Sample Collection and Analytical Procedures 6

2.1 Measurement and calculation of pCO_2^{sea} and estimation of air-sea CO_2 flux . 7

2.1.1 Measurements of pCO_2^{sea} in the Greenland Sea and the Barents Sea 7

2.1.2 Measurements pCO_2^{sea} and pCO_2^{air} in the Southern Ocean 9

2.1.3 Calculation of pCO_2 and air-sea CO_2 flux 10

2.2 Measurements of DIC and $\delta^{13}C$ 11

2.2.1 Collection of seawater sample 11

2.2.2 DIC Analyses 11

2.2.3 Mass Spectrometer Analyses of $\delta^{13}C$ 13

Chapter 3

Temporal and Spatial Variations of pCO_2^{sea} and air-sea CO_2 Flux in the Greenland Sea and the Barents Sea 26

3.1 Long-term trend of pCO_2^{sea} and pCO_2^{air} 27

3.2 pCO_2^{sea}-SST relationships 28

3.3 monthly pCO_2^{sea} maps 29

3.4 Seasonal variation of the air-sea CO_2 flux 33

3.5 Interannual variability of the CO_2 flux 36

Chapter 4

Temporal and Spatial Variations of Carbon System in the Southern Ocean 51

4.1 Variation of pCO_2^{sea} measured on Umitaka-Maru cruise in 2003 52

4.1.1 Fronts and zones in the Southern Ocean 52

4.1.2 Latitudinal and longitudinal distributions of pCO_2^{sea}, SST and SSS 53

4.1.3 pCO_2^{sea} -SST relationship 54

4.1.4 Spatial distributions of pCO_2^{sea} and air-sea CO_2 flux 55

4.2 Variations of pCO_2^{sea} in the western Pacific sector in the summer of 2002 ... 57

4.2.1 Aurora Australis cruise 57

4.2.2 Hakuho-maru (KH-01-3) cruise 58

4.2.3 JARE43 Tangaroa cruise 59

4.2.4 JARE43 Shirase cruise 59

4.2.5 Temporal and spatial variations of pCO_2^{sea} and air-sea CO_2 flux 60

4.2.6 Comparison of the seasonal variations of pCO_2^{sea} and air-sea CO_2 flux in the Southern Ocean, the Greenland Sea and the Barents Sea 62

4.3 Variations of DIC in the western Pacific Sector in summer 64

4.3.1 Spatial distribution of nDIC 64

4.3.2 Temporal variation of nDIC 65

4.4 Temporal variations of pCO_2^{sea}, DIC and $\delta^{13}C$ over 10 years 66

4.4.1 Variation of pCO_2^{sea} 67

4.4.2 Variations of DIC and $\delta^{13}C$ 68

Chapter 5

Summary **106**

References

Chapter 1

Introduction

The terrestrial atmosphere contains many greenhouse gases such as carbon dioxide (CO_2), methane and nitrous oxide, and CO_2 is one of the most important greenhouse gases in maintaining and changing the climate. The atmospheric CO_2 concentration has been increased from 280 ppmv in pre-industrial era to about 375 ppmv in 2003, due to fossil fuel combustion and deforestation, which was demonstrated by recent direct atmospheric measurements and analyses of ancient air occluded in polar ice cores (Barnola et al., 1987; Conway et al., 1994; Etheridge et al., 1996; Keeling et al, 1989, 1995; Nakazawa et al., 1993, 1997; Neftel et al., 1985; Kawamura et al., 2000; Ishidoya 2003). Therefore, it is crucial for predicting future possible climate change to understand the global carbon cycle, i.e. to quantify CO_2 uptake and release by the oceans and the terrestrial biosphere.

The ocean is a major carbon reservoir on the Earth's surface, and it absorbs a certain amount of anthropogenic CO_2 emitted into the atmosphere. The oceanic CO_2 uptake has been estimated using various methods such as measurements of atmospheric O_2/N_2 ratio and carbon isotopic ratio of CO_2 and model inversion analyses (Keeling and Shertz, 1992; Francey et al., 1995; Keeling et al., 1995; Rayner et al., 1999; Le Quéré et al., 2003), but there are still large uncertainties in their estimates. For example, Prentice et al. (2001) reported an average oceanic CO_2 uptake of 1.9 GtC yr^{-1} with uncertainty of 0.7 GtC yr^{-1} for the 1990s, based on atmospheric O_2/N_2 observations. However, Takahashi et al. (1997) reported that the global ocean as a whole is nearly in equilibrium with atmospheric CO_2, but locally in disequilibrium by as much as 30%. They also suggested that high latitude oceans act as a CO_2 sink, due to strong wind and lower partial CO_2 pressure in the surface ocean (pCO_2^{sea}) than in the atmosphere (pCO_2^{air}).

It is considered that the vertical transport of carbon from the surface ocean to the deep layer plays a key role in oceanic carbon uptake. Once carbon is transported from the surface ocean to abyssal depths, either by physical or biological processes, it

can be effectively sequestered away from the atmosphere over 1000 years (Broeker and Peng, 1982). In this context, high latitude oceans, such as the Greenland Sea and the Southern Ocean, are thought to be an important sink for atmospheric CO_2 (Anderson, 1995; Noji et al., 2000). In the central Greenland Sea gyre, the Greenland Sea Deep Water, which is source water that ventilates North Atlantic Deep Water, is formed (Aagaard et al., 1985).

In the Greenland Sea gyre, Hood et al. (1999) evaluated an annual average ΔfCO_2 (CO_2 fugacity difference between the atmosphere and the ocean) of 71 μatm, based on 6-month measurements by CARIOCA drift buoys. They also estimated the oceanic CO_2 uptake to be 2.4-4.2 x 10^{-3} GtC yr^{-1} for the Greenland Sea gyre (74°-76°N, 10°W-5°E; 0.15 x 10^6 km^2) during the period from August 1996 to July 1997. Skjelvan et al. (1999) derived the CO_2 uptake of 1.2 ± 0.15 x 10^{-1} GtC yr^{-1} for the Greenland Sea (0.81 x 10^6 km^2) and the Norwegian Sea (1.39 x 10^6 km^2), based on their observed data from the regions of 74.5°-75.5°N and 5°W-3°E (25.6 x 10^3 km^2) and 64.5°-70.5°N and 7°W-5°E (33.8 x 10^3 km^2) during the 1996-1997 period. By analyzing the fCO_2^{sea} values measured during 9 cruises between 1982 and 1998, Olsen et al. (2003) reported the CO_2 uptake of 8.2 x 10^{-2} GtC yr^{-1} for the northern North Atlantic (45°-80°N) in the wintertime (October to March), with interannual variability of about ± 7 % due mostly to changes in wind speed and fCO_2^{air}.

The formation of intermediate/deep water also occurs in the Barents Sea (Kaltin et al., 2002). High dense water is formed on the shelf of the Barents Sea by surface cooling and brine rejection due to sea ice formation, and then penetrates into the intermediate/deep layers in the Arctic Ocean. Schlosser et al. (1990) pointed out that atmospheric CO_2 absorbed by the Barents Sea would be stored in the Arctic Ocean for more than 100 years. Based on measurements of the total dissolved inorganic carbon, total alkalinity, temperature, salinity, and nitrate in the water column, Kaltin et al.

(2002) calculated the oceanic CO_2 uptake to be 29 ± 11 gC m^{-2} for 3 months starting from the late winter of 1999.

The Southern Ocean is also considered to be an important region for the anthropogenic CO_2 uptake, mainly due to its large area and high wind speeds (Sabine and Key, 1998), although biological activities are rather limited by lower iron supply (Martin et al., 1990). However, there are large differences among oceanic CO_2 uptake estimated by previous studies. For example, Takahashi et al. (2002) estimated the Southern Ocean CO_2 uptake to be 0.6 GtC yr^{-1} based on global measurements of ΔpCO_2, while Rayner et al. (1999) found to be about 0.1 GtC yr^{-1} using their atmospheric inverse model.

Recently, another importance about carbon cycle in the Southern Ocean was pointed out. Orr et al. (2005) reported that Southern Ocean surface waters would begin to become under-saturated with respect to aragonite, a metastable form of calcium carbonate ($CaCO_3$), by the year 2050 due to acidification of seawater caused by taking up CO_2, and that this undersaturation could extend throughout the entire Southern Ocean and into the sub-arctic Pacific Ocean by 2100. Therefore, it is important, not only for quantifying the oceanic CO_2 uptake but also for predicting the influence of absorbed CO_2 on marine biological activities, to examine temporal and spatial variations of carbon system in the Southern Ocean.

The purpose of this thesis is to collect data of pCO_2^{sea} and its relevant factors extensively and discuss temporal/spatial variations of carbonate system in the northern and southern polar oceans based on those data. For this purpose, we measured pCO_2^{sea} in the Greenland Sea and the Barents Sea for the period 1992-2001, calculated the air-sea CO_2 flux, and examined seasonal/interannual variations of the oceanic CO_2 uptake in terms of CO_2 partial pressure difference between the ocean and the atmosphere

($\Delta pCO_2 = pCO_2^{sea} - pCO_2^{air}$), sea surface temperature (SST), wind speed and sea ice area to show what controls the air-sea CO_2 flux in the northern polar oceans. The results will be presented and discussed in detail in Chapter 3, after describing our experimental procedures employed in Chapter 2.

In addition to measurements in the Greenland Sea and the Barents Sea, we also acquired the pCO_2^{sea} data on the Umitaka-Maru cruise in the Indian (110°-140°E) and western Pacific (140°-150°E) sectors of the Southern Ocean from January to February 2003. The collection of pCO_2^{sea}, Dissolved Inorganic Carbon (DIC) and its $\delta^{13}C$ data were further made on the Aurora Australis, Hakuho-Maru, Tangaroa and Shirase cruises in the western Pacific sector (140°-150°E) in 2001 and 2002. Based on these measurements, we derived spatial variations of pCO_2^{sea} and air-sea CO_2 flux, as well as summertime variation of carbon system, for the Southern Ocean. The examination was also made on temporal variations of pCO_2^{sea}, DIC and its $\delta^{13}C$ in this ocean, using their data from previous studies (Hashida, 1993; Ishii et al., 1998). Furthermore, we compared the air-sea CO_2 flux for the Southern Ocean with those for the Greenland Sea and the Barents Sea, to characterize the CO_2 uptake by the northern and southern polar oceans. The results and discussion will be presented in Chapter 4.

Chapter 2

Sample Collection and Analytical Procedures

In order to elucidate spatial and temporal variations of partial CO_2 pressure in the surface sea (pCO_2^{sea}), air-sea CO_2 flux, dissolved inorganic carbon (DIC) and its carbon isotopic ratio ($d^{13}C$) in northern and southern polar oceans, we collected sea water samples and air samples equilibrated with surface seawater on board research vessels in the Greenland Sea, the Barents Sea and the Southern Ocean. In this section, we describe our experimental and analytical procedures employed for these components.

2.1 Measurement and calculation of pCO_2^{sea} and estimation of air-sea CO_2 flux

2.1.1 Measurements of pCO_2^{sea} in the Greenland Sea and the Barents Sea

Comprehensive measurements of pCO_2^{sea} and its relevant factors were made on 9 cruises in the eastern Greenland Sea and the western Barents Sea during the period August 1992-April 2001, as outlined in Table 2-1. Hydrographic stations for the pCO_2^{sea} measurements, major current system (Furevik, 2001), and minimum/maximum sea ice areas found from the NCEP/NCAR reanalysis data (Kalnay et al., 1996) in both seas are depicted in Fig. 2-1. There are two branches of the warm Norwegian Atlantic Current that flow northward off the Norwegian coast; one is the West Spitsbergen Current and the other is the branch that enters the Barents Sea (Furevik, 2001; Kaltin et al., 2002). The cold Eastern Greenland Current flows southward along the Greenland coastline.

In these measurements, the pCO_2^{sea} values were obtained using a discrete flask sampling with subsequent laboratory analysis. A schematic diagram of our sampling system for air equilibrated with seawater is given in Fig. 2-2. The system consists of a shower-head type equilibrator, a diaphragm pump, a chemical desiccant column ($Mg(ClO_4)_2$), a four-way valve, and a stainless flask (1 L) with two stopcocks at both

ends (Watai et al., 1998). Seawater introduced into the equilibrator was vented to the atmosphere so that air samples were collected at ambient pressures. All the flasks were evacuated at 1.3 x 10^{-5} Pa at 120 °C for 24 hours in our laboratory before shipping, and each flask was thoroughly flushed by uncontaminated air aboard ship before sampling. After connecting the flask to the sampling system, the air was circulated at a flow rate of 0.5 L min^{-1} for 15 minutes to ensure equilibrium in CO_2 between seawater and air (Watai et al., 1998), and then collected in the flask.

From August 1992 to January 1999, seawater was taken 3-5 m below the surface using a submersible pump (> 100 L min^{-1}), and part of it (12 L min^{-1}) was diverted into the equilibrator. It was found that the temperature of seawater in the equilibrator agreed well with SST to within ± 0.1 °C. During November 1999-April 2001, uncontaminated seawater was taken from the sea-chest of the vessel, and it was observed that the temperature of seawater in the equilibrator was higher than SST by 0.55 °C in November 1999 and 0.82 °C in April 2001. In October 2000, we did not measure the seawater temperature rise in the equilibrator. Therefore, the average of the two values for November 1999 and April 2001 (0.68 °C) was taken to be the rise in seawater temperature from the inlet to the equilibrator. The uncertainty in the temperature rise was considered to be 0.14 °C in October 2000, but this does not affect the results of the present study (see Chapter 3).

All the flasks filled with air samples were sent to our laboratory, and their CO_2 concentrations were determined against our air-based CO_2 standard gases with a precision of ± 0.5 ppmv within 3 months of sampling using a gas-chromatograph equipped with a flamed ionization detector and a converter of CO_2 to CH_4 (Watai et al., 1998). The CO_2 concentrations of our standard gases are traceable to the WMO standards (Tanaka et al., 1987; http://gaw.kishou.go.jp/wcc/co2/co2comparison). We also confirmed that the CO_2 concentrations of air samples stored in our flasks were

stable to within ± 0.1 ppmv for 3 months (Nakazawa et al., 1997).

2.1.2 Measurements pCO_2^{sea} and pCO_2^{air} in the Southern Ocean

Observations of pCO_2^{sea} and pCO_2^{air} (atmospheric CO_2 partial pressure) were made from October 2001 to March 2002 in the western Pacific sector (140°-150°E) using R/V Aurora Australis belonging to the Australian Commonwealth Scientific and Research Organization (CSIRO), R/V Hakuho-Maru belonging to the University of Tokyo, R/V Tangaroa chartered by the National Institute of Polar Research, icebreaker "Shirase" belonging to the NIPR. In 2003, pCO_2^{sea} measurements were made between the Indian (110°-140°E) and western Pacific (140°-150°E) sectors of the Southern Ocean, using R/V Umitaka-Maru belonging to Tokyo University of Marine Science and Technology. The observations by these ships are summarized in Table 2-2. The tracks of the 2001-02 and 2003 cruises and the locations of fronts in the Southern Ocean determined according to Chaigneau and Morrow (2002) to be described in Chapter 4 are depicted in Figs. 2-3 and 2-4.

On these cruises, pCO_2^{sea} was continuously measured. The measurement system used is similar to that shown in Fig. 2-2, except that part of a four-way valve, the sampling flask and their relevant tubing was replaced with a non-dispersive infrared (NDIR) CO_2 analyzer and a gas-handling system for CO_2 standard gases and air equilibrated with seawater. The gas-handling system was also equipped with a tubing to measure the atmospheric CO_2 concentration. The CO_2 standard gases were introduced into the NDIR analyzer every 1 hour for calibrating its output relative to the CO_2 concentration.

Uncontaminated seawater was taken from the sea-chest of the vessel and introduced into the equilibrator at approximately 10 L min^{-1}. It was found that the

temperature of seawater in the equilibrator was higher than SST, which is similar to the measurements in the Greenland Sea and the Barents Sea. The temperature rises measured on these cruises are shown in Table 2-3.

In situ measurements of pCO_2^{air} were also carried out using the above-mentioned system, except for the Umitaka-Maru cruise. To calculate air-sea CO_2 flux for the Umitaka-Maru cruise, we used the atmospheric CO_2 concentration data at Syowa Station (69°S, 39°E).

2.1.3 Calculation of pCO_2 and air-sea CO_2 flux

The values of pCO_2^{sea} and pCO_2^{air} were calculated by the equation,

$$pCO_2 = xCO_2 \times (P - p(H_2O)). \quad (2\text{-}1)$$

Here, xCO_2 is the measured CO_2 concentration of dry air equilibrated with seawater or that of ambient dry air, P is the barometric pressure, and $p(H_2O)$ is the saturated vapor pressure. As mentioned above, the temperature rise of seawater between its inlet and the equilibrator was observed on three cruises after 1999 in the Greenland Sea and the Barents Sea , as well as on all cruises in the Southern Ocean. The effect of temperature rise on the measured value of pCO_2 was corrected using the iso-chemical temperature dependence of pCO_2 given by Takahashi et al. (1993),

$$\frac{\delta \ln(pCO_2)}{\delta T} = 4.23\,(\%^{\circ}C^{-1}). \quad (2\text{-}2)$$

The CO_2 flux (f) between the air and the sea is conventionally given by the product of the gas transfer velocity K_{CO2} as a function of wind speed (Wanninkhof, 1992; Wanninkhof and McGills, 1999), the solubility of CO_2 β (Weiss, 1974), and the partial pressure difference ΔpCO_2;

$$f = K_{CO2} \cdot \beta \cdot (pCO_2^{air} - pCO_2^{sea}) = K_{CO2} \cdot \beta \cdot \Delta pCO_2 = E \cdot \Delta pCO_2. \quad (2\text{-}3)$$

Here, E represents the gas transfer coefficient, which is usually assumed to be independent of SST, since K_{CO2} and β counteract their temperature dependence (Tans et al., 1990).

2.2 Measurements of DIC and $\delta^{13}C$

2.2.1 Collection of seawater sample

In the Southern Ocean, seawater samples were collected from the deep layer to the surface by using a Niskin bottle, and then each sample was filled into a 100 ml vial for analyses of DIC and its $\delta^{13}C$. A small amount (0.03 g) of mercury (II) chloride ($HgCl_2$) was added to the samples to kill plankton contained in the samples, by which the influence by plankton activities during sample storage can be avoided. The seawater samples collected were kept under cool and dark conditions until they were analyzed for DIC and its $\delta^{13}C$. The samples were sent to Meteorological Research Institute, Japan and CSIRO, Australia, and then analyzed for DIC by using a coulometer. Some samples were also sent to Tohoku University for a mass spectrometer analysis of $\delta^{13}C$ in DIC.

2.2.2 DIC Analyses

DIC in the seawater sample was analyzed using a carbon coulometer (UIC Co., Ltd., model 5011 or 5012) (Ishii et al., 1998) and its improved model (Nippon ANS Co.). The analysis system of DIC used comprises a CO_2 extraction unit, a coulometer, a standard gas injector and a control unit (Fig. 2-5). The extraction unit is used to extract CO_2 from seawater sample by mixing it with phosphoric acid, as well as to transfer the

extracted CO_2 to the coulometer. The standard gas injector carries the CO_2/N_2 standard gases to the coulometer to watch whether the analyzer operates normally. The control unit manages analytical procedures of DIC and data storage. CO_2 gas transferred by N_2 carrier gas from the extraction unit to the coulometer is absorbed by cathode solution in an electrolysis cell and titrated coulometrically. The coulometer used is as follows.

The electrolysis cell was separated by ceramic so that chemical reaction between the cathode and anode sides proceeds gently. The electrolysis cell on the cathode side was filled by the cathode solution after the magnetic stirrer was injected and then attached with a platinum electrode. The cathode solution was a mixture of dimethyl sulfoxide, water, mono-ethanolamine and tymolphthalein. The electrolysis cell on the anode side was filled by the anode solution saturated with potassium iodide and then attached with a silver electrode. When CO_2 extracted from seawater is introduced into the cathode side by N_2 carrier gas, the respective reactions occur on the cathode and anode sides:

Cathode side: $CO_2 + HO(CH_2)_2NH_2 \rightarrow HO(CH_2)_2NHCOOH$ (2-4)

$2H_2O + 2e^- \rightarrow H_2(g) + 2OH^-$ (2-5)

$HO(CH_2)_2NHCOOH + OH^- \rightarrow HO(CH_2)_2NHCOO^- + H_2O$ (2-6)

Anode side: $Ag^0(s) \rightarrow Ag^+ + e^-$ (2-7)

$2Ag^+ + 4I^- \rightarrow 2AgI_2^-$ (2-8)

These reactions are rewritten as:

$$Ag^0 + 2I^- + CO_2 + HOCH_2CH_2NH_2 \rightarrow AgI_2^- + 1/2H_2 + HO(CH_2)_2NHCOO^- \quad (2\text{-}9)$$

Therefore, electron equivalent to CO_2 participating in this reaction flows between the

electrodes. The total amount of CO_2 is calculated by counting electrical quantity.

2.2.3 Mass Spectrometer Analyses of $\delta^{13}C$

$\delta^{13}C$ in DIC was determined by analyzing CO_2 gas extracted from seawater sample. Our CO_2 extraction system consists of a Pyrex glass flask in which sample seawater is reacted with phosphoric acid (H_3PO_4), H_2O trap at about -100°C and two H_2O/CO_2 traps at -197°C, a sample tube and a rotary pump. A schematic diagram of the system is shown in Fig. 2-6. The traps were made of Pyrex glass and contained many thin glass tubes to trap CO_2 or H_2O effectively.

The CO_2 extraction procedures were as follows. Firstly, water sample and H_3PO_4 of about 5 ml were introduced into the evacuated glass flask, and mixed well using a magnetic stirrer. Then, CO_2 gas released was transported from the reaction flask to the traps by evacuating the whole system by the rotary pump. CO_2 collected in the trap was sublimated by increasing its temperature to about -100°C and transferred to the sample tube cooled at –197°C by liquid nitrogen. After completing the collection of CO_2 gas, the sample tube was flamed off.

A mass spectrometer used in this study was a Finnigan MAT-δS, which consists of an inlet system for sample and standard, an analyzer system and a signal and data processing system. The inlet system is shown in Fig. 2-7. This system comprises two separate inlets for sample and standard gases, of which structures are designed to be the same to allow an alternative introduction of the two gases into the analyzer under the same condition. Each inlet has a variable volume for reserving the gas to be analyzed and an inlet capillary with an inner diameter of 0.5 mm connected to the analyzer. The inlet for the sample has also a tube cracker in which sample tube is broken to introduce CO_2 into the analyzer. To minimize an influence of non-linear response of the pre-

amplifiers of the detectors, ion beam intensities for the sample and standard have to be identical. This can be attained by adjusting the pressure in the respective variable volumes, of which the volume is adjustable within a range from about 3.5 to 40 ml.

The analyzer system is evacuated with a turbo molecular pump till the pressure is about 5 x 10^{-6} Pa. The introduced CO_2 sample is first fed to ionization chamber in the analyzer system. The ions leave from the ionization chamber through some lenses and enter into the magnetic sector field. After deflected by the magnetic field, the ions are caught by Faraday cup collectors suitably placed for each mass and are converted to ion current proportional to numbers of the ions arrived there. Our MAT-δS has 6 collectors, but three collectors of them were employed to obtain the ion current for mass 44, 45 and 46 of CO_2, so that values of δ^{45} and δ^{46} of the sample against the standard are calculated. The definitions of δ^{45} and δ^{46} are:

$$\delta^{45} = \left(\frac{R_{sa}^{45}}{R_{st}^{45}} - 1 \right), \tag{2-10}$$

$$\delta^{46} = \left(\frac{R_{sa}^{46}}{R_{st}^{46}} - 1 \right), \tag{2-11}$$

where R denotes the ion current ratios of mass 45 or 46 against that of mass 44 and subscripts 'sa' and 'st' denote the sample and standard, respectively. Values of $\delta^{13}C$ and $\delta^{18}O$ of a CO_2 sample are calculated from the measured δ^{45} and δ^{46} by using the formulas described in Morimoto (1993).

Analytical procedures of CO_2 samples were as follows. The sample tube, in which the extracted CO_2 was sealed, was cleaned using ethanol and put into the tube cracker mad of Pylex grass. The tube cracker was connected to the inlet system by an air-tight coupler with O-rings, and the inlet system including the tube cracker was evacuated using a rotary pump first and then a turbo molecular pump for 8 minutes. After evacuation, the sample tube was cracked and the released CO_2 was introduced into

the variable volume for sample. After this, the procedures proceeded automatically by control of the personal computer. The ion beam was focused again by tuning the accelerating voltage finely. Then, the respective ion currents for mass 44, 45 and 46 of the standard and sample were measured 8 times alternately and the measured values were averaged to obtain the δ^{45} and δ^{46} values. Outliers of the measurements, which were defined as those lying more than 2 standard deviations from the respective average value, were excluded. It took about 12 minutes to analyze one CO_2 sample. Precisions of our MAT-δS were estimated to be ± 0.02 and ± 0.05‰ for $\delta^{13}C$ and $\delta^{18}O$, respectively (Morimoto 1993). Our laboratory standards of isotope analysis of CO_2 are pure CO_2 gases prepare by reacting NBC-18 ($\delta^{13}C$ of -5.03‰ and $\delta^{18}O$ of -23.04‰ relative to V-PDB) and NBS-19 ($\delta^{13}C$ of +1.95‰ and $\delta^{18}O$ of -2.2‰ relative to V-PDB) with 100% phosphoric acid at 25°C.

Table 2-1. Summary of cruises in the Greenland Sea and the Barents Sea for the 1992-2001 period

Year	Month	Cruise Name	Vessel Name	Observed Territory	Sampling Method
1992	Aug.	-	Lance	75°-79°N 11°W-9°E	Anchor
1993	Aug.	-	Lance	74°-79°N 13°W-9°E	Anchor
1994	April-May	-	Polar Ship	70°-75°N 18°W-10°W	Anchor
1995	June	ICE BAR	Lance	74°-78°N 19°E-35°E	Anchor
1996	July-Aug.	ICE BAR	Lance	74°-81°N 17°E-35°E	Anchor
1999	Jan.-Feb.	- / VEINS	Ian Petrov/Lance	70°-80°N 0°-30°E	Anchor
1999	Nov.	VEINS	Lance	71°-80°N 11°E-20°E	Underway
2000	October	-	Lance	71°-78°N 13°E-19°E	Underway
2001	April	CONVECTION	Lance	71°-77°N 11°W-19°E	Underway

Table 2-2. Summary of cruises for pCO_2^{sea} measurements in the Southern Ocean for the 2001-2003 period

Year	Month	Cruise Name	Vessel Name	Observed Territory
2001	Oct.-Dec.	-	Aurora Australis	44°-67°S 140°-147°E
2002	Jan.	KH-01-3	Hakuho-Maru	45°-65°S 140°-170°E
2002	Jan.-Feb.	JARE43	Tangaroa	44°-66°S 140°-150°E
2002/2003	March	JARE43	Shirase	47°-66°S 70°-150°E
2003	Jan.-Feb.	-	Umitaka-Maru	20°-67°S 110°-147°E

Table 2-3. Temperature rise occurred between the sea surface and the equilibrator for the respective cruises.

Year	Vessel Name	Temperature rise from SST (°C)
2001	Aurora Australis	0.7
2002	Hakuho-Maru	0.4
2002	Tangaroa	0.9
2002/2003	Shirase	Temp(eq)*0.07-0.77 (Temp(eq)<11) 0 (Temp(eq)>11)
2003	Umitaka-Maru	1.1

For the Shirase cruise, the temperature rise can be expressed as a function of temperature in the equilibrator.

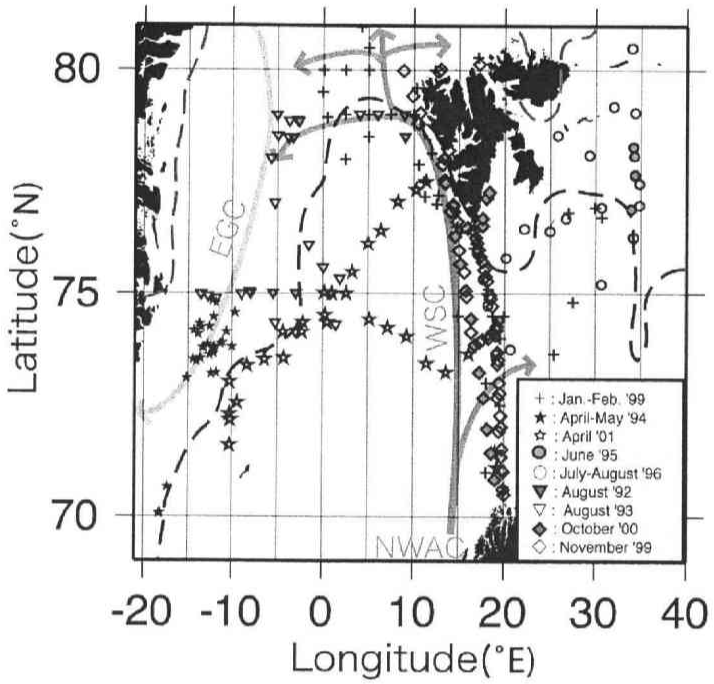

Fig. 2-1. Geographical locations where pCO_2^{sea} measurements were made from 1992 through 2001. Dashed gray and black lines show the climatological boundaries of sea ice area in August and January, respectively. Arrows represent major currents in the Greenland Sea and the Barents Sea (Furevik et al., 2001), including the Norwegian Atlantic Current (NWAC), West Spitsbergen Current (WSC), and East Greenland Current (EGC). The atmospheric CO_2 data used to calculate pCO_2^{air} in this study were taken at Ny-Ålesund in Svarbard Islands (79°N, 12°E).

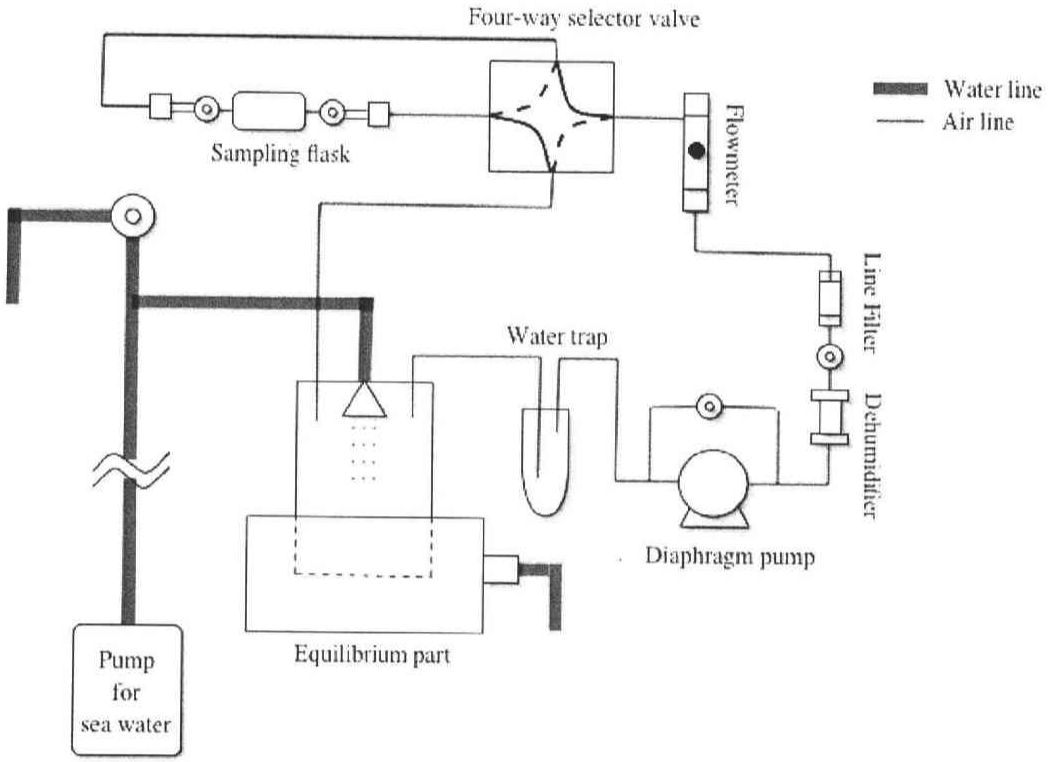

Fig. 2-2. Sampling equipment for air equilibrated with seawater used in the Greenland Sea and the Barents Sea

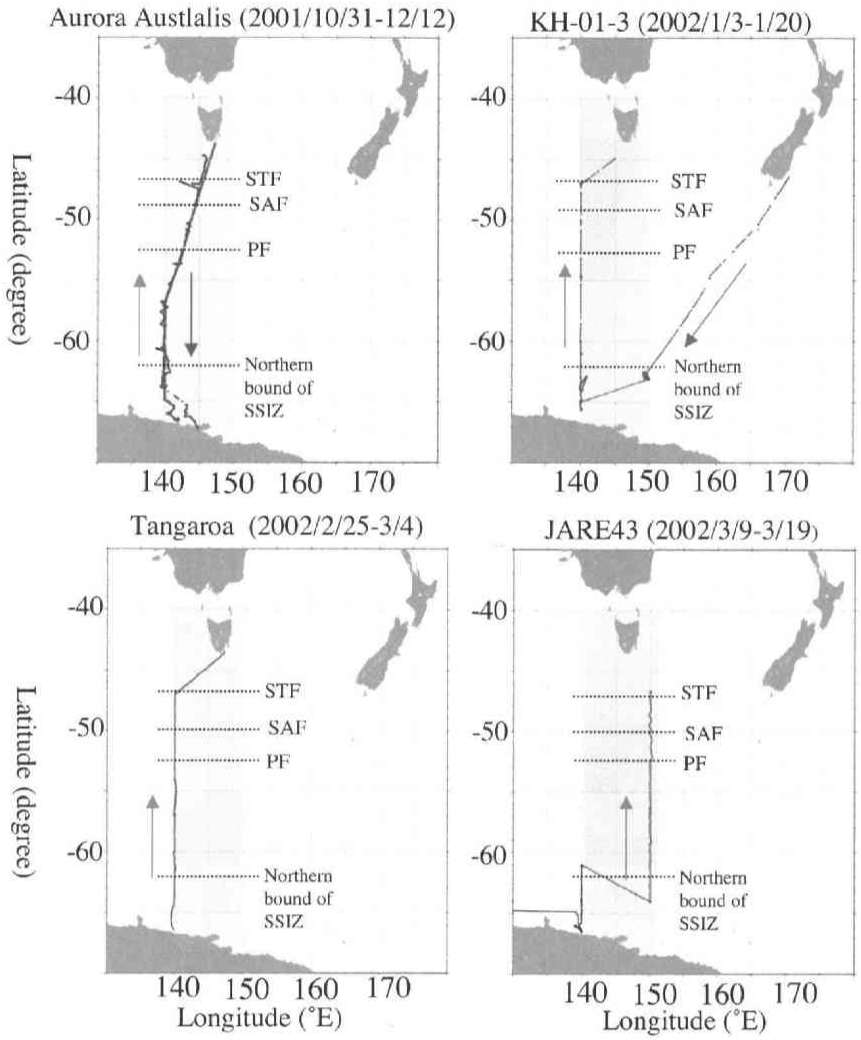

Fig. 2-3. Cruise tracks of R/Vs Aurora Australis, Hakuho-maru, Tangaroa and Shirase. Light green show areas where temporal variations of pCO_2^{sea} and air-sea CO_2 flux were examined in this study. The locations of fronts defined according to Chaigneau and Morrow (2002) and zones in the Southern Ocean are also depicted.

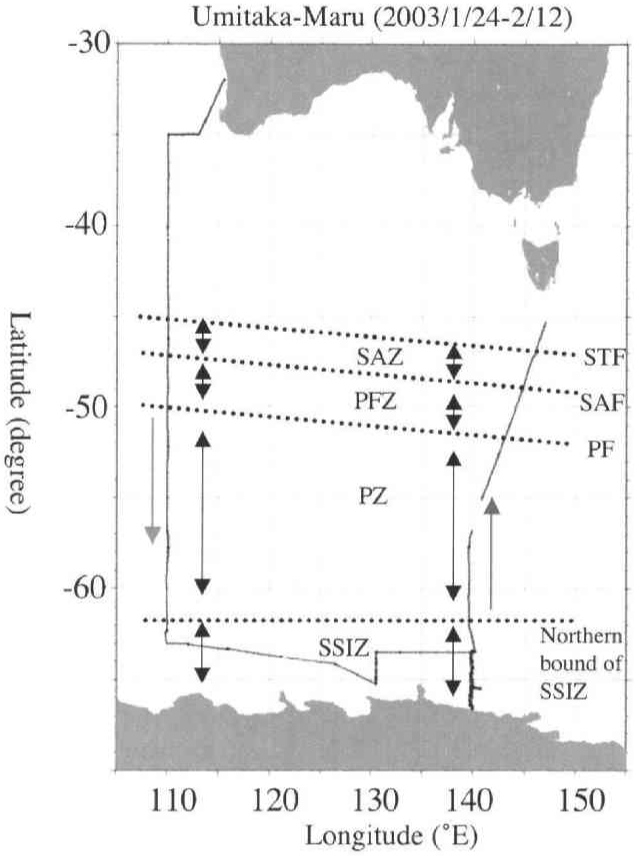

Fig. 2-4. Cruise track of Umitaka-Maru, and locations of fronts defined according to Chaigneau and Morrow (2002) and zones in the Southern Ocean

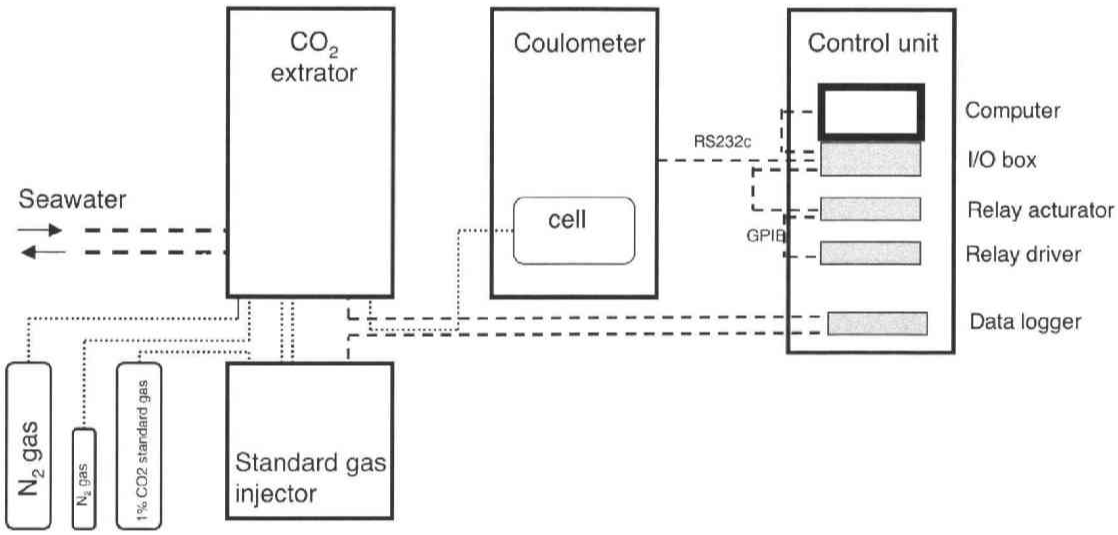

Fig. 2-5. Schematic diagram of the DIC measurement system used in this study

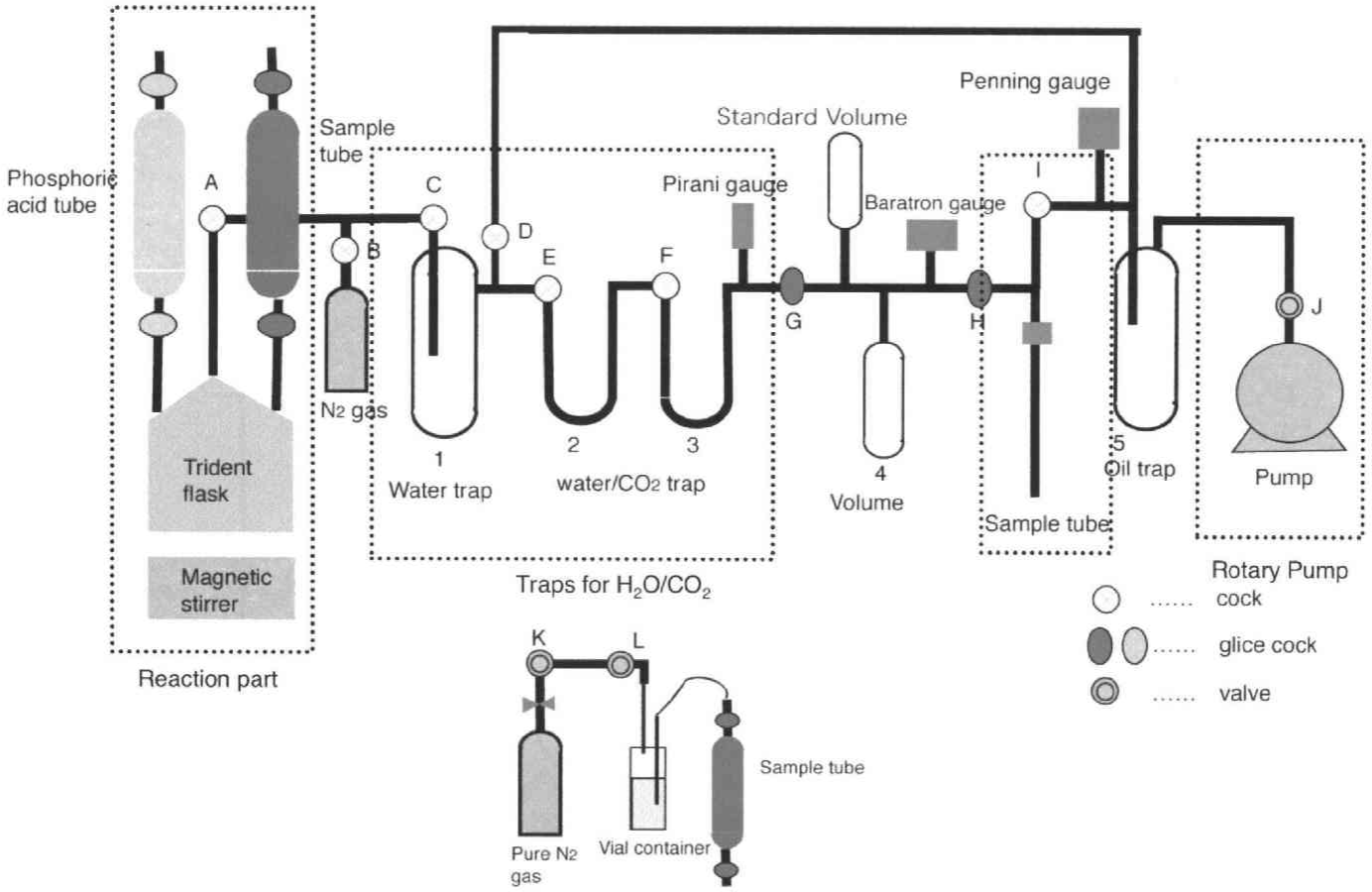

Fig. 2-6. Schematic diagram of the CO_2 extraction system used in this study

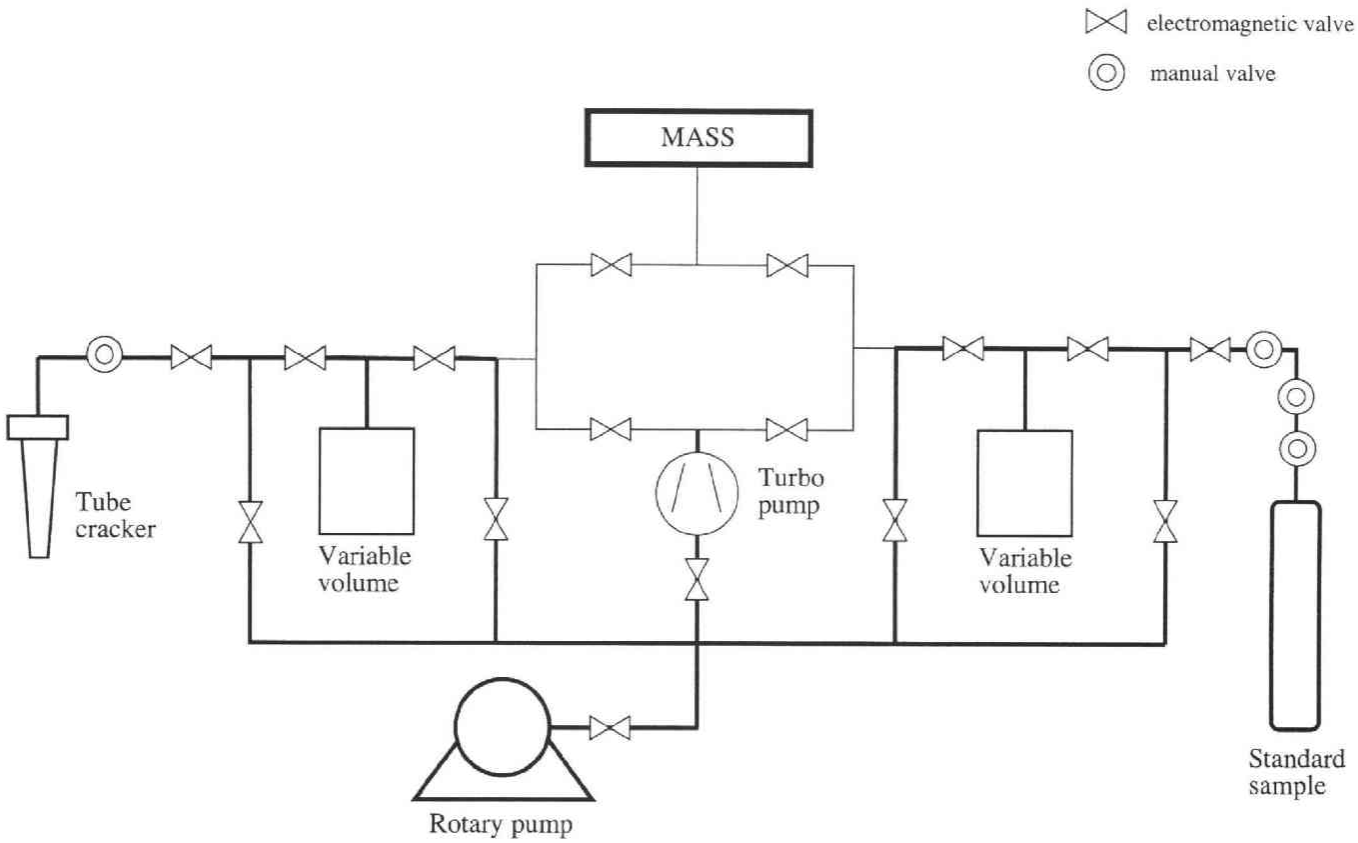

Fig. 2-7. Inlet system of the mass spectrometer, MAT-δS

Chapter 3

Temporal and Spatial Variations of pCO_2^{sea} and air-sea CO_2 Flux in the Greenland Sea and the Barents Sea

In order to understand temporal and spatial variations of pCO_2^{sea} and air-sea CO_2 flux in the Greenland Sea and the Barents Sea, pCO_2^{sea} was measured 9 times during the period 1992-2001. In this chapter, the results of pCO_2^{sea} obtained from these measurements, as well as the air-sea CO_2 fluxes calculated from the differences between measured values of pCO_2^{air} and pCO_2^{sea}, will be reported. Based on these results, the seasonal and interannual variations of pCO_2^{sea} and air-sea CO_2 flux will be discussed. The discussion will also be made for the relationship between North Atlantic Oscillation and oceanic CO_2 anomaly.

3.1 Long-term trend of pCO_2^{sea} and pCO_2^{air}

The pCO_2^{sea} values obtained in the western Greenland Sea in April 1994 and in the same month in 2001 were compared to determine the long-term trend. The comparison indicated a pCO_2^{sea} increase of 28 ± 21 μatm, on average, during that period. However, further detailed discussion of the long-term trend is beyond the scope of this paper because the spatial variability is too large and time series data are not available for that region.

Recent studies have revealed a secular increase of pCO_2^{sea} in the subtropics (Gruber et al., 2002; Keeling et al., 2004; Midorikawa et al., 2005) and even in the high latitudes, such as the Southern Ocean (Inoue and Ishii, 2005) and northern North Atlantic, where deep convection occurs in winter. In the Barents Sea, Omar et al. (2003) compared the fCO_2^{sea} data taken in 1967 and in 2000-2001. They found that fCO_2^{sea} has increased at a rate similar to the atmospheric CO_2 increase over the past 33 years. By inspecting observational data from the northern North Atlantic, Olsen et al. (2003) found that the pCO_2^{sea} has increased at a rate larger than that of the pCO_2^{air}. Furthermore,

Lefèvre et al. (2004) reported that the pCO_2^{sea} has increased at a rate of 1.8 μatm yr^{-1} in recent decades, which is slightly higher than that of the pCO_2^{air}, in the North Atlantic (50°-70°N, 80°-10°W).

In this study, we simply assumed that the pCO_2^{sea} has increased at a rate equal to that observed for pCO_2^{air} (Olsen et al., 2003; Omar et al., 2003). The pCO_2^{air} values were derived from the atmospheric CO_2 concentration data at Ny-Ålesund (Morimoto et al., 2001), which show an average increase rate of 1.5 ppmv yr^{-1} for the 1992-2001 period. By assuming the increase rate to be 1.5 μatm yr^{-1} for pCO_2^{sea}, we normalized all the observed data of pCO_2^{sea} to the year 1995 ($pCO_{2,95}^{sea}$) to evaluate the seasonal variation in the air-sea CO_2 flux.

3.2 pCO_2^{sea}-SST relationships

The data of pCO_2^{sea} are unevenly distributed in space and time; thus, it is necessary to interpolate/extrapolate the observed pCO_2^{sea} values to evaluate the annual CO_2 uptake in the Greenland Sea and the Barents Sea. It is known that variations in pCO_2^{sea} are mainly due to changes in temperature, mixing of the upper ocean, and marine biological activities (Broecker and Peng, 1982). The pCO_2^{sea} variations are often apparently related to SST (e.g., Tans et al., 1990; Inoue et al., 1995; Cosca et al., 2003). Seasonal variation in the relative contribution of those processes influencing pCO_2^{sea} leads to a different temperature dependence of pCO_2^{sea}. Therefore, we determined the apparent relationships between the pCO_2^{sea} and SST for each month and combined them with the dataset of SST that is available throughout these seas.

Figure 3-1 shows the relationships between the $pCO_{2,95}^{sea}$ and SST for the Greenland Sea and the Barents Sea. The temperature dependence of $pCO_{2,95}^{sea}$ is

noticeably different for different seasons.

The $pCO_{2,95}^{sea}$ increases with increasing SST, except for May and June. The temperature dependence of $pCO_{2,95}^{sea}$ varied from 1 to 3 %°C^{-1} from August to April. These temperature dependences deviate from that of the solubility (Eq. 2-2), which suggests the effect of the mixing of the upper ocean and biological activities against SST change. In May, when SST was lower than 1 °C, we found a negative correlation between $pCO_{2,95}^{sea}$ and SST. This relationship may be closely related to the biological CO_2 uptake, which starts in the western area of the Greenland Sea at this time of the year (Skjelvan et al., 1999; Anderson et al., 2000). In June, a higher $pCO_{2,95}^{sea}$ (>250 μatm) was observed when SST > 2 °C and < -1 °C, and a lower $pCO_{2,95}^{sea}$ (<200 μatm) was observed when SST was about 1 °C. A large temperature dependence of $pCO_{2,95}^{sea}$ was noted in July (6 %°C^{-1}). This might be caused by the CO_2 drawdown close to the sea ice in the western Barents Sea (Fig. 3-2). Such a complicated $pCO_{2,95}^{sea}$-SST relationship also indicates that processes other than solubility, possibly biological activities (spring bloom), predominantly control the variation in $pCO_{2,95}^{sea}$. Therefore, we tried to derive the $pCO_{2,95}^{sea}$ values during the spring bloom using SST and chlorophyll-a data. However, $pCO_{2,95}^{sea}$ could not be approximated by these two parameters alone, as pointed out in the equatorial Pacific by Dandonneau (1995) earlier. To document the pCO_2^{sea} distribution during the spring bloom, it is necessary to use variables that are directly related to the photosynthesis/respiration of phytoplankton, such as nitrate and phosphate (Wanninkhof et al., 1996).

3.3 monthly pCO_2^{sea} maps

In order to draw monthly maps of $pCO_{2,95}^{sea}$ for the Greenland Sea and the Barents

Sea, we used seasonally different $pCO_{2,95}^{sea}$-SST relationships obtained by fitting the data given in Fig. 3-2 with,

$$pCO_{2,95}^{sea}(t) = a(t) \times SST + b(t), \quad (3\text{-}1)$$

where $a(t)$ is the slope and $b(t)$ the intercept at a given time (month) t. In this procedure, since the pCO_2^{sea} values observed at SST higher than 2 °C in June are fairly close to those for July, we included those data to derive the $pCO_{2,95}^{sea}$-SST relationship for July. We also assumed that the negative relationship found in May is valid at SST lower than 0.55 °C in June, and the positive relationship at SST higher than 0.55 °C in June/July is applicable to the same SST range in May. The temperature of 0.55 °C is the intersecting point of the two $pCO_{2,95}^{sea}$-SST regression lines shown in Fig. 3-2(B). For January and February, the same positive $pCO_{2,95}^{sea}$-SST relationship was used, considering active deep convection and low marine biological activities in this period of the year. Furthermore, under the assumption that the $pCO_{2,95}^{sea}$-SST relationship varies smoothly with time, the slope and the intercept for March, September, and December with no observational data were deduced by interpolating linearly the results of contiguous months. The respective parameters obtained by fitting to Eq. 3-1 are summarized in Table 3-1. As shown in Fig. 3-3, the values of $pCO_{2,95}^{sea}$ calculated using Eq. 3-1 with the best-fit parameters agreed well with the observed $pCO_{2,95}^{sea}$ values with a standard deviation of ± 14 μatm for the differences between the observed and calculated values.

To see the seasonal cycles of $pCO_{2,95}^{sea}$ calculated by Eq. 3-1 and to examine whether they could reconstruct the actual features throughout the year, we compared the $pCO_{2,95}^{sea}$ values by Eq. 3-1 and observational data taken in the present with those of earlier studies (Anderson et al., 2000; Hood et al., 1999; Olsen et al., 2003; Omar et al., 2003; Takahashi et al., 2002; Weiss et al., 1992) for two sites at 75°N, 0° in the central Greenland Sea and at 74°N, 17.5°E in the western Barents Sea (Fig. 3-4). The $pCO_{2,95}^{sea}$

values calculated in this study are 15-30 μatm higher than those observed by Weiss et al. (1992) in the Greenland Sea in July 1981 and in March 1982. However, if the pCO_2^{sea} increased at the same rate as pCO_2^{air} from 1981 to 1995, the calculated pCO_2^{sea} values agree well with the observed values within a range of –9 to 6 μatm. This means that our assumption about the annual increase of pCO_2^{sea} is generally reasonable.

The calculated $pCO_{2,95}^{sea}$ in the central Greenland Sea (Fig. 3-4 (A)) shows a seasonal variation of about 95 μatm, with two maxima, one in April and another in November, and a minimum in June. Anderson et al. (2000) reported a seasonal variation of fCO_2^{sea} with a maximum in November and a minimum in August. Furthermore, we compared our $pCO_{2,95}^{sea}$ values with those of Olsen et al. (2003). Their equation gives the pCO_2^{sea} values in the year 1995 and is applicable to the period from October to March. The values of pCO_2^{sea} calculated by Olsen et al. (2003) for the October-March period agree well with our results within a range of 3 to 14 μatm, except for October. In October, a large difference of 32 μatm was found between the pCO_2^{sea} values of this study and those observed by Olsen et al.(2003). The fCO_2^{sea} values given by Hood et al. (1999) and Anderson et al. (2000) are generally higher than our calculated values. On the other hand, the average values of pCO_2^{sea} obtained by Takahashi et al. (2002) for two sites (76°N, 2.5°W and 76°N, 2.5°E) are 15-25 μatm lower than those of our results, showing a seasonal variation with high values in February/March and low values in July.

As seen in Fig. 3-4(B), $pCO_{2,95}^{sea}$ varied largely on a time scale of a few months in the western edge of the Barents Sea. The $pCO_{2,95}^{sea}$ showed a hump in July, which is caused by the large temperature dependence of $pCO_{2,95}^{sea}$ in June and July (Table 3-1). The $pCO_{2,95}^{sea}$ values calculated for March also agreed well with those obtained by Weiss et al. (1992), if their pCO_2^{sea} values are shifted up by an amount equivalent to the rise in pCO_2^{air} over the period in question. Omar et al. (2003) obtained a pCO_2^{sea} value

for October that was slightly lower than our values, and the results by Olsen et al. (2003) for the October-March period agree well with ours, except for October. In October, a large difference of 32 μatm was also found between the $pCO_{2,95}^{sea}$ values and those observed by Olsen et al. (2003). The pCO_2^{sea} values by Olsen et al. (2003) deviate largely from ours in the Greenland Sea and the Barents Sea in October, due to the difference in temperature dependence of pCO_2^{sea} between both studies.

The average values of pCO_2^{sea} given by Takahashi et al. (2002) for two sites (76°N, 17.5°E and 72°N, 17.5°E) show a rapid increase from February to April, with a gradual monotonic decrease thereafter towards the minimum in autumn and winter; the seasonal evolution identified by Takahashi et al. (2002) has a noticeably different temporal behavior than that in our results.

The $pCO_{2,95}^{sea}$ of the western Barents Sea is higher than that of the central Greenland Sea. However, the seasonal variation in the $pCO_{2,95}^{sea}$ of the western Barents Sea showed a different pattern from that of the central Greenland Sea (Figs. 3-4(A) and 3-4(B)). These variations were caused by the monthly varying temperature dependence of the $pCO_{2,95}^{sea}$ and SST distribution. In the western Barents Sea, SST is about 2-3 °C higher than the SST in the central Greenland Sea throughout the year.

The monthly distributions of $pCO_{2,95}^{sea}$ for the Greenland Sea and the Barents Sea are presented in Fig. 3-5. The area of sea ice was at its minimum in August and at its maximum in January (Fig. 3-2). The warm West Spitsbergen Current and the cold Eastern Greenland Current produce the longitudinal characteristics of a $pCO_{2,95}^{sea}$ distribution that is high on the east side and low on the west side, reflecting mainly the temperature dependence of $pCO_{2,95}^{sea}$. The current flowing northeastward in the Barents Sea originated from the Norwegian Atlantic Current (Fig. 3-2) shows relatively high $pCO_{2,95}^{sea}$ in comparison with the surrounding areas.

In May and June, $pCO_{2,95}^{sea}$ in the western Greenland Sea decreases to levels

lower than 250 μatm, depending on SST. In the spring of 1995, Skjelvan et al. (1999) found that the values of fCO_2^{sea} measured along 75°N were similar to the winter values in the eastern area of the Greenland Sea and that fCO_2^{sea} decreased rapidly from about 320 to 240 μatm at 3°W due to the CO_2 drawdown by biological activities in the western area. However, in the spring of 1997, they also found that the fCO_2^{sea} values in the western area were relatively constant (270-300 μatm), probably due to unusually cold temperatures at that time (Chierici, personal communication).

3.4 Seasonal variation of the air-sea CO_2 flux

Based on the monthly distributions of $pCO_{2,95}^{sea}$ given in Fig. 3-5 and pCO_2^{air} at Ny-Ålesund, the air-sea CO_2 fluxes in the Greenland Sea and the Barents Sea were calculated for the respective months. To calculate the monthly averaged CO_2 fluxes for the 1992-2001 period, we used the NCEP/NCAR reanalysis data (Kalnay et al., 1996) for the SST, wind speed, atmospheric pressure, and sea ice distribution. Since the NCEP/NCAR reanalysis data are prepared for each grid of 1.875° by 1.904°, the air-sea CO_2 fluxes were also obtained on the same spatial resolution. Therefore, the total CO_2 flux in the whole area is presented by the equation,

$$F = \sum_{i=0}^{n} (E_i \cdot \Delta pCO_{2,i} \cdot S_i). \qquad (3\text{-}2)$$

Here, i represents the grid number, and S shows the sea area. In this calculation, we assumed that the CO_2 exchange across the air-sea interface is thoroughly prevented by the sea ice.

The results are shown in Fig. 3-6. In general, the Greenland Sea and the Barents Sea are sinks for the atmospheric CO_2. The flux is small (< 2 mol $m^{-2} yr^{-1}$) in the eastern

Greenland Sea because warm currents with small ΔpCO_2 are flowing in this region (Skjelvan et al., 1999; Olsen et al., 2003). By contrast, larger CO_2 fluxes (> 6 mol m^{-2} yr^{-1}) are found in the northwestern area for the period of December to March, which is ascribed to strong winds (7-9 m s^{-1}) as well as to low $pCO_{2,95}^{sea}$. In May and June, larger air-to-sea CO_2 fluxes are inferred in the areas where the negative $pCO_{2,95}^{sea}$-SST relationship was applied to derive $pCO_{2,95}^{sea}$. During the period from July to September, when the wind speed ranges between 3 and 6 m s^{-1}, the CO_2 flux is reduced by 70 % compared with the wintertime value, even for the same ΔpCO_2.

The air-sea CO_2 fluxes estimated for the Greenland Sea and the Barents Sea are summarized in Tables 3-2 and 3-3, respectively, along with those reported in earlier studies. Our result for the Greenland Sea (52 ± 20 gC m^{-2} yr^{-1}) agrees well with those of earlier studies. From the calculation of fCO_2^{sea} based on measurements of the total dissolved inorganic carbon, total alkalinity, temperature, salinity, and phosphorous concentrations in the central Greenland Sea (75°N, 0°) for the 1993-1997 period, Anderson et al. (2000) estimated the average annual CO_2 flux to be 53 ± 4 gC m^{-2} yr^{-1}. Hood et al. (1999) also reported a CO_2 flux of 55 gC m^{-2} yr^{-1} for the last two years of the period, 1996 and 1997. On the other hand, Skjelvan et al. (1999) gave a somewhat larger CO_2 flux of 71 gC m^{-2} yr^{-1} for the 1993-1995 period. For the Barents Sea, we estimated the annual CO_2 flux to be 46 ± 27 gC m^{-2} yr^{-1}. This value also agrees well with that of 44 ± 10 gC m^{-2} yr^{-1} derived by Fransson et al. (2001).

However, a more detailed inspection of Tables 3-2 and 3-3 indicates noticeable differences in the seasonal behavior of the CO_2 flux observed in the present and earlier studies. The CO_2 uptake estimated by Skjelvan et al. (1999) for the Greenland Sea in summer and autumn is larger than ours. This difference can be attributed to the wind speed used to calculate the air-sea CO_2 flux. Compared with our values, the ΔpCO_2 values given by Skjelvan et al. (1999) are about 13 μatm higher in summer and 11 μatm

lower in autumn. These differences would yield only a 10 % difference in the air-sea CO_2 flux under the same wind conditions. On the other hand, the NCEP/NCAR data used in this study give average wind speeds of 5.4 and 8.5 m s^{-1} for summer and autumn, respectively, and Skjelvan et al. (1999) used wind speeds of 7.2 and 11.2 m s^{-1} for the respective seasons in their analysis. By changing the wind speed in the range covered by both studies, the air-sea CO_2 flux can be altered by a factor of 2. For winter and spring, Skjelvan et al. (1999) used almost the same wind and ΔpCO_2 fields as ours. Therefore, there is better agreement between the results of both studies for these seasons than for summer and autumn.

The CO_2 fluxes derived by Hood et al. (1999) using the ECMWF wind data agree well with our results within our estimated uncertainties. The oceanic CO_2 uptake estimated by Kaltin et al. (2002) for the Barents Sea depends largely on the C/N ratio of new production. Their estimate of the CO_2 flux, 44 ± 40 gC m^{-2} yr^{-1}, agrees fairly well with the estimate in this study when the C/N ratio is assumed to be 6.6.

It is important to clarify how the seasonal evolution of the CO_2 uptake in the Greenland Sea and the Barents Sea is controlled by various oceanic and atmospheric phenomena. Figure 3-7 shows the monthly averages of the ΔpCO_2, relative ice cover, wind speed, and the CO_2 uptake for the region (70°-80°N, 20°W-40°E) covered by the Greenland Sea and the Barents Sea. In general, the seasonal variation of ΔpCO_2 is negatively correlated with the wind speed, and, to a lesser extent, with the ice cover. The monthly CO_2 uptake reaches low values (0.034 GtC yr^{-1}) in April and November and high values (0.062 GtC yr^{-1}) in May and September, reflecting different seasonal variations of the variables used in its calculation. In order to quantify how ΔpCO_2, the gas transfer velocity, and the relative ice cover affect the CO_2 uptake, we used the equation,

$$F_{a.f.}(t) = \overline{E}(t) \cdot \Delta\overline{pCO_2}(t) \cdot S(t), \qquad (3\text{-}3)$$

where $F_{a.f.}(t)$ is the total CO_2 uptake in the Greenland Sea and the Barents Sea, $S(t)$ is the ice-free sea area, $\Delta\overline{pCO_2}(t)$ is the spatially averaged value of ΔpCO_2 at month t, and $\overline{E}(t)$ is the spatially averaged value of the gas transfer velocity $E(t)$. This equation disregards the covariance term between the transfer velocity and the ΔpCO_2. The differential of $F_{a.f.}(t)$ with respect to time can be written as,

$$\frac{\delta F_{a.f.}}{\delta t} = \frac{\delta\overline{E(t)}}{\delta t} \cdot \Delta\overline{pCO_2(t)} \cdot S(t) + \overline{E(t)} \cdot \frac{\delta\Delta\overline{pCO_2(t)}}{\delta t} \cdot S(t) + \overline{E(t)} \cdot \Delta\overline{pCO_2(t)} \cdot \frac{\delta S(t)}{\delta t}, \qquad (3\text{-}4)$$

where the first, second, and third terms on the right-hand side of Eq. 3-4 represent changes in the CO_2 uptake caused by temporal variations in the gas transfer coefficient, ΔpCO_2, and the sea area, respectively. The calculated values of the respective terms and their sum are given in Fig. 3-8. The decrease in the CO_2 uptake seen from March to April is caused by the reduction in both ΔpCO_2 and the wind speed. From April to May, these contributions tend to counteract each other, but the contribution from the pCO_2^{sea} decrease becomes so large that the CO_2 uptake increases. For the period of August to October, the wind speed is a major factor for controlling the air-sea CO_2 flux. In November and December, the air-sea CO_2 flux increases, mainly due to rapid changes in ΔpCO_2. The seasonally varying sea ice area contributes to the decrease in the CO_2 uptake from September to November to a certain extent, but, compared with the wind speed and ΔpCO_2, it has a minor effect on the variations in the CO_2 uptake.

3.5 Interannual variability of the CO_2 flux

We examined the interannual variability of the air-sea CO_2 flux in the same way

as Olsen et al. (2003) did. We assumed that the only intercept values given in Table 3-1 for the empirical pCO_2^{sea}-SST relationships varied with the atmospheric CO_2 increase rate (1.5 μatm yr^{-1}) over the period from 1992 to 2001. This assumption means that the ΔpCO_2 was not affected by the uptake of anthropogenic CO_2. Figure 3-9 shows the monthly and 1-year running mean anomalies of the ΔpCO_2, sea ice area, wind speed, CO_2 uptake, and the monthly and 1-year running means of the North Atlantic Oscillation Index (NAOI) during the same period. By comparing these anomalies with the average values of the CO_2 uptake and its relevant factors, i.e., the wind speed, ΔpCO_2, and sea ice area, we estimated the contributions of the anomalies of the respective factors to the CO_2 uptake to be 13, 4, and 15 %, respectively. Considering the anomalies of the wind speed, SST, and sea ice area, the interannual variability of the CO_2 uptake amounts was found to be 18 % of its average value. Contrary to the equatorial Pacific, where large interannual variations in the air-sea CO_2 flux occur due to changes in the ΔpCO_2 distribution (Feely et al., 2002), the Greenland Sea and the Barents Seas are the oceans in which ΔpCO_2 is a minor factor in determining the interannual variability. Olsen et al. (2003) reported that the interannual variability of the CO_2 uptake for the entire north Atlantic Ocean in the winter season between 1981 and 2001 was about 7 %. They also reported that changes in the wind speed and fCO_2^{air} accounted for most of its interannual variations. Their finding that the wind speed is crucial for the interannual variations of the air-sea CO_2 flux is in agreement with our results. The NAOI is an index derived from the north-south distribution of the sea level pressure over the North Atlantic Ocean. Therefore, the NAOI is closely related to the wind speed over the northern North Atlantic. The anomaly of the CO_2 uptake varies similarly with those of the wind speed and the NAOI. The anomalies of ΔpCO_2 and the sea ice area are negatively correlated with the NAOI. In the North Atlantic sector, the climate variability on a time scale of months to decades is dominated by the North

Atlantic Oscillation (Wallace and Gutzler, 1981). Therefore, both the decadal change in CO_2 uptake and the interanuual variation could occur in the Greenland Sea and the Barents Sea.

Overland and Wang (2005) reported that the ice area has decreased by about 20% over the past two and a half decades, primarily in the western Arctic ocean, and a decrease in sea ice has occurred in the last decade, as shown in Fig.3-9 in their paper. Jones et al. (2001) reported an SST increase of 0.18 °C per decade in the Northern Hemisphere over the same period. The wind speed also seemed to decrease slightly, but not significantly, when an rms deviation of ± 3.0 m s^{-1} is taken into account (Smith et al., 2001). If these long-term trends are added to Eq. 3-1, the CO_2 uptake is consequently expected to increase at a rate of 8 x 10^{-4} GtC yr^{-2}, which is mostly caused by the decrease in the sea ice area. Skjelvan et al. (1999) also suggested an increasing trend in the CO_2 uptake of about 9 x 10^{-4} GtC yr^{-2} in the Greenland Sea. These results indicate that more anthropogenic CO_2 will possibly be stored in the Greenland Sea and the Barents Sea due to a decrease in sea ice area in the near future. However, the oceanic dynamics and biological activities in the near future may be different from the present conditions. Therefore, extended observations and analyses are needed to forecast the variation of air-sea CO_2 flux in the Greenland Sea and the Barents Sea.

Table 3-1. Coefficients of the linear function (Eq. 3-1 in the text) expressing the pCO_2^{sea}-SST relationships for the respective months derived on the basis of the pCO_2^{sea} data taken in the Greenland Sea and the Barents Sea for the 1992-2001 period. a, b, N, σ, r, and ci represent the slope (μatm $^{\circ}C^{-1}$) and intercept (μatm) of the linear function determined by a least-squares fit, the volume of data used, the standard deviation (μatm), the correlation coefficient of the fit, and the 95 % confidence interval, respectively.

Month	a	b	N	σ	r	ci
1	7.10	294.02	22	10	0.88	0.73 - 0.95
2	7.10	294.02	18	10	0.88	0.70 - 0.95
3	5.90	305.37	-		-	-
4	4.35	320.05	40	14	0.60	0.35 - 0.77
5-6 (SST<0.55°C)	-33.99	235.85	20	11	-0.59	-0.82 - -0.20
5-6 (SST>0.55°C)	16.37	208.08	7	28	0.82	0.18 - 0.97
7	16.37	208.08	14	17	0.94	0.82 - 0.98
8	8.11	222.09	27	15	0.64	0.34 - 0.82
9	4.77	250.55	-		-	-
10	5.23	279.45	21	5	0.92	0.81 - 0.97
11	4.67	310.10	48	13	0.63	0.42 - 0.78
12	5.99	301.39	-		-	-

Table 3-2. Air-sea CO_2 fluxes (gC m^{-2} yr^{-1}) in winter (January to March), spring (April to June), summer (July to September), and autumn (October to December), and annual CO_2 fluxes in the open water areas of the central Greenland Sea.

	Winter	Spring	Summer	Autumn	Annual
Hood et al. (1999)	58	64	52	43	55
Skjelvan et al. (1999)	$58 \pm 14_{(1995)}$	$52 \pm 21_{(1995)}$	$77 \pm 26_{(1993)}$	$85 \pm 16_{(1995)}$	71
Anderson et al. (2000)	-	-	-	-	53 ± 4
Olsen et al. (2003)	$44 \sim 61_{(Feb.)}$	-	-	$35 \sim 53_{(Nov.)}$	-
This work	72 ± 25	45 ± 21	37 ± 14	54 ± 21	52 ± 20

The uncertainties of Skjelvan et al. (1999) are estimated based on the standard deviations in wind speed and natural variability observed in the fCO_2^{sea} measurements. The uncertainty of Anderson et al. (2000) is due to the variability in the wind field and extent of sea ice from 1993 to 1997.

Table 3-3. Air-sea CO_2 fluxes (gC m^{-2} yr^{-1}) in winter (January to March), spring (April to June), summer (July to September), and autumn (October to December), and annual CO_2 fluxes in the open water areas of the Barents Sea.

	Winter	Spring	Summer	Autumn	Annual
Fransson et al. (2001)	-	-	-	-	44 ± 10
Kaltin et al. (2002)	-	116 ± 44 (C/N = 8.75) 44 ± 40 (C/N = 6.6)	-	-	-
This work	63 ± 22	28 ± 13	43 ± 17	49 ± 18	46 ± 18

The uncertainties of Kaltin et al. (2002) include the analytical error, the variability in the source water concentration, and the uncertainty in the fresh water estimates. The oceanic uptake of atmospheric CO_2 by Fransson et al. (2001) was determined by the difference in the export production computed from the nutrient deficit and the observed deficit of dissolved inorganic carbon. The uncertainty for this calculation procedure was estimated.

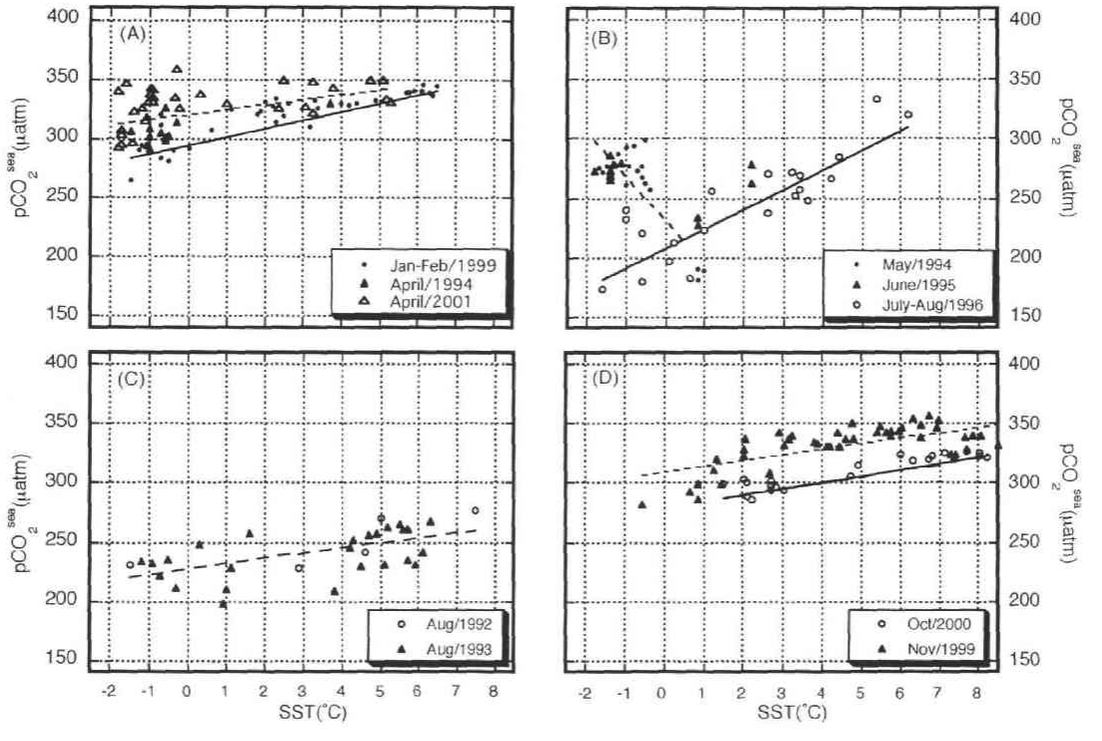

Fig. 3-1. Relationships between pCO_2^{sea} and SST for the Greenland Sea and the Barents Sea for the periods of January to April (A), May to early August (B), late August (C), and October to November (D). All the pCO_2^{sea} values plotted were normalized to the year 1995, assuming that they have increased secularly at the same rate as pCO_2^{air} (1.5 μatm yr^{-1}). The solid and dashed lines show the values obtained by applying a least-squares fit to the data.

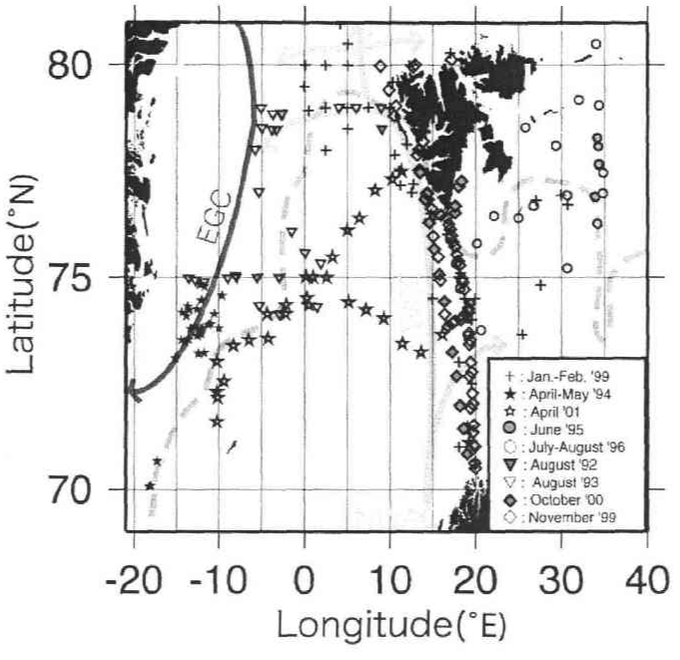

Fig. 3-2. The same as in Fig.2-1. Geographical locations where pCO_2^{sea} measurements were made from 1992 through 2001. The atmospheric CO_2 data used to calculate pCO_2^{air} in this study were taken at Ny-Ålesund in the Svarbard Islands (79°N, 12°E). The dashed gray line shows the boundary of the climatological sea ice area in August, and the dashed black line shows the climatological sea ice area in January. The arrows represent the major currents in the Greenland Sea and the Barents Sea (Furevik et al., 2001), including the Norwegian Atlantic Current (NWAC), West Spitsbergen Current (WSC), and East Greenland Current (EGC).

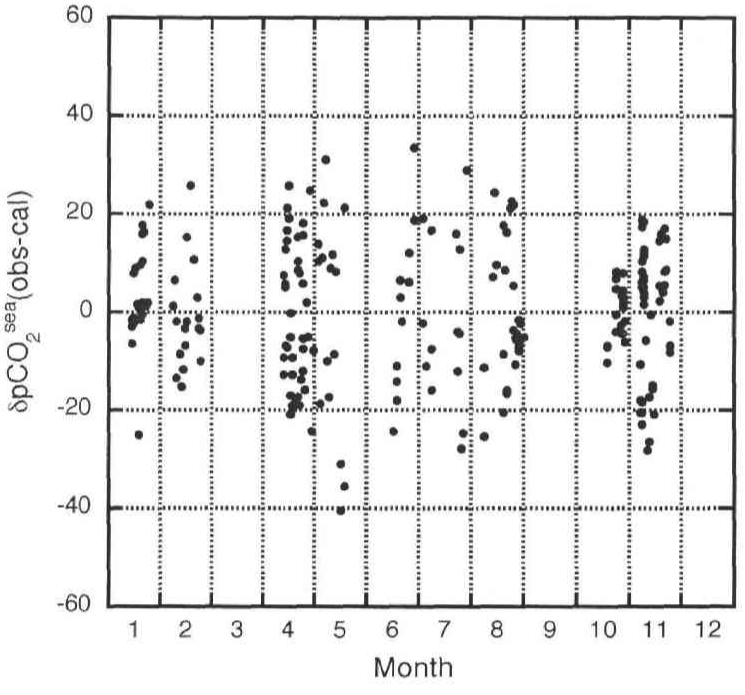

Fig. 3-3. Differences between the observed and calculated pCO_2^{sea} values for the Greenland Sea and the Barents Sea. The calculated values were obtained from the empirically derived pCO_2^{sea}-SST relationships and the SST data (cf. text).

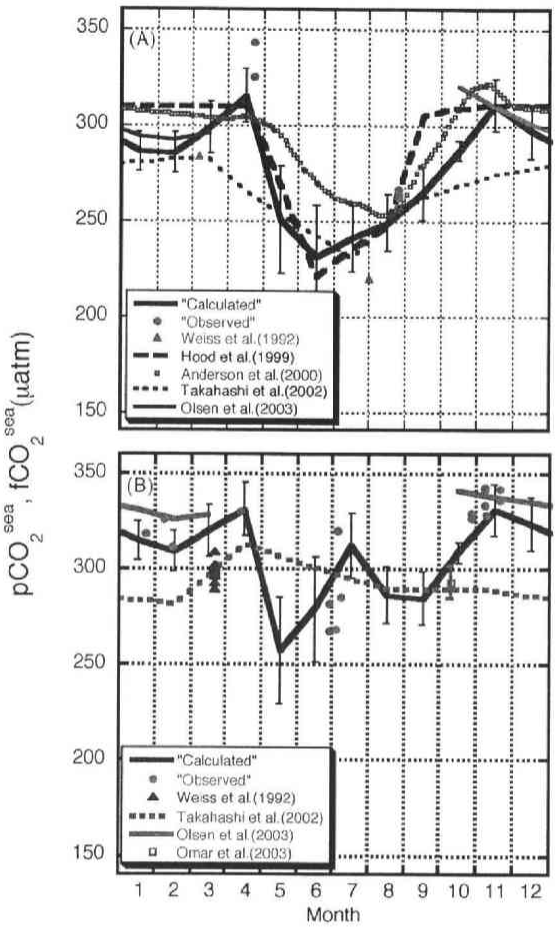

Fig. 3-4. Seasonal variations of pCO_2^{sea} in the central Greenland Sea (panel A) and the western Barents Sea (panel B). The blue thick solid lines in the upper and lower panels show the pCO_2^{sea} values calculated for the respective locations at 75°N and 0° and 74°N and 17.5°E using the empirical pCO_2^{sea}-SST relationships with coefficients given in Table 3-1. The red circles represent our observed pCO_2^{sea} values normalized to the year 1995. In panel A, the purple triangles denote the pCO_2^{sea} observed by Weiss et al. (1992) for 1981 and 1982, the green dotted line, the fCO_2^{sea} by Hood et al. (1999), the aqua rectangle, the fCO_2^{sea} by Anderson et al. (2000), the gray dashed line, the pCO_2^{sea} by Takahashi et al. (2002), and the solid purple line, the fCO_2^{sea} calculated using the fCO_2^{sea}-SST relationships given empirically by Olsen et al. (2003). In panel B, the purple triangles show the pCO_2^{sea} values observed by Weiss et al. (1992) for 1981 and 1982, the gray dashed line, the pCO_2^{sea} by Takahashi et al. (2002), and the gray rectangle, the pCO_2^{sea} derived for an SST of 5.7°C from the results obtained by Omar et al. (2003) for October.

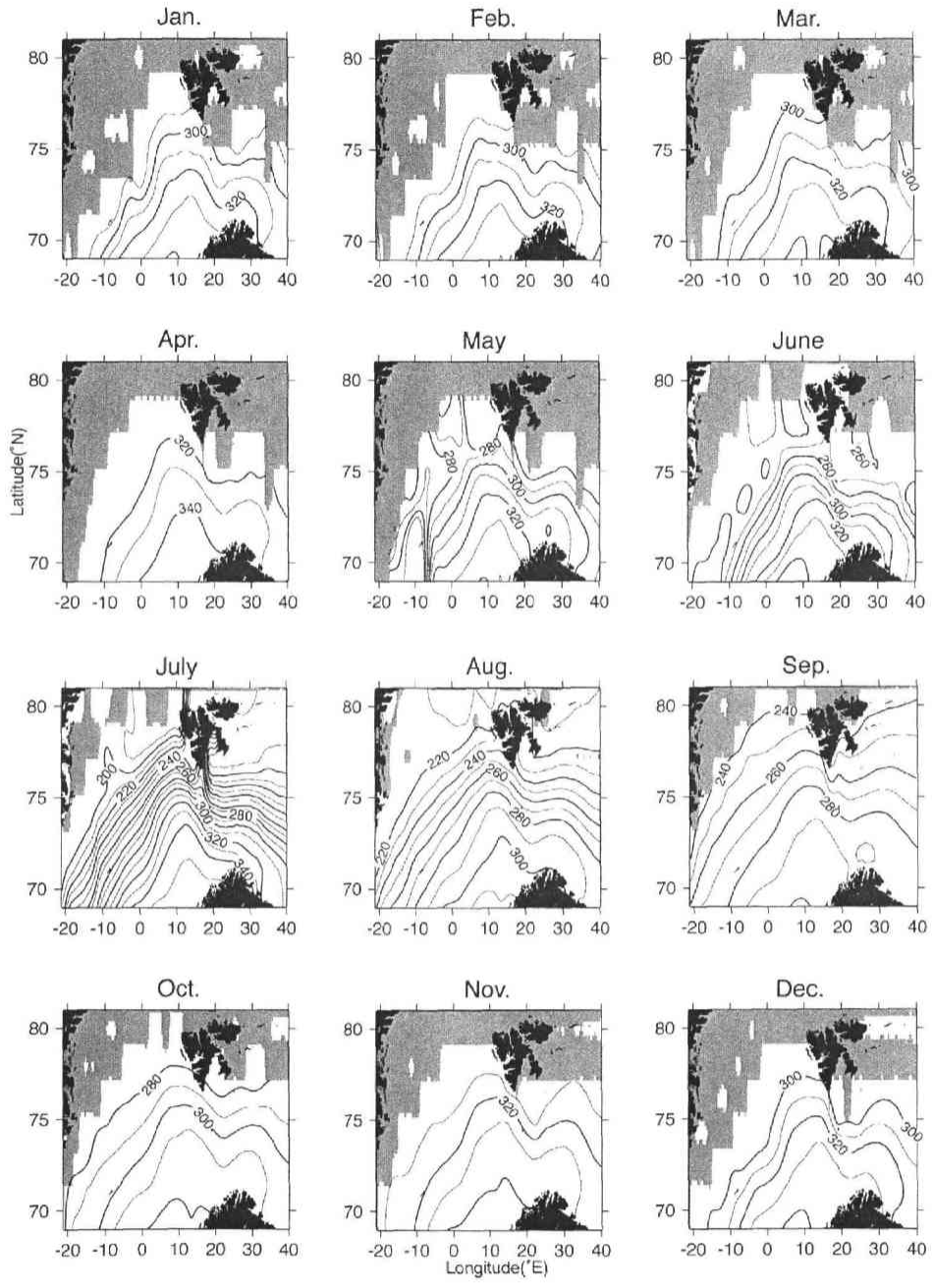

Fig. 3-5. Distributions of the monthly pCO_2^{sea} values (μatm) calculated for 1995 using the empirical pCO_2^{sea}-SST relationships and the NCEP/NCAR reanalysis SST data. The shaded areas show the sea ice estimated based on the NCEP/NCAR reanalysis data.

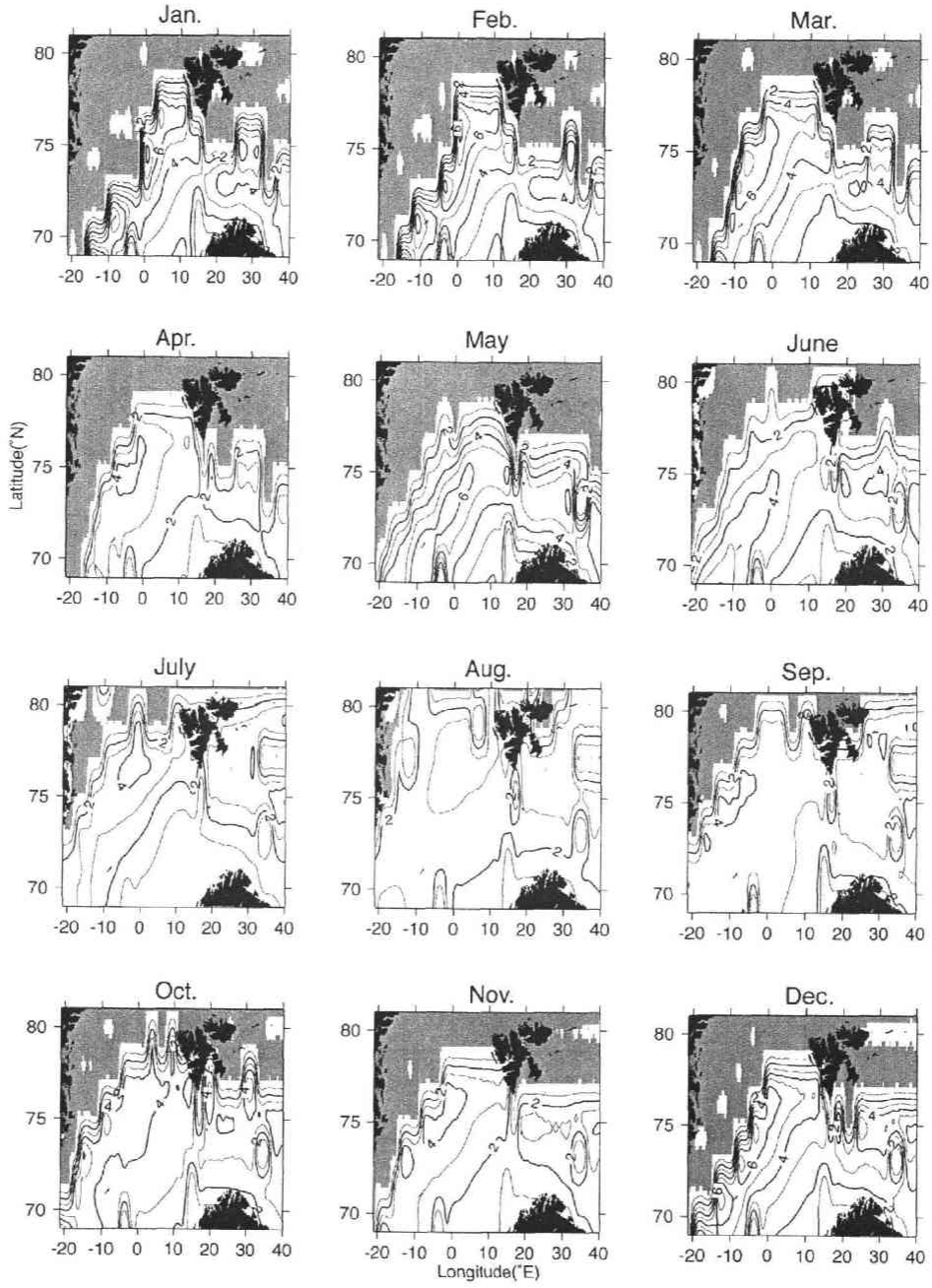

Fig. 3-6. Distributions of the monthly air-sea CO_2 fluxes (mol m^{-2} yr^{-1}) calculated for 1995 using the gas transfer velocity given by Wanninkhof (1992) and the monthly average wind fields derived from the NCEP/NCAR reanalysis data for the 1992-2001 period. The positive flux values indicate the uptake of atmospheric CO_2 by the ocean, and the shaded areas show sea ice.

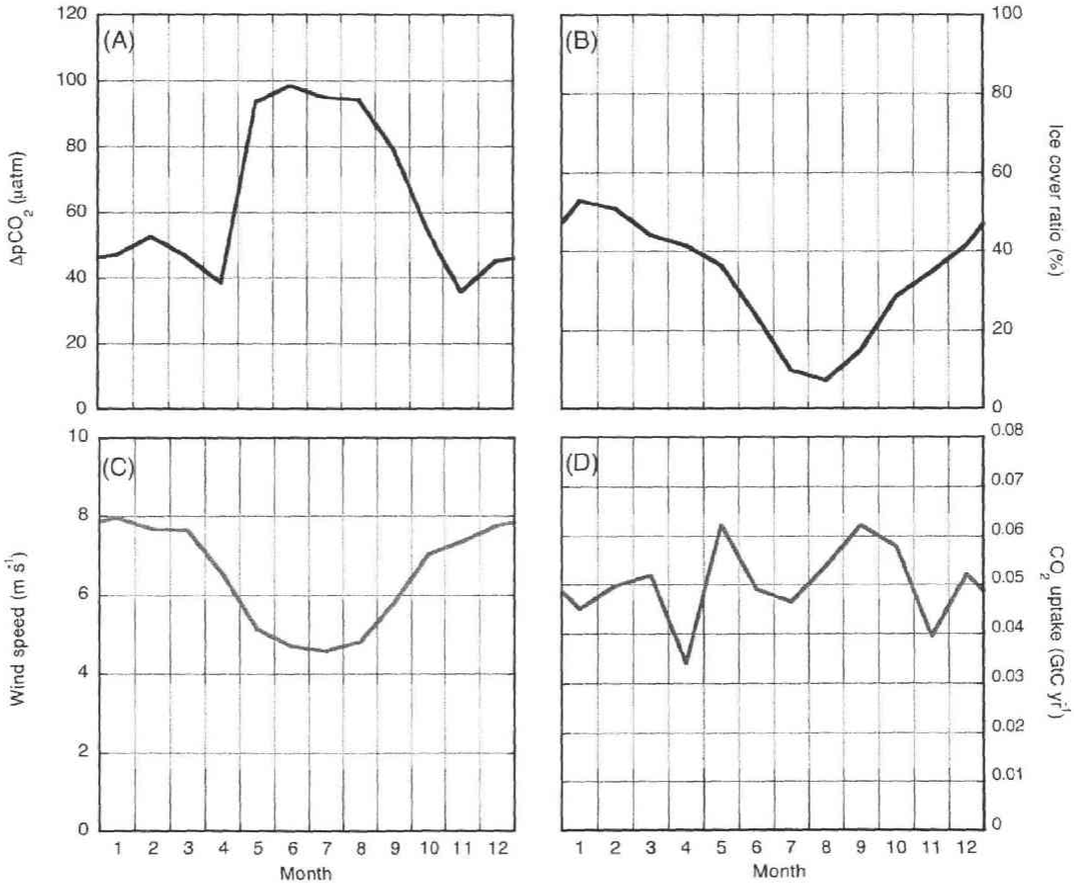

Fig. 3-7. Seasonal variations of ΔpCO_2 (A), the sea ice cover (B), the wind speed (C), and the CO_2 uptake (D) in the Greenland Sea and the Barents Sea (70°-80°N, 20°W-40°E).

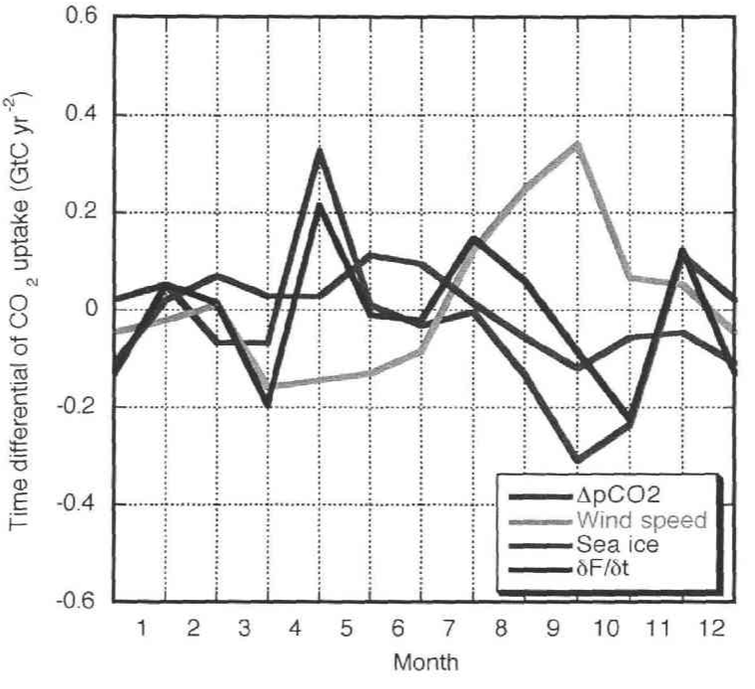

Fig. 3-8. Respective contributions of ΔpCO_2, the wind speed, and the sea ice area to the seasonal variation of the oceanic CO_2 uptake in the Greenland Sea and the Barents Sea (cf. text). The positive and negative values mean the acceleration and suppression of the CO_2 uptake, respectively.

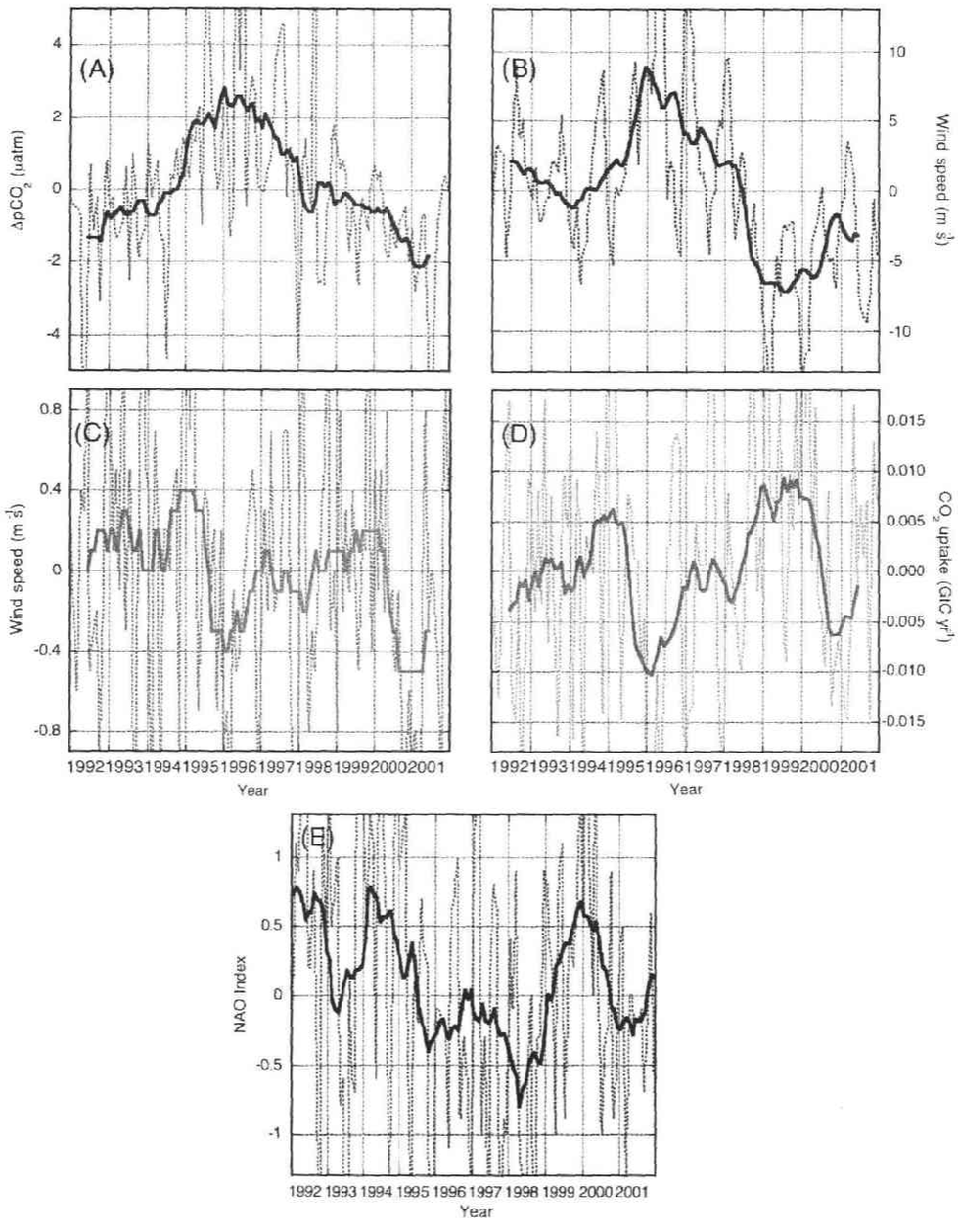

Fig. 3-9. Anomalies of ΔpCO_2 (A), the ice cover (B), the wind speed (C), and the CO_2 uptake (D) in the Greenland Sea and the Barents Sea, and those of the NAOI (E). The dashed lines represent the anomalies of the monthly means, and the solid lines show their 1 year-running means.

Chapter 4

Temporal and Spatial Variations of Carbon System in the Southern Ocean

In order to understand spatial and seasonal variations of carbon system in the Southern Ocean, measurements of pCO_2^{sea}, DIC and its $\delta^{13}C$ were made in the Indian sector (110°-140°E) and the western Pacific sector (140°-150°E) of the ocean during the period 2001-2003. In this chapter, the results obtained from these measurements will be reported and discussed.

4.1 Variation of pCO_2^{sea} measured on Umitaka-Maru cruise in 2003

In this section, we discuss spatial distributions of pCO_2^{sea} measured using R/V Umitaka-Maru in the Indian and western Pacific sectors, as well as those of air-sea CO_2 flux derived on the basis of the measurement results of pCO_2^{sea}.

4.1.1 Fronts and zones in the Southern Ocean

Significant characteristic of the Southern Ocean is that there are several circumpolar fronts, by which vertical structures of water temperature, salinity and chemical components such as nutrients are changed greatly. Their locations are defined based on vertical structures of water temperature and salinity (Nagata et al., 1988; Orsi et al., 1995) or variations of the two factors in the surface ocean (Chaigneau and Morrow, 2002). The fronts are labeled Sub Tropical Front (STF), Sub Antarctic Front (SAF) and Polar Front (PF) in order from north to south. Furthermore, ocean zones being separated by the fronts are also important to characterize the Southern Ocean. These zones are named Sub Antarctic Zone (SAZ), Polar Frontal Zone (PFZ), Polar Zone (Polar Zone) and Seasonal Sea Ice Zone (SSIZ). The locations of these fronts and zones are shown in Fig. 4-1 for the Umitaka-Maru cruise. We determined the locations of STF, SAF and PF in accordance with their definitions by Chaigneau and Morrow

(2002). The northern boundary of SSIZ was assumed to be 62°S on the basis of the distributions of surface salinity and ice concentration from NCEP/NCAR reanalysis data (Enomoto and Ohmura, 1990). The locations of the respective fronts and SSIZ determined for the Umitaka-Maru cruise are summarized in Table 4-1. This table shows that the respective fronts on the 110°E line are located about 2.5 degrees north of those on the 140°E line, while the locations of SSIZ on 110° and 140°E lines existed at the same latitude.

4.1.2 Latitudinal and longitudinal distributions of pCO_2^{sea}, SST and SSS

The measurements on board Umitaka-Maru were made for the period of 24 January to 12 February, 2003, along the tack shown in Fig. 4-1. Measured values of SST, Sea Surface Salinity (SSS) and pCO_2^{sea} are plotted in Fig. 4-2 against latitude. It can be seen from this figure that the pCO_2^{sea} values are generally lower than pCO_2^{air}, but the differences between both values are not so large.

In the north side of PF (50°S) along 110°E, SST and SSS decreased and pCO_2^{sea} increased with increasing latitude. In PZ (50°-62°S), SST decreased with increasing latitude, and SSS and pCO_2^{sea} showed relatively constant values of 33.5 and 355 μatm, respectively. In SSIZ (south of 62°S), SST and SSS decreased with increasing latitude, and pCO_2^{sea} showed a fairly constant value of 350 μatm.

The latitudinal distributions of SST, SSS and pCO_2^{sea} along 140°E are similar to those along 110°E, but there are some differences between the results from the two journeys. For example, the SST values on the 110°E line were generally higher by about 2°-3°C than the values on the 140°E line, reflecting the fact that the fronts on the 110°E line were located north of those on the 140°E line. The values of SSS along 110°E were higher by about 0.3 than the values along 140°E, except for SSIZ. In SSIZ,

SSS on the 110°E line decreased with increasing latitude, while SSS on the 140°E line showed a fairly constant value of 33.2 and increased rapidly from 33.0 to 33.6 south of 65°S. The pCO_2^{sea} values obtained from the two journeys were fairly close to each other, but slight differences of about 5 μatm were seen in the south side of 60°S. The variability of pCO_2^{sea} on the 140°E line in SSIZ was relatively larger than that on the 110°E line.

Figure 4-3 shows the longitudinal distributions of SST, SSS and pCO_2^{sea} along the Antarctic continental coastline. It can be seen from this figure that the values of these parameters distributed evenly against longitude and their variability was fairly small. The values of SST, SSS and pCO_2^{sea} ranged between -0.5°C and 3.5°C, between 33.0 and 33.5, and between 350 and 365 μatm, respectively.

4.1.3 pCO_2^{sea} -SST relationship

As described in Chapter 3, it is very useful for estimating pCO_2^{sea} in areas without measurement to investigate the relationship between pCO_2^{sea} and SST using their existing data. Therefore, we examined the temperature dependence of pCO_2^{sea} measured on the Umitaka-Maru cruise, to make a distribution map of pCO_2^{sea} for the Indian and western Pacific sectors with a longitudinal interval of 110°-150°E. The results are shown in Fig. 4-4. The pCO_2^{sea}-SST relationships derived for the 110°E line, Antarctic continental coastline and 140°E line are similar to each other. The pCO_2^{sea} values showed a general trend of decreasing with increasing SST, but such a relationship was not clearly seen when SST was lower than 5°C. Previous measurements in the Southern Ocean (Hashida, 1993; Metzl et al., 1999; Inoue and Ishii. 2005) also reported the negative relationship between pCO_2^{sea} and SST, but more detailed inspection of the results indicated that there are noticeable differences between

the pCO_2^{sea}-SST relationships obtained by the present and other studies. Hashida (1993) obtained the negative and positive relationships between pCO_2^{sea} and SST in March when SST was lower and higher than 15°C, respectively. Metzl et al. (1999) also showed the negative relationship between pCO_2^{sea} and SST, which is similar to that by Hashida (1993), but they observed the strong positive relationship in January 1995 when SST was lower than 0°C. Inoue and Ishii (2005) reported that the weak positive relationship was found when SST was lower than 10°C, the relationship was negative when SST was in a range between 10° and 15°C and the positive relationship was observed when SST was higher than 15°C. The differences among these results are caused mainly by seasonal/interannual variations of water transport or biological activities.

4.1.4 Spatial distributions of pCO_2^{sea} and air-sea CO_2 flux

In order to draw a pCO_2^{sea} distribution map in the Indian (110°-140°E) and western Pacific (140°-150°E) sectors, we used the pCO_2^{sea}-SST relationship,

$$pCO_2^{sea} = 358.7 - 0.75 \times SST\ , \qquad (4\text{-}1)$$

which was obtained by fitting to the data given in Fig. 4-4. As seen from Fig. 4-5, the values of pCO_2^{sea} calculated using Eq. 4-1 agree well with the observed values, and the standard deviation for differences between the observed and calculated values was estimated to be 4.1 μatm.

For the calculation of pCO_2^{sea} in the Indian and western Pacific sectors, we used the average SST data for January and February 2003, taken from the NCEP/NCAR Reanalysis data (Kalnay et al. 1996) as done in Chapter 3. The latitude-

longitude distribution of calculated pCO_2^{sea} value for the Indian and western Pacific sectors are presented in Fig. 4-6, together with that of SST. The results show a characteristic feature of low pCO_2^{sea} values of about 345 μatm on the Australian side and high values of 360 μatm on the Antarctic side, reflecting the north-south SST difference, as depicted in Fig. 4-6 (a), and the temperature dependence of pCO_2^{sea}, as given in Fig. 4-4.

Based on the distribution of pCO_2^{sea} given in Fig. 4-6 and pCO_2^{air} measured at Syowa Station (69°S, 39°E), the distribution of average air-sea CO_2 flux for the two months of January and February 2003 was calculated for the Indian and western Pacific sectors. The calculated results are shown in Figure 4-7, together with the wind speed data used. In general, the Indian and western Pacific sectors of the Southern Ocean act as sink for atmospheric CO_2, and the CO_2 flux ranges between 0 and 3 mol m^{-2} yr^{-1}. Small air-sea CO_2 fluxes (less than 1.5 mol m^{-2} yr^{-1}) are found south of PF, as well as south of Australia, due to relatively low wind speeds. On the other hand, large CO_2 fluxes (more than 2.5 mol m^{-2} yr^{-1}) are seen around SAZ, although strong winds (more than 16 m s^{-1}) are observed in PFZ. For the comparison with our results, the air-sea CO_2 fluxes calculated by Takahashi et al. (2002) for the same area are shown in Fig. 4-8. Our results for the Indian and western Pacific sectors are similar to those by Takahashi et al. (2002), except for PZ of the western Pacific sector where the Takahashi et al.'s distribution indicates CO_2 source area, while ours implies weak sink.

Based on the results of the above-mentioned calculation, we estimated the summertime oceanic CO_2 uptake in the Indian and western Pacific sectors to be 0.012 GtC $month^{-1}$. By assuming that this flux is applicable to the whole Southern Ocean, the CO_2 uptake of 0.14 GtC $month^{-1}$ is obtained. On the other hand, Takahashi et al. (2002) reported that the summertime oceanic CO_2 uptake for the same area was 0.009 GtC $month^{-1}$ for the Indian and western Pacific sectors, and 0.12 GtC $month^{-1}$ for the whole

Southern Ocean.

4.2 Variations of pCO_2^{sea} in the western Pacific sector in the summer of 2002

Our pCO_2^{sea} measurements in the western Pacific sector (140°-150°E) were made in March of the respective years from 2001 to 2003 using R/V Shirase. Since our measurements are temporally discrete, we describe our results briefly here.

As described above, it is important for discussing pCO_2^{sea} variations in the Southern Ocean to understand where oceanic fronts existed. We determined the locations of Sub Tropical Front, Sub Antarctic Front and Polar Front, in accordance with their definitions by Chaigneau and Morrow (2002). The northern boundary of Seasonal Sea Ice Zone (SSIZ) was assumed to be 62°S on the basis of surface salinity and ice concentration distributions from NCEP/NCAR Reanalysis data (Enomoto and Ohmura, 1990). The locations of the fronts and zone determined for four cruises are summarized in Table 4-2.

4.2.1 Aurora Australis cruise

The measurements on board Aurora Australis were made for the period of 31 October, 2001 to 12 December, 2001. Measured values of SST, SSS and pCO_2^{sea} are plotted in Fig. 4-9 against latitude. It can be seen from this figure that the results obtained during the southward (outward) and northward (homeward) journeys are similar to each other, but there are also some differences between the results from the two journeys. North of STF (47°S) and in SAZ (47°-49°S), SST and SSS decreased and

pCO_2^{sea} increased from 300 to 350 μatm with increasing latitude. In PFZ (49°-53°S), SST and SSS showed humps at 50.5° and 51°S for the southward and northward voyages, respectively, and pCO_2^{sea} decreased slightly from 360 to 347 μatm, going southward. In PZ (53°–62°S), SST decreased with increasing latitude, while SSS and pCO_2^{sea} showed almost constant values of about 33.8-33.9 and 350-360 μatm, respectively. In SSIZ (south of 62°S), SST showed a constant value of about -1.5 °C, and SSS increased with latitude after showing a minimum value of 33.5 at 63°S. The latitudinal distribution of pCO_2^{sea} is similar to that of SSS, with a minimum value of 310 μatm at 63°S and a maximum value of over 400 μatm around 67°S. The values of pCO_2^{sea} observed in this zone are higher than those of pCO_2^{air}.

4.2.2 Hakuho-maru (KH-01-3) cruise

The measurement by Hakuho-maru was made from 3 January, 2002 to 20 January, 2002. Figure 4-10 shows the latitudinal distributions of SST, SSS and pCO_2^{sea} measured on this cruise. North of STF (47°S) and in SAZ (47°-49°S), SST and SSS decreased and pCO_2^{sea} increased from 285 μatm to 310 μatm with increasing latitude. In the northern part of PFZ (49°-50°S), SST and SSS showed a rapid decrease around 49°S and pCO_2^{sea} increased rapidly from 310 to 350 μatm with increasing latitude. On the other hand, going southward in the southern part of PFZ (50°-53°S), SST and SSS decreased and pCO_2^{sea} also decreased slightly from 350 to 340 μatm. In PZ (53°-62°S), SST decreased with increasing latitude and pCO_2^{sea} varied from 333 to 350 μatm, but SSS showed a fairly constant value of about 33.8. In SSIZ (south of 62°S), SST was almost constant at around 1 °C, a slight southward decrease of SSS occurred, and pCO_2^{sea} decreased remarkably to lower than 200 μatm due to marine biological photosynthesis especially south of 65°S. Compared with the results from the Aurora

Australis cruise, a large difference can be seen in the pCO_2^{sea} distribution in SSIZ.

4.2.3 JARE43 Tangaroa cruise

Figure 4-11 shows SST, SSS and pCO_2^{sea} measured on the Tangaroa cruise for the period of 25 February, 2002 to 4 March, 2002. North of STF (47°S) and in SAZ (47°-50°S), SST and SSS decreased with increasing latitude, while pCO_2^{sea} increased from 300 to 340 μatm. In PFZ (50°-52°S), SST and SSS were rapidly lowered and pCO_2^{sea} increased from 340 to 355 μatm, going southward. In PZ (52°-62°S), SST decreased with increasing latitude and pCO_2^{sea} varied from 342 to 360 μatm, but SSS showed almost constant values of approximately 33.8. In SSIZ (south of 62°S), SST decreased gradually going southward, and SSS increased with latitude after showing a minimum value of 33.7 at 63.5°S. pCO_2^{sea} showed a minimum value of 305 μatm at 65°S.

4.2.4 JARE43 Shirase cruise

Shirase cruise was made from 9 March, 2002 to 19 March, 2002. The measured values of SST, SSS and pCO_2^{sea} are plotted in Fig. 4-12 against latitude. It should be noted that the locations of fronts such as STF, defined by surface SSS, might be incorrect because the SSS data obtained by Shirase were sparse. In SAZ (45°-49°S), SST and SSS decreased and pCO_2^{sea} increased from 340 to 355 μatm, going southward. In PFZ (49°-53.5°S), SST showed a hump at 52°S and then decreased with latitude, and SSS decreased monotonically and pCO_2^{sea} decreased from 357 to 347 μatm toward high latitudes. In PZ (53.5°-62°S), SST decreased with increasing latitude, showing a fairly constant SSS of about 33.8 and a similar value of pCO_2^{sea} around 350 μatm. In

SSIZ (south of 62°S), SST and pCO_2^{sea} decreased and SSS decreased with increasing latitude.

4.2.5 Temporal and spatial variations of pCO_2^{sea} and air-sea CO_2 flux

We derived summertime average fields of SST, SSS and pCO_2^{sea} for the Southern Ocean, using the results from the above-mentioned cruises. Their average latitudinal distributions obtained are shown in Fig. 4-13. In general, temporal and spatial variability of pCO_2^{sea} in the Southern Ocean was larger than that of pCO_2^{air}, as well as that of pCO_2^{sea} in other oceans (see Chapter 3). The values of pCO_2^{sea}, including one standard deviation represented as a shaded area in Fig. 4-13, were always lower than those of pCO_2^{air}, except for parts of SSIZ and PFZ. The variability of pCO_2^{sea} and SSS was much larger in the southern part of SSIZ (64°-66°S) than in other areas of the Southern Ocean, while SST showed almost the same variability as in other areas. The average values of pCO_2^{sea} plotted in Fig. 4-13 show low values of about 315 μatm in SAZ and about 300 μatm in SSIZ and high values of about 355 μatm in PFZ. Based on measurements of pCO_2^{sea} and pCO_2^{air}, the air-sea CO_2 fluxes at the respective latitudes were calculated for the above-mentioned individual cruises and then averaged to estimate the summertime fluxes in this ocean area. The average air-sea CO_2 fluxes obtained are plotted in Fig. 4-14. The air-sea CO_2 flux indicated low values of less than 1mol m^{-2} yr^{-1} in PFZ and high values of more than 3 mol m^{-2} yr^{-1} north of STF and SSIZ, reflecting mainly the distribution of ΔpCO_2. It is also seen that the air-sea CO_2 flux fluctuates irregularly in SSIZ due to large variability of pCO_2^{sea} observed in this zone.

In order to examine variations of pCO_2^{sea} in summer, SST, SSS and pCO_2^{sea} observed at the respective latitudes of 45°, 48°, 53°, 58°, 63° and 66°S are plotted in Fig.

4-15 against time. As shown above, SST in this ocean was always high at lower latitudes and decreased going southward. On the other hand, SSS was highest at 45°S, and the respective values at 48°, 66°, 53°, 58° and 63°S decreased in order. Although SSS is expected to be low off the coast of the Antarctic Continent due to the inflow of fresh water originated in melted ice sheet into the Southern Ocean, the values at 66°S were high, especially in November and December. pCO_2^{sea} at 66°S also indicated the high values of over 400 μatm for these two months, which are higher than pCO_2^{air}, and then decreased rapidly to 200 μatm. These temporal variations of SSS and pCO_2^{sea} are ascribed to physical and biological processes in the ocean: Deep waters with high salinity, containing high nutrients, iron and CO_2, were transported to the surface in November and December 2001. By this upwelling, photosynthesis of marine biota became active and then weak one month after, probably due to limitation of iron supply in the Southern Ocean (Martin et al., 1990). In this regard, our measurements indicated that the concentrations of nitrate ranged from 30 μmol kg^{-1} to 13 μmol kg^{-1} for the two months, while that of iron obtained by Lai et al. (personal communication) was 0.922 nM in January. Martin et al. (1990) also found in the Southern Ocean that the iron concentration increased from 0.05 to 0.7 nmol Fe kg^{-1} with increasing depth between the surface and 1500 m. As a result, pCO_2^{sea} off the coast of the Antarctic Continent (66°S) varied in a range of over 100 μatm during a few months. On the other hand, pCO_2^{sea} at the other latitudes of 45° to 63°S showed a small variability of less than 25 μatm.

Figure 4-16 shows the temporal variations of air-sea CO_2 flux at the respective latitudes of 45°, 48°, 53°, 58°, 63° and 66°S. The values ranged from -2 mol m^{-2} yr^{-1} at 66°S in December to 6 mol m^{-2} yr^{-1} at 63°S in January, depending on both ΔpCO_2 and wind speed. At most latitudes, the air-sea CO_2 fluxes showed a maximum value in January, due to the largest ΔpCO_2 value in that month. The average air-sea

CO_2 flux in the ocean area covered by this study is plotted in Fig. 4-17 against time. The y-axis of the figure also represents the CO_2 uptake for the Southern Ocean which were calculated by assuming that the average air-sea CO_2 flux derived for the present area with a longitudinal interval of 140°-150°E can be applicable to the whole Southern Ocean. The CO_2 flux reached a minimum value of 1 mol m^{-2} yr^{-1} in December and a maximum value of 3 mol m^{-2} yr^{-1} in January, and the total CO_2 uptake by the ocean for the five summer months amounted to 0.037 GtC yr^{-1} for the present measurement area and 1.4 GtC yr^{-1} for the whole Southern Ocean. Metzl et al. (1999) measured a clear seasonal variation of air-sea CO_2 flux at 40°-50°S in the Indian sector, as depicted in Fig. 4-18. The air-sea CO_2 fluxes in this area are higher by 1-2 mol m^{-2} yr^{-1}, on average, than those in the Southern Ocean, but close to those at 45° and 48°S due to a large CO_2 sink in SAZ (Fig. 4-14). If it can be assumed that the average CO_2 flux in the area covered by this study shows a temporal variation similar to that derived by Metzl et al. (1999), it is suggested that the CO_2 uptake in the Southern Ocean varies seasonally, with the maximum in January-February and the minimum in September. Metzl et al. (1999) also reported that the CO_2 uptake at 40°-50°S in the Southern Ocean amounted to 1.05 GtC yr^{-1}, and Takahashi et al. (2002) evaluated the CO_2 uptake in the Southern Ocean (south of 50°S) to be 0.6 GtC yr^{-1}. These estimates are smaller than our annual CO_2 uptake of 1.4 GtC yr^{-1} calculated on the basis of the five-month measurements. The cause of this difference is attributable to the fact that the summertime oceanic CO_2 uptake is highest through the year (Metzl et al., 1999). Even if this is the case, our results certainly imply that the Southern Ocean acts as an important CO_2 sink.

4.2.6 Comparison of the seasonal variations of pCO_2^{sea} and air-sea CO_2 flux in the Southern Ocean, the Greenland Sea and the Barents Sea

To examine the air-sea CO_2 exchange in the Southern Ocean in more detail, we compare the present results with those from the Greenland Sea and the Barents Sea, which are described in Chapter 3. The temporal variations of pCO_2^{sea} at the respective latitudes in the Southern Ocean are shown in Fig. 4-19, together with those in the Greenland Sea (75°N, 0°) and the Barents Sea (70°N, 40°E). The pCO_2^{sea} values observed in the two northern seas were usually lower than those in the Southern Ocean. The pCO_2^{sea} value at 66°S varied rapidly between 200 and 400 μatm during three summer months, which is much larger than those in the Greenland Sea and the Barents Sea in summer. This difference is attributable to different biological activities in the two ocean areas. As described above, Martin et al. (1990) pointed out that the marine biological activity in the Southern Ocean is strongly controlled by iron. To examine the importance of biological activity in the air-sea CO_2 exchange, ΔpCO_2, wind speeds and air-sea CO_2 fluxes at the respective latitudes in the Southern Ocean, as well as in the Greenland Sea and the Barents Sea, are summarized in Table 4-3. The average ΔpCO_2 value was calculated to be 31 μatm for the Southern Ocean and 80 μatm for the Greenland Sea and the Barents Sea. The fact that ΔpCO_2 is larger in the Greenland Sea and the Barents Sea than in the Southern Ocean is due to strong biological activities in the former seas. However, the wind speed in the Southern Ocean is higher by 2.7 m s^{-1}, on average, than that in the Greenland Sea and the Barents Sea, reflecting a strong circumpolar westerly in the Antarctic region. Consequently, the air-sea CO_2 flux is smaller by 0.8 mol m^{-2} yr^{-1} in the Southern Ocean than in the Greenland Sea and the Barents Sea. These results suggest that even in summer, the physical process is much more essential than the biological process for the oceanic CO_2 uptake in the Southern Ocean, while the biological process is important for the summertime CO_2 uptake in the Greenland Sea and the Barents Sea.

4.3 Variations of DIC in the western Pacific Sector in summer

It is very important for understanding the air-sea CO_2 exchange to elucidate not only the distribution of surface pCO_2^{sea} but also that of Dissolved Inorganic Carbon (DIC), since DIC varies temporally and spatially by marine biological activities and water transport processes. In this section, we discuss temporal and spatial variations of DIC in the western Pacific Sector in summer, which were measured on the Aurora Australis cruise in November and December 2001, the Hakuho-Maru cruise in January 2002 and the JARE43 Tangaroa cruise in January 2002.

4.3.1 Spatial distribution of nDIC

The latitude-depth distributions of water temperature and salinity measured on the Aurora Australis cruise are shown in Fig. 4-20, and the distribution of nDIC (DIC normalized to a salinity of 34 p.s.u.) is shown in Fig. 4-21. In general, the water temperature was high in the surface and at low latitudes, and low in the deep sea and at high latitudes, while nDIC showed an opposite behavior, i.e. low in the surface and at low latitudes, and high in the deep sea and at high latitudes. Such a distribution of DIC is formed mainly in relation to a temperature dependence of CO_2 solubility, biological consumption of inorganic carbon and re-mineralization of organic matter. On the other hand, the distribution of salinity is more complicated than those of the water temperature and nDIC. However, isothermals and isohalines of the figures indicate that the water temperature and salinity were fairly constant from the deep layer to the surface in the ocean south of 65°S. High DIC concentrations of over 2000 μmol kg^{-1} were also seen south of 65°S. These facts would support our assumption that the deep water rich in nutrient, salinity, CO_2 and iron was transported to the surface in

November and December, as described in section 4.2.5.

The water temperature distribution measured on the Hakuho-Maru cruise, shown in Fig. 4-22, is similar to that on the Aurora Australis cruise. However, the salinity distributions on both cruises were different, especially at low latitudes. One possible cause of such a difference may be attributable to complicated water transport in this area, but it is also thought that the distribution of salinity for the Hakuho-Maru cruise is not well represented due to its sparse measurements. The cross-sectional representation of nDIC is given in Fig. 4-23. This distribution is also similar to that on the Aurora Australis cruise, but the low values of nDIC were found in the surface ocean around 65°S due to biological activities. These low values were observed being coincident with the low values of pCO_2^{sea}.

The water temperature and salinity measured on the Tangaroa cruise south of 60°S are shown in Fig. 4-24, and nDIC in Fig. 4-25. It is seen from Fig. 4-24 that the water temperature varied between -1° and 2°C, and salinity was low in the surface and increased with depth. Remarkably low values of nDIC were found near 70 m at 62.5 °S due to biological activities, and pCO_2^{sea} decreased slightly with increasing latitude.

4.3.2 Temporal variation of nDIC

To examine temporal changes of nDIC in the Southern Ocean, the differences between the nDIC values measured on the Hakuho-Maru and Aurora Australis cruises (ΔnDIC) were calculated. Its latitude-depth representation is given in Fig. 4-(g). In general, ΔnDIC shows negative values at depths above 200 m, since biological activity was high when Hakuho-Maru cruised. The low values of nDIC measured on the Hakuho-Maru cruise were obtained from December to January when the pCO_2^{sea} value was low, as shown in Fig.4-26. Large negative values of ΔnDIC of

less than -100 μmol kg^{-1} were found at 65°S where pCO_2^{sea} was remarkably low. On the other hand, slightly positive values of ΔnDIC were observed below 200 m at latitudes between 44° and 60°S, as well as below 100 m south of 61°S. This observed distribution of ΔnDIC is formed by the fact that DIC is consumed by marine biological activities in the surface and resultant organic matter is re-mineralize below 200 m.

The differences between the nDIC values measured on the Tangaroa and Hakuho-Maru cruises (ΔnDIC) are shown in Figs. 4-27. This figure shows that DIC generally increased with time for 1-2 months between both cruises, especially at 65°S, though large negative values of ΔnDIC were seen around 70 m at 62.5°S. This result clearly suggests that biological activities for the period when the Hakuho-Maru cruised were generally stronger than those when Tangaroa cruised. The ΔnDIC values for the Tangaroa and Aurora Australis cruises are also given in Fig. 4-27, which shows the results for four summer months. The ΔnDIC values were negative in the surface ocean, due to biological activities enhanced at the Tangaroa cruise more than at the Aurora Australis cruise. On the other hand, small positive values of ΔnDIC were seen below 100 m due to re-mineralization of organic matter enhanced when Tangaroa cruised. The ΔnDIC distribution obtained from the Tangaroa and Aurora Australis cruises is similar to that from the Hakuho-Maru and Aurora Australis cruises.

4.4 Temporal variations of pCO_2^{sea}, DIC and $\delta^{13}C$ over 10 years

In this section, we discuss temporal variations of pCO_2^{sea}, DIC and $\delta^{13}C$ over 10 years to estimate their long-term trends in the Southern Ocean.

4.4.1 Variation of pCO_2^{sea}

The pCO_2^{sea} values measured by JARE30 in 1989, JARE31 in1990, JARE32 in 1991 and JARE43 in 2002 using R/V Shirase are plotted in Fig. 4-28 against latitude. It is seen from this figure that pCO_2^{sea} increased for the period 1989-2002, especially at low latitudes, but the increase rate of pCO_2^{sea} for this period cannot be explicitly derived, since its year-to-year variation is too large to detect a clear trend. For example, pCO_2^{sea} increased from 315 to 335 μatm between 1990 and 1991 at 48°S, while it decreased from 350 to 330 μatm between 1989 and 1990 and increased from 330 μatm to 340 between 1990 and 1991 at 53°S. Jabaud-Jan et al. (2004) also reported that changes in pCO_2^{sea} between 1998 and 2000 were -14.6 and 37.9 μatm for 50-56° and 58-60°S in the Southern Ocean, respectively, due to anomalously warm weather conditions in the summer of 1998. Therefore, considering that the year-to-year variation of pCO_2^{sea} is caused by changeable water transport and the temperature dependence of pCO_2^{sea}, we examined the long-term trend of pCO_2^{sea} in the following way.

Figure 4-29 shows the relationships between SST and pCO_2^{sea} obtained for the respective JARE cruises. It is evident from this figure that a significant difference of pCO_2^{sea} between 1989 and 1991 is not clearly seen. For example, a hump of pCO_2^{sea} found at 47°S by the JARE32 cruise, as seen in Fig. 4-28, is not found in Fig. 4-29. Therefore, it is thought that for detecting the long-term trend of pCO_2^{sea}, to examine the relationship between SST and pCO_2^{sea} is more essential than to examine the distribution of pCO_2^{sea}. By inspecting Fig. 4-29 from this viewpoint, it is found that pCO_2^{sea} in a temperature range of over 9°C was increased by 20-28 μatm for 13 years. This amount of increase corresponds to the increase rates of 1.5-2.2 μatm yr^{-1}. On the other hand, a significant increase of pCO_2^{sea} was not clearly seen under 8°C, probably

being strongly influenced by biological activities. Especially, the pCO_2^{sea} values measured by JARE43 at SSTs lower than 3°C were lower by about 20 μatm than those measured on earlier cruises, due to biological activities enhanced especially when the JARE43 cruise was made. Inoue and Ishii (2005) reported, from their observations for the period 1969-2002, that the pCO_2^{sea} increase rate ranged between 0.7 and 1.8 μatm yr^{-1}, and that the increase trend of pCO_2^{sea} was not clearly observable in SSIZ, since biological activities negated the long-term increase of pCO_2^{sea}. The increase rate of pCO_2^{sea} by Inoue and Ishii (2005) is generally lower by 0.6-0.8 μatm yr^{-1} than ours, but both results for SSIZ are identical to each other, suggesting that it is difficult to detect the long-term trend of pCO_2^{sea} for SSIZ based on its direct observations in summer.

4.4.2 Variations of DIC and $\delta^{13}C$

In order to derive the long-term trend of nDIC over 10 years, we compare the temperature dependence of nDIC for the JARE34 Shirase cruise with that for the JARE44 Tangaroa 2003 cruise. As described below, it is difficult to detect its long-term trend based on 10-year observations even at the same location. Figure 4-30 shows the vertical profiles of nDIC measured at a location of 57°S and 148°E in 1993 on the JARE34 cruise and at a location of 55°S and 140°E in 2001 on the Hakuho-Maru cruise. It is seen from this figure that differences between nDIC at depths below 100 m from the JARE34 and Hakuho-Maru cruises were 7-19 μmol kg^{-1}, probably due to anthropogenic CO_2 uptake by the ocean. However, in the surface layer shallower than 100 m, the values of nDIC measured on the JARE34 cruise were higher than those on the Hakuho-Maru cruise, while the situation was reversed at a deeper layer. The lower values of nDIC measured in the surface layer on the Hakuho-Maru cruise may imply that biological activities negated the effect of anthropogenic CO_2 uptake by the ocean

occurred for 10 years.

Figure 4-31 shows the relationships between the water temperature and nDIC for SSIZ, obtained by the two cruises of JARE34 and Tangaroa in 1993. It is known that the relationship between the two parameters for the Southern Ocean can be expressed by two different regression lines (Ishii et al., 1998). Ishii et al. (1998) also reported from their JARE34 cruise measurements that nDIC measured for water masses with temperatures of -1.7°C or lower in SSIZ preserves their wintertime state in the mixed layer. Ishii et al. (1998) estimated the wintertime nDIC value of the mixed layer to be 2184 μmol kg^{-1}, based on the JARE34 measurement data shown in Fig. 4-31(a). In this study, we also employed the same value of 2184 μmol kg^{-1}. On the other hand, we found from Fig. 4-31(b) that the wintertime mixed layer nDIC value was 2196 μmol kg^{-1} when Tangaroa cruised. By comparing these two values for SSIZ, a change in nDIC for 10 years was estimated to be about 12 μmol kg^{-1}, showing an average increase rate of 1.2 μmol kg^{-1} yr^{-1}.

As described above, it is difficult to detect the long-term increase of pCO_2^{sea} in SSIZ based on its direct measurements in summer. Therefore, we tried to calculate the increase rate of pCO_2^{sea} by using the Buffer factor, our measurement results and related parameters. The time change in pCO_2^{sea} can be calculated by the equation,

$$\delta pCO_2(\delta t) = R \times \frac{\delta nDIC(\delta t)}{nDIC} \times pCO_2. \qquad (4\text{-}2)$$

Here, nDIC, pCO_2, $\delta pCO_2(\delta t)$, $\delta nDIC(\delta t)$ and R denote the wintertime values of nDIC and pCO_2^{sea}, the changes in pCO_2^{sea} and nDIC for 10 years, and the Buffer factor, respectively. In this calculation, we employed 14 (Inoue and Ishii, 2005), 12 μmol kg^{-1} per decade, 2184 μmol kg^{-1} and 340 μatm for the respective values of R, $\delta nDIC(\delta t)$,

nDIC and pCO_2. The value employed for pCO_2 of 340 μatm was taken from the result obtained by Takahashi et al. (2002) in the winter of 1995. Consequently, the average increase rate of pCO_2^{sea} for 10 years was estimated to be 2.6 μatm yr^{-1}. This estimation of the pCO_2^{sea} increase rate was made rather roughly, but 2.6 μatm yr^{-1} derived here for SSIZ is fairly comparable to 1.5-2.2 μatm yr^{-1} obtained above for the Southern Ocean except for SSIZ on the basis of direct pCO_2^{sea} measurements, both values being higher than 1.4 μatm yr^{-1} of pCO_2^{air}.

To detect the long-term trend of $\delta^{13}C$ for 10 years, we investigated the relationships between the water temperature and $\delta^{13}C$ in DIC for the JARE34 and Tangaroa cruises in 2003. The measured values of water temperature and $\delta^{13}C$ on these cruises are shown in Fig. 4-32. As seen in this figure, the relationship between both parameters for SSIZ can be also expressed by two different regression lines. Taking this into account, the results suggest that the $\delta^{13}C$ values measured on both cruises indicate around 0.9 ‰ for the wintertime mixed layer value and no significant difference of $\delta^{13}C$ is detectable in the mixed layer for 10 years. If the nDIC increase rate of 1.2 μmol kg^{-1} yr^{-1} was caused by anthropogenic CO_2 uptake by the ocean, the long-term change of $\delta^{13}C$ in the wintertime mixed layer for 10 years should be -0.04 ‰ per decade. This discrepancy suggests that further measurements of $\delta^{13}C$ are needed to quantify the anthropogenic CO_2 uptake in the Southern Ocean.

Table 4-1. Locations of oceanographic fronts along 110° and 140°E lines determined according to definitions by Chaigneau and Morrow (2002). STF, SAF, PF and SSI represent Sub Tropical Front, Sub Antarctic Front, Polar Front and Seasonal Sea Ice Zone, respectively.

	110°E	140°E
STF	45°S	47-48°S
SAF	47°S	49-50°S
PF	50°S	52-53°S
Northern bound of SSIZ	62°S	62°S

Table 4-2. The positions of oceanographic fronts in Southern Ocean. They are decided by Chaigneau and Morrow (2002). STF, SAF, PF and SSIZ represent Sub Tropical Front, Sub Antarctic Front, Polar Front and Seasonal Sea Ice Zone, respectively.

	Aurora Australis	Hakuho-Maru	Tangaroa	Shirase
STF	47-48°S	47°S	47°S	45°S
SAF	48.5-49°S	49°S	50°S	49°S
PF	53°S	53°S	52°S	54°S
Northern bound of SSIZ	62°S	62°S	62°S	62°S

Table 4- 3. Average values of ΔpCO_2, wind speed and air-sea CO_2 flux for the Southern Ocean (140°-150°E) from November to March, and the Greenland Sea and the Barents Sea from May to September

Southern Ocean (140°-150°E)	ΔpCO_2 (μatm)	Wind Speed (m/s)	CO_2 flux (mol/m^2/yr)
45°S (North of STF)	47	7.4	3.0
48°S (SAZ)	32	8.0	2.4
53°S (PZ)	18	8.7	1.4
58°S (PZ)	14	9.9	1.5
63°S (SSIZ)	35	8.0	2.8
66°S (SSIZ)	37	6.1	1.9
Average	31	8.0	2.2
Greenland Sea Barents Sea	80	5.3	3.0

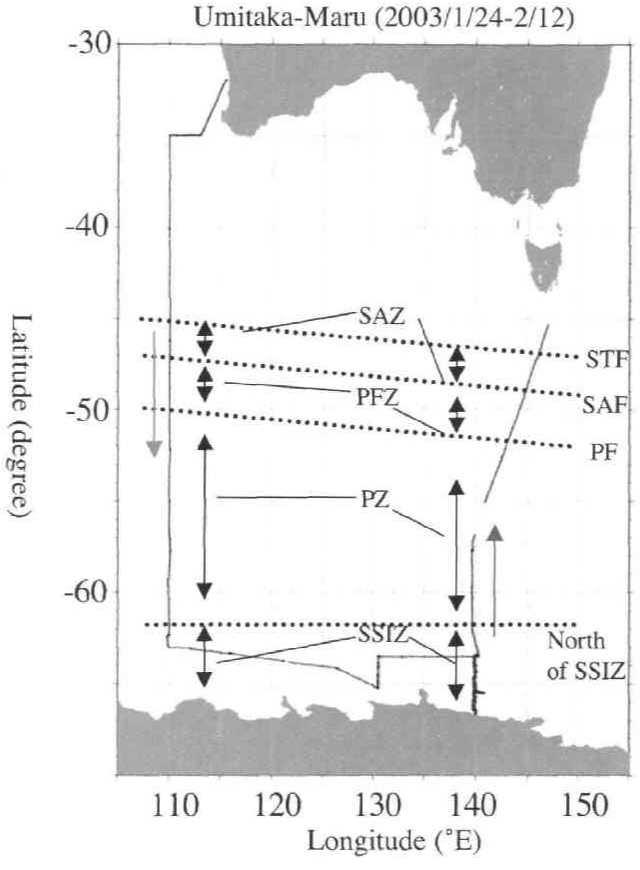

Fig. 4-1. Cruise track of Umitaka-Maru for the period January 24-February 12, 2003, and locations of oceanographic fronts and zones.

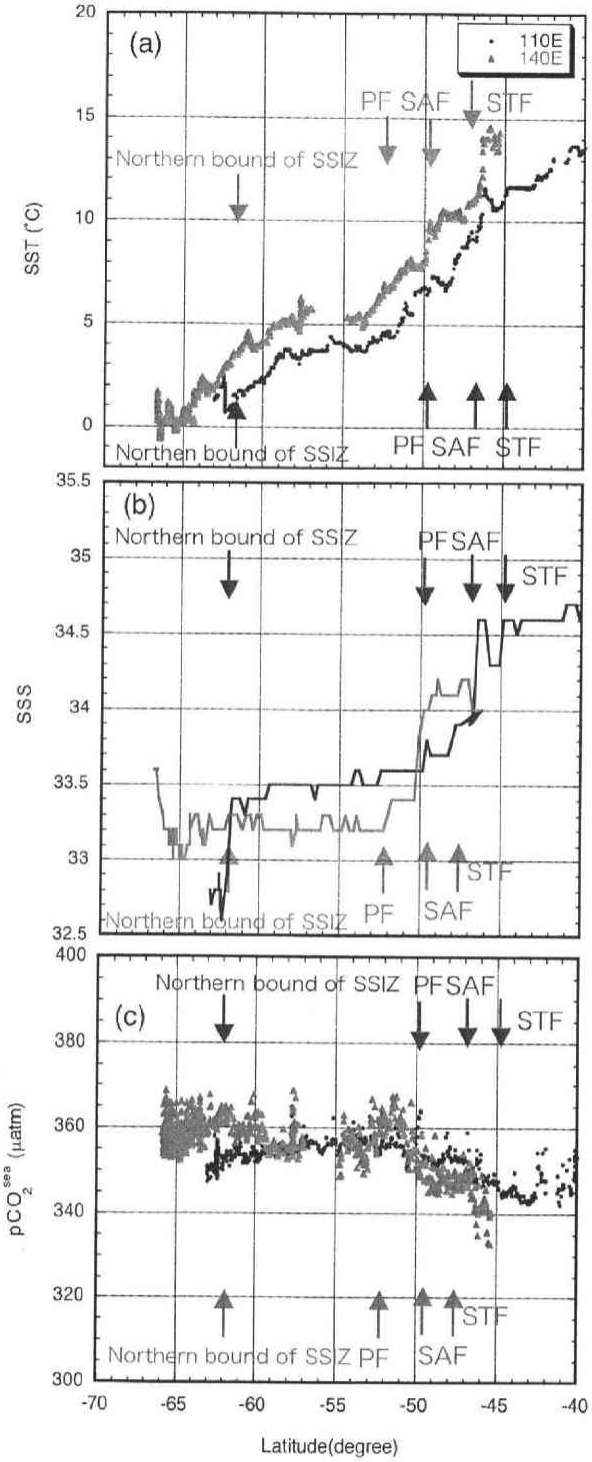

Fig. 4-2. Latitudinal distributions of SST (a), SSS (b) and pCO_2^{sea} (c) measured on the Umitaka-Maru cruise. Blue and red circles represent the results obtained along 110° and 140°E lines, respectively. Blue and red arrows represent the locations of the southern bound of Seasonal Sea Ice Zone, Polar Front, Sub Antarctic Front and Sub Tropical Front determined for the respective measurements along 110° and 140°E.

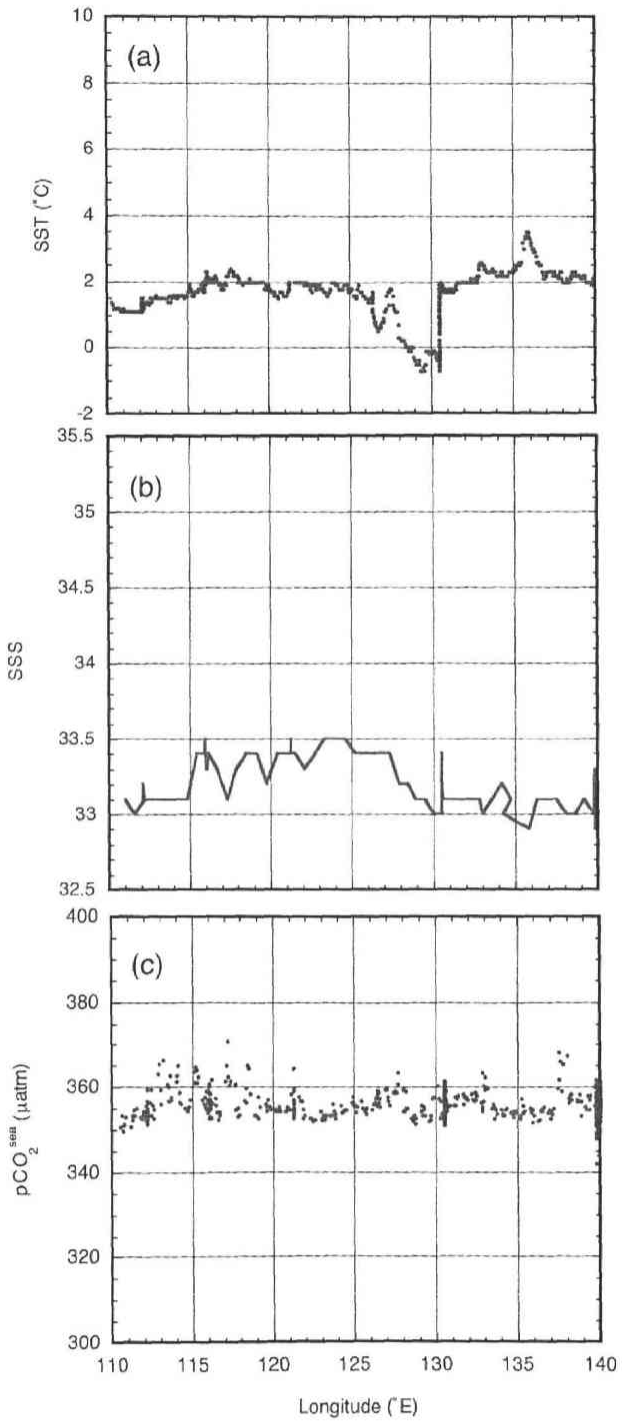

Fig. 4-3. Longitudinal distributions of SST (a), SSS (b) and pCO_2^{sea} (c) measured on the Umitaka-Maru cruise along the Antarctic Continental coastline.

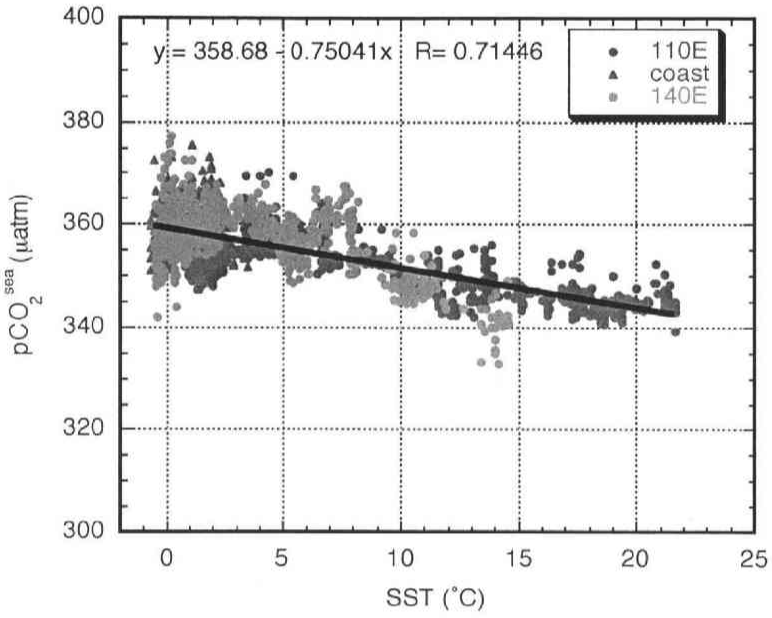

Fig. 4-4. Relationship between pCO_2^{sea} and SST obtained for the Umitaka-Maru cruise in the Southern Ocean during January 24-February 12, 2003. Blue circles, purple triangles and red circles represent the values of pCO_2^{sea} measured along the 110°E line, continental coastline and 140°E line, respectively. Solid line shows the best-fit line to the data obtained by applying a least-squares fit.

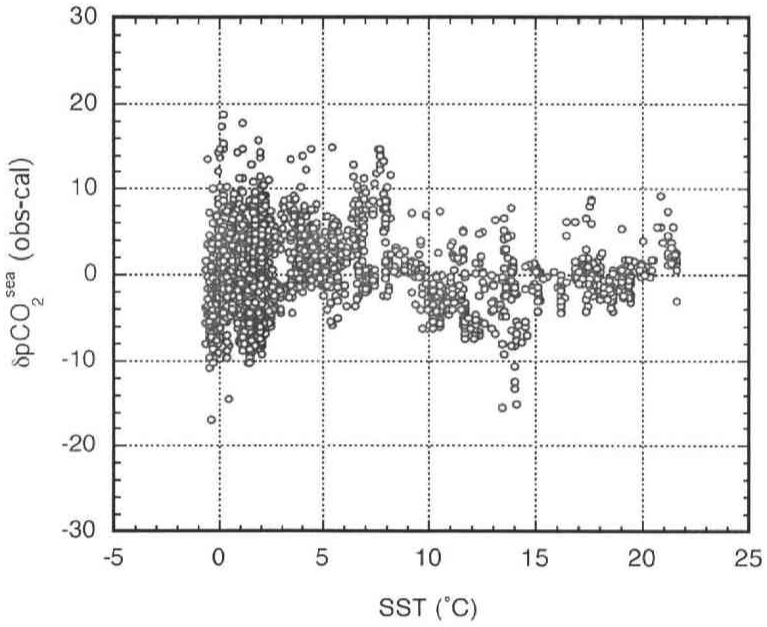

Fig. 4-5. Differences between the observed and calculated pCO_2^{sea} values for the Umitaka-Maru cruise in the Southern Ocean during January 24-February 12, 2003. The calculated values were obtained using the empirically derived pCO_2^{sea}-SST relationship and the SST data.

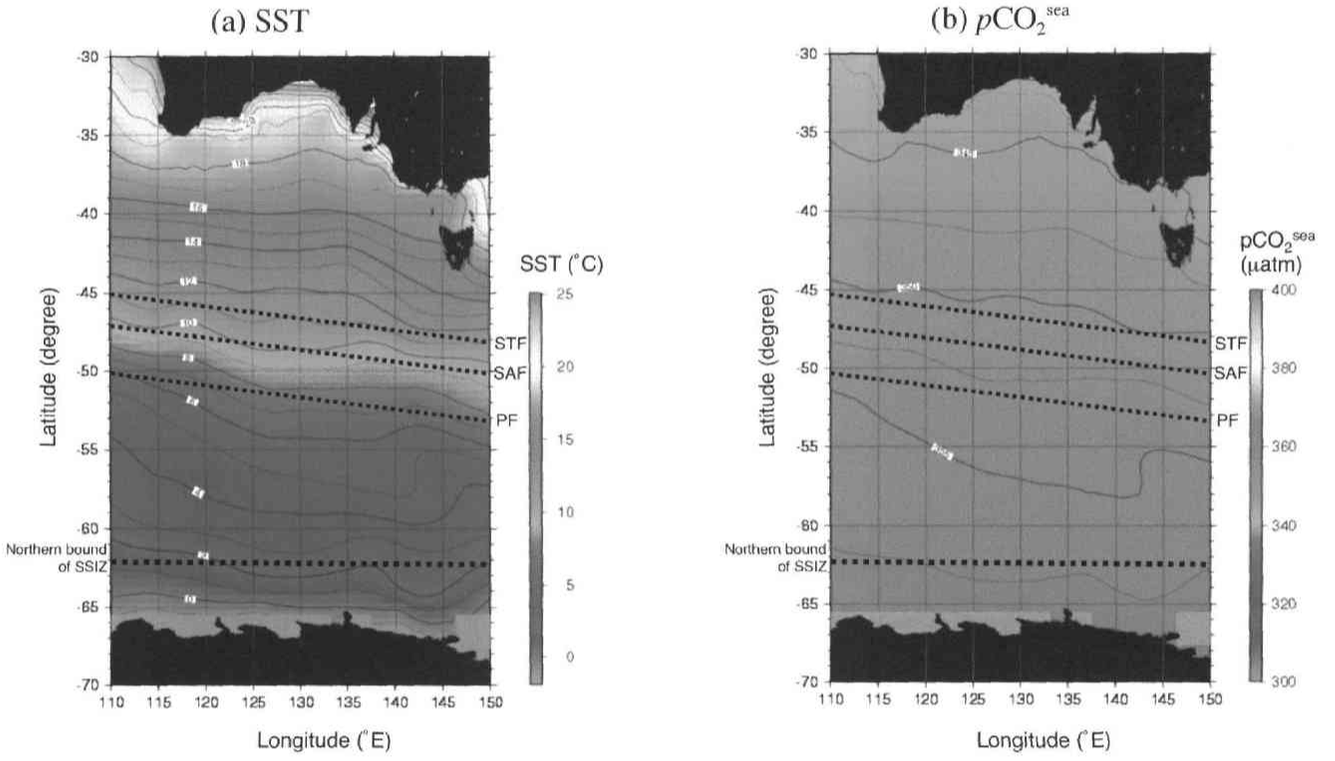

Fig. 4-6. Latitude-longitude distributions of the average SST (°C) (a) and pCO_2^{sea} (μatm) calculated for January and February 2003 using the NCEP/NCAR reanalysis SST data and the empirically derived pCO_2^{sea}-SST relationship (b). Gray shades show sea ice areas found from the NCEP/NCAR reanalysis data. Dashed lines represent the locations of STF, SAF, PF and northern bound of SSIZ, respectively.

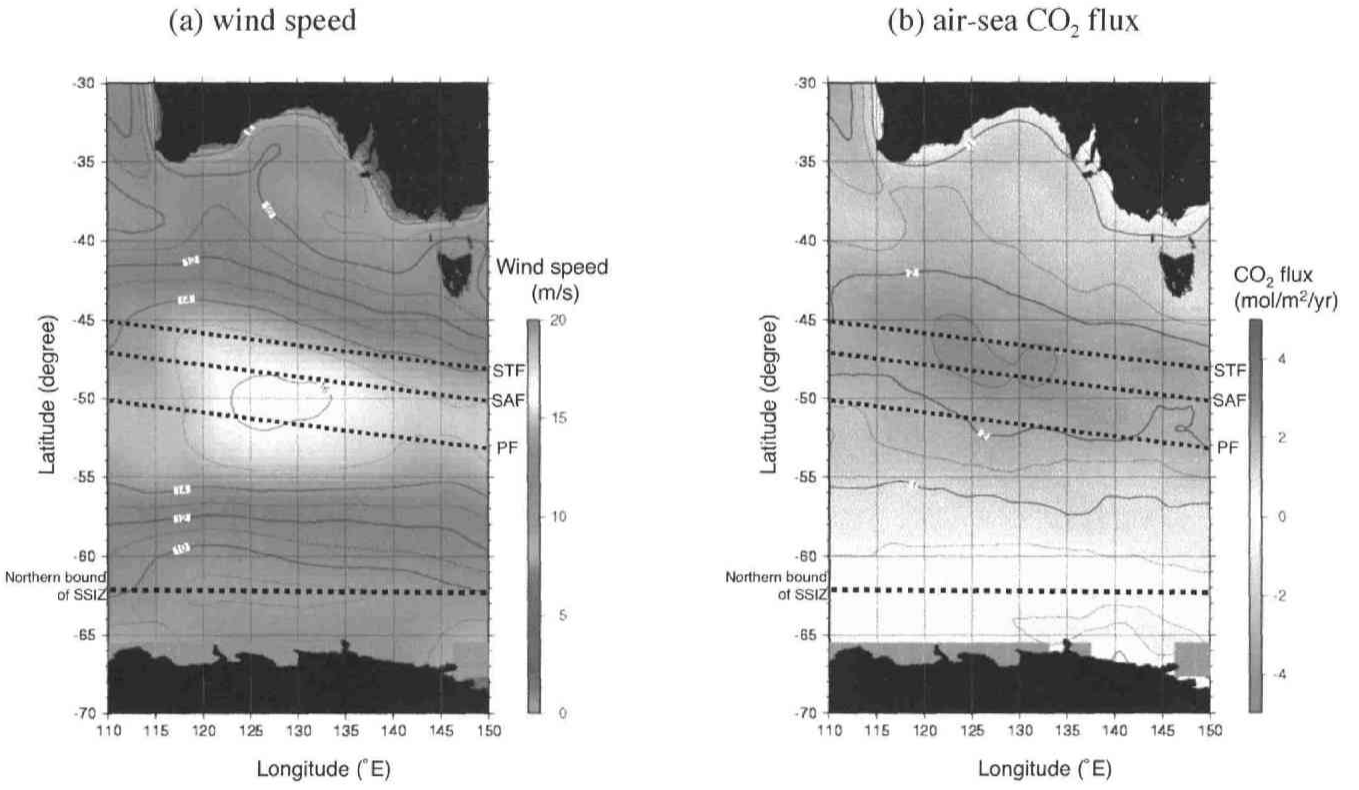

Fig. 4-7. Latitude-longitude distributions of the average wind speed (m s^{-1}) (a) and calculated air-sea CO_2 flux (mol m^{-2} yr^{-1}) for January and February 2003 using the NCEP/NCAR reanalysis wind data. Gray shades show sea ice areas found from the NCEP/NCAR reanalysis data. Dashed lines represent STF, SAF, PF and northern bound of SSIZ, respectively. The positive value of air-sea CO_2 flux means oceanic CO_2 uptake from the atmosphere.

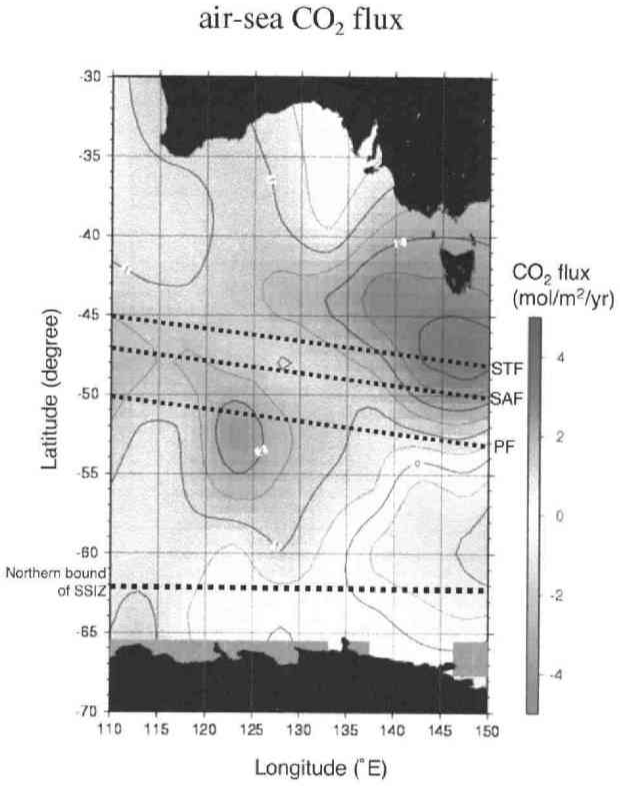

Fig. 4-8. Latitude-longitude distribution of the average air-sea CO_2 flux (mol m^{-2} yr^{-1}) calculated for January and February 1995 on the basis of Takahashi et al. (2002) (http://www.ldeo.columbia.edu/res/pi/CO2/carbondioxide/air_sea_flux/fluxdata.txt).
Gray shades show sea ice areas found from the NCEP/NCAR reanalysis data. Dashed lines represent the locations of STF, SAF, PF and northern bound of SSIZ estimated for our Umitaka-Maru cruise. The positive value of air-sea CO_2 flux means oceanic CO_2 uptake from the atmosphere.

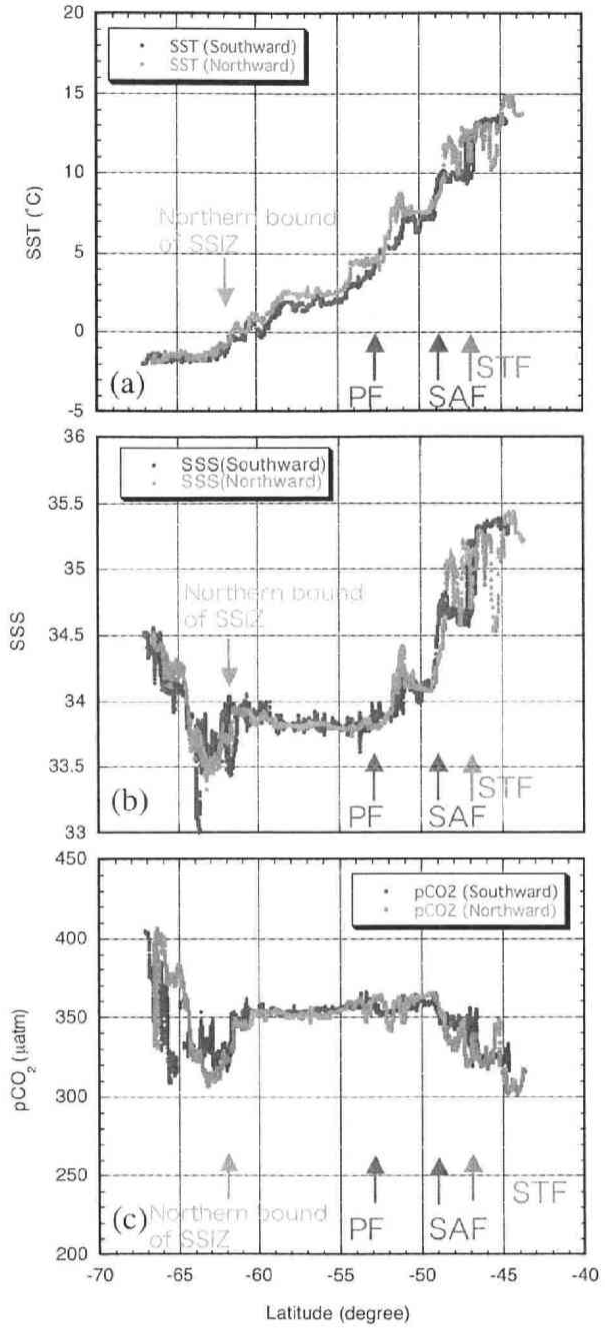

Fig. 4-9. Latitudinal distributions of SST (a), SSS (b) and pCO_2^{sea} (c) in Aurora Australis cruise, respectively. The blue points represent the southward, and the red the northward. Each colored arrows represent the position of South of Seasonal Sea Ice Zone (gray) Polar Front (purple), Sub Antarctic Front (blue), Sub Tropical Front (red), respectively.

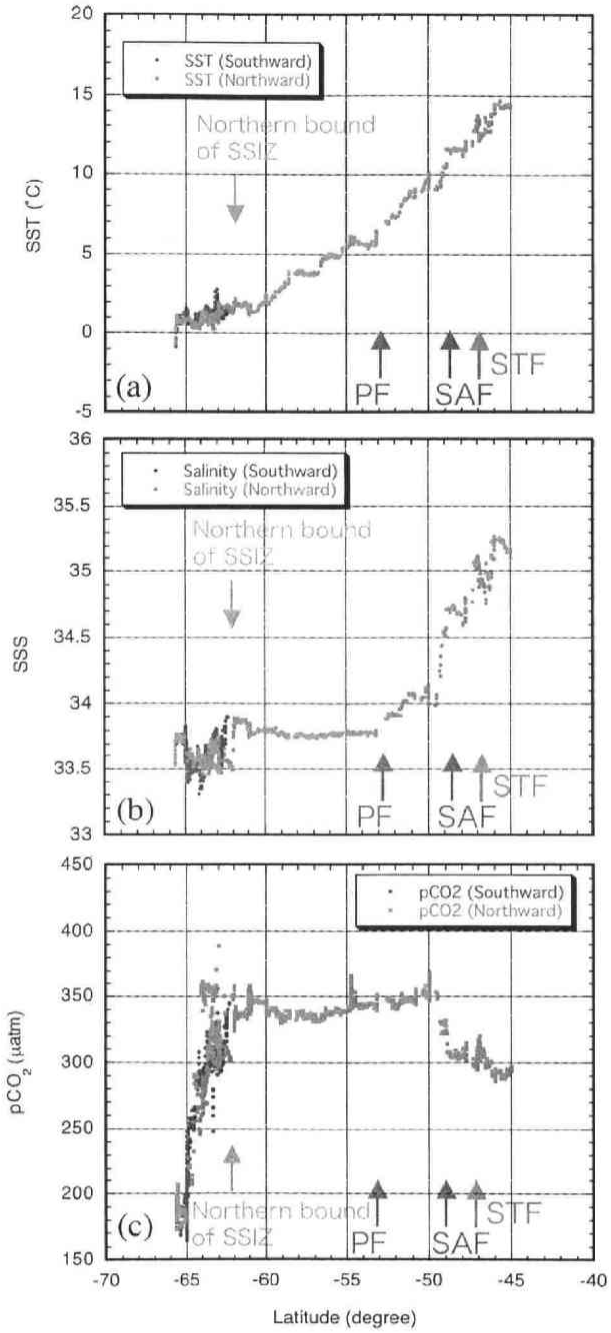

Fig. 4-10. The same as in Figure 4-9, but in Hakuho-maru cruise

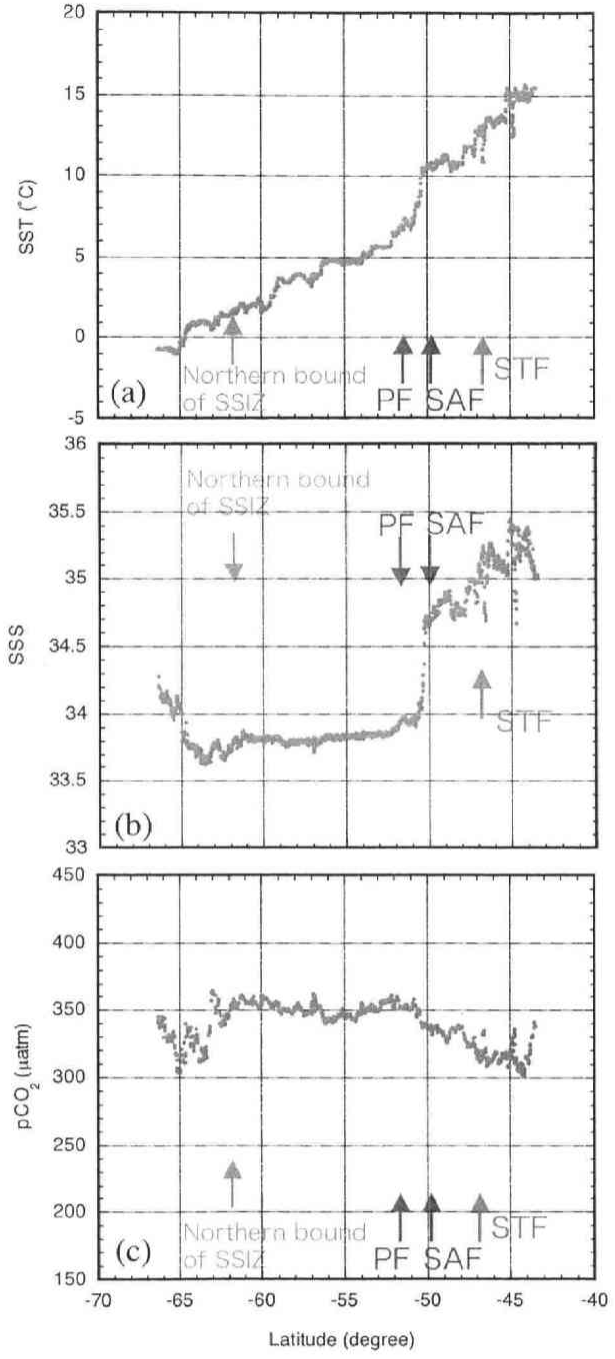

Fig. 4-11. The same as in Figure 4-9, but in Tangaroa cruise

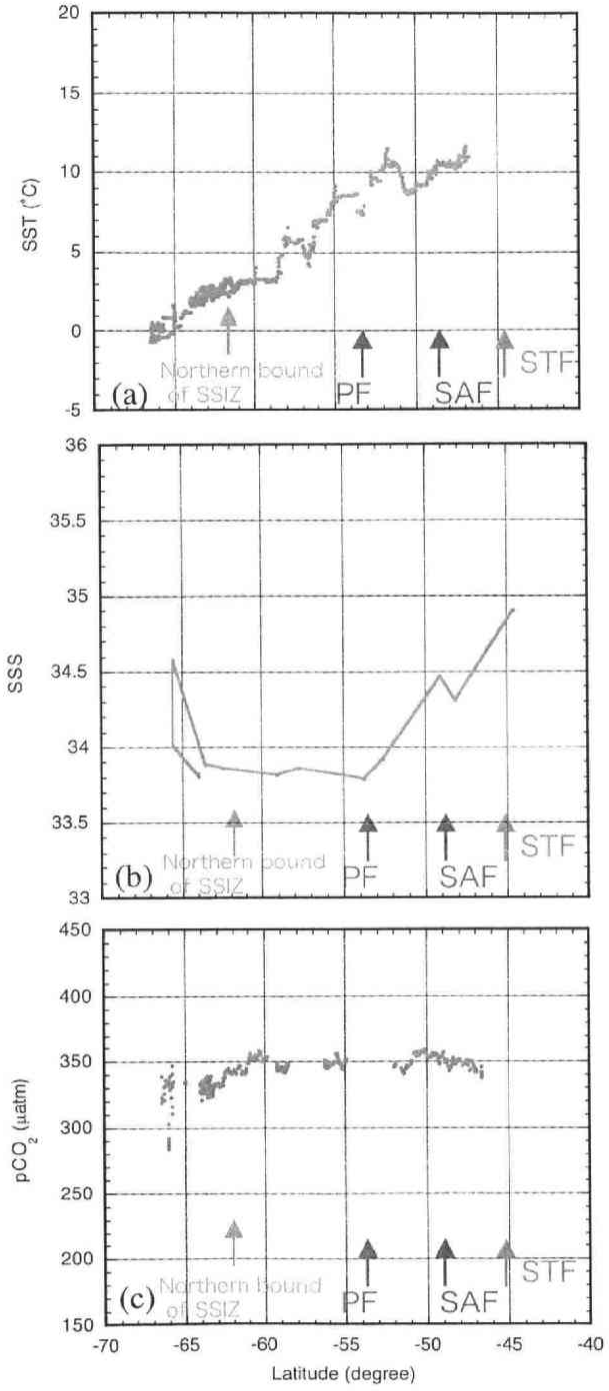

Fig. 4-12. The same as in Figure 4-9, but in JARE43 Shirase cruise

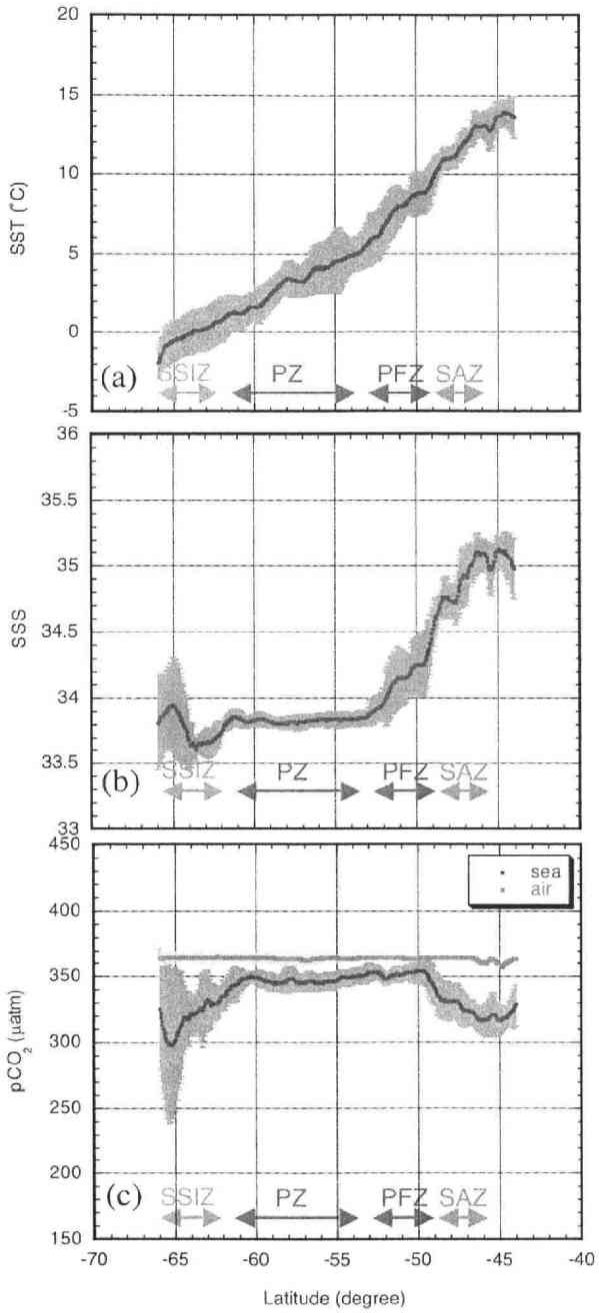

Fig. 4-13. Latitudinal distribution of averaged SST (a), SSS (b) and $pCO_2^{air/sea}$ (c) in summer (Oct. 2001 – Mar. 2002), respectively. The shaded areas show the deviations of temporal variation of respective parametors in summer.

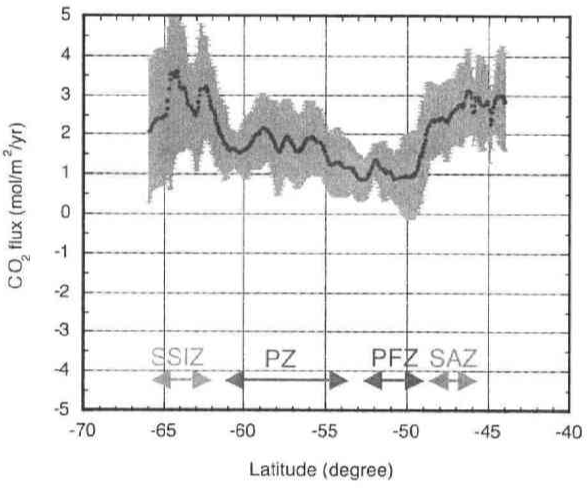

Fig. 4-14. Latitudinal distribution of averaged air-sea CO_2 flux. The shaded areas show the deviations of temporal variations of air-sea CO_2 flux for summer. The positive value means oceanic CO_2 uptake in this study.

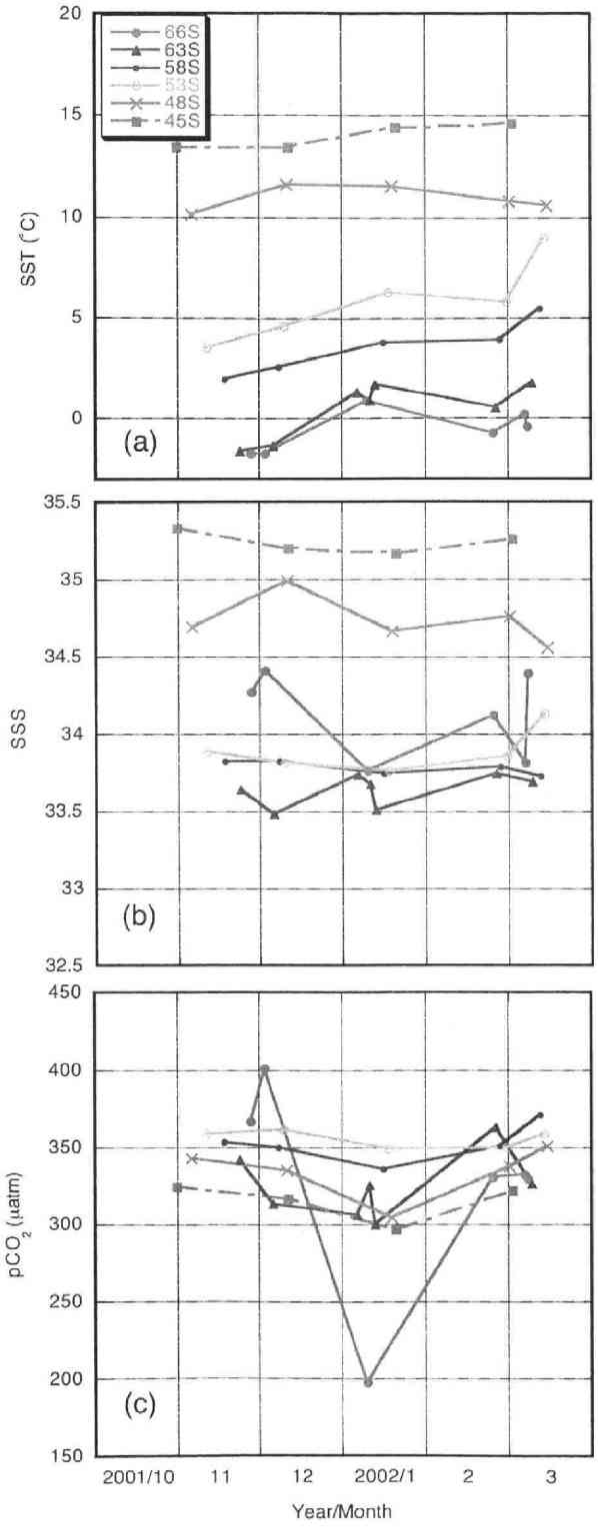

Fig. 4-15. Summer-time variations of SST (a), SSS (b) and the pCO_2^{sea} (c) in 45°S (red square), 48°S (red cross), 53°S (orange circle), 58°S (green circle), 63°S (blue triangle) and 66°S (purple circle), respectively.

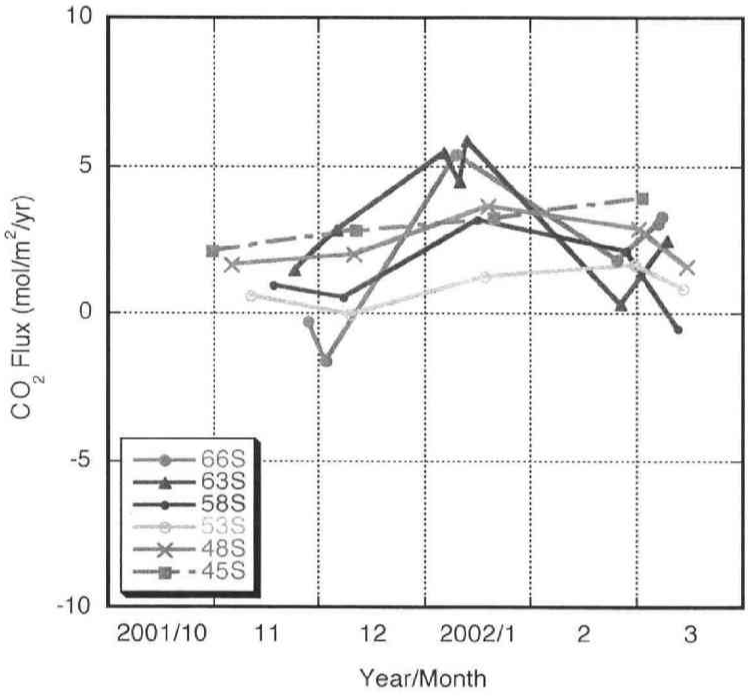

Fig. 4-16. Summer-time variations of air-sea CO_2 flux in 45°S (red square), 48°S (red cross), 53°S (orange circle), 58°S (green circle), 63°S (blue triangle) and 66°S (purple circle), respectively.

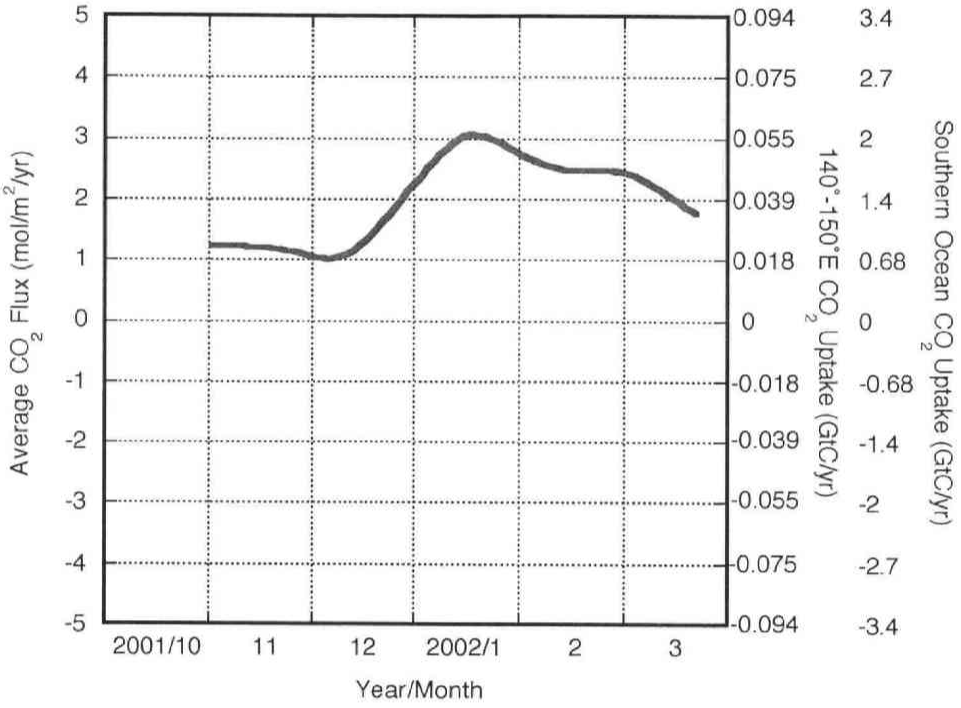

Fig. 4-17. Temporal variation of the average air-sea CO_2 flux (left y-axis) in the present measurement area in summer. The right scales of y-axis represent CO_2 uptake calculated from the average air-sea CO_2 flux for the present measurement area and the whole Southern Ocean, respectively. The positive value means that the ocean takes up CO_2 from the atmosphere.

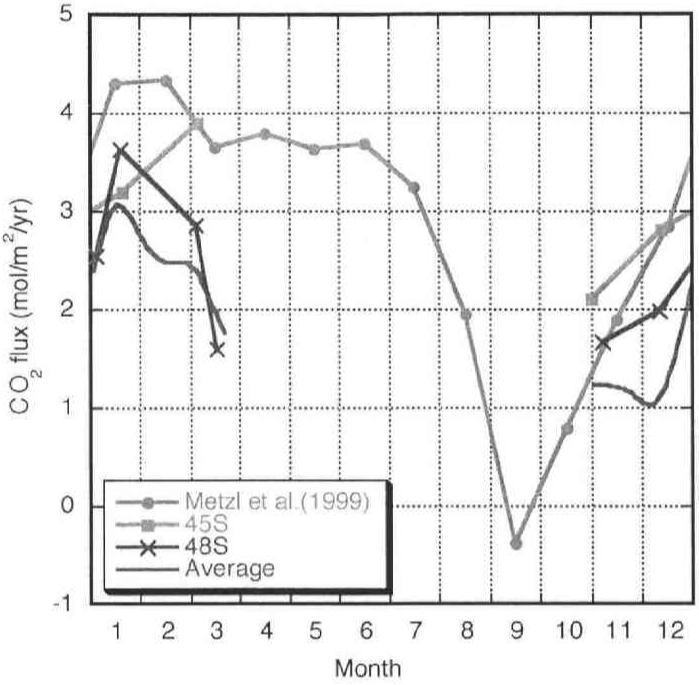

Fig. 4-18. Seasonal variations of the average air-sea CO_2 flux observed in this study. Red lines with squares and green lines with crosses show the CO_2 fluxes observed at 45° and 48°S, respectively, and blue lines represent the average between 44° and 66°S. Purple line shows the CO_2 flux values obtained by Metzl et al. (1999) in 40°-50°S in the Indian sector.

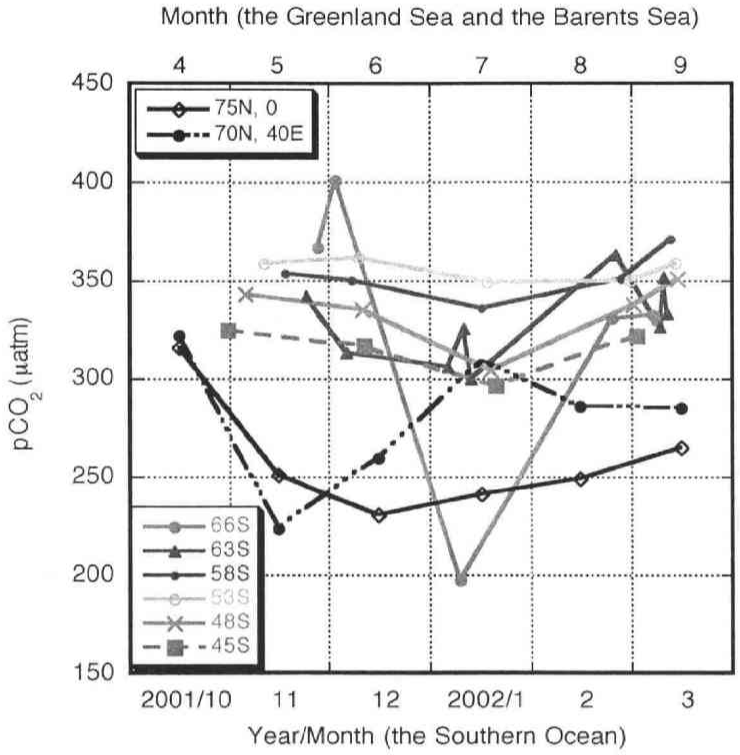

Fig. 4-19. Temporal variations of pCO_2^{sea} in the Southern Ocean (140°-150°E), the central Greenland Sea (75°N, 0°, black line with diamonds) and the Barents Sea (70°N, 40°E, dashed line with solid circles). Color lines represent the results at the respective latitudes in the Southern Ocean. The months on the top of x-axis are shifted by a half year from the bottom axis, so that the northern hemispheric seasonal variations are easily compared with the southern hemispheric variations.

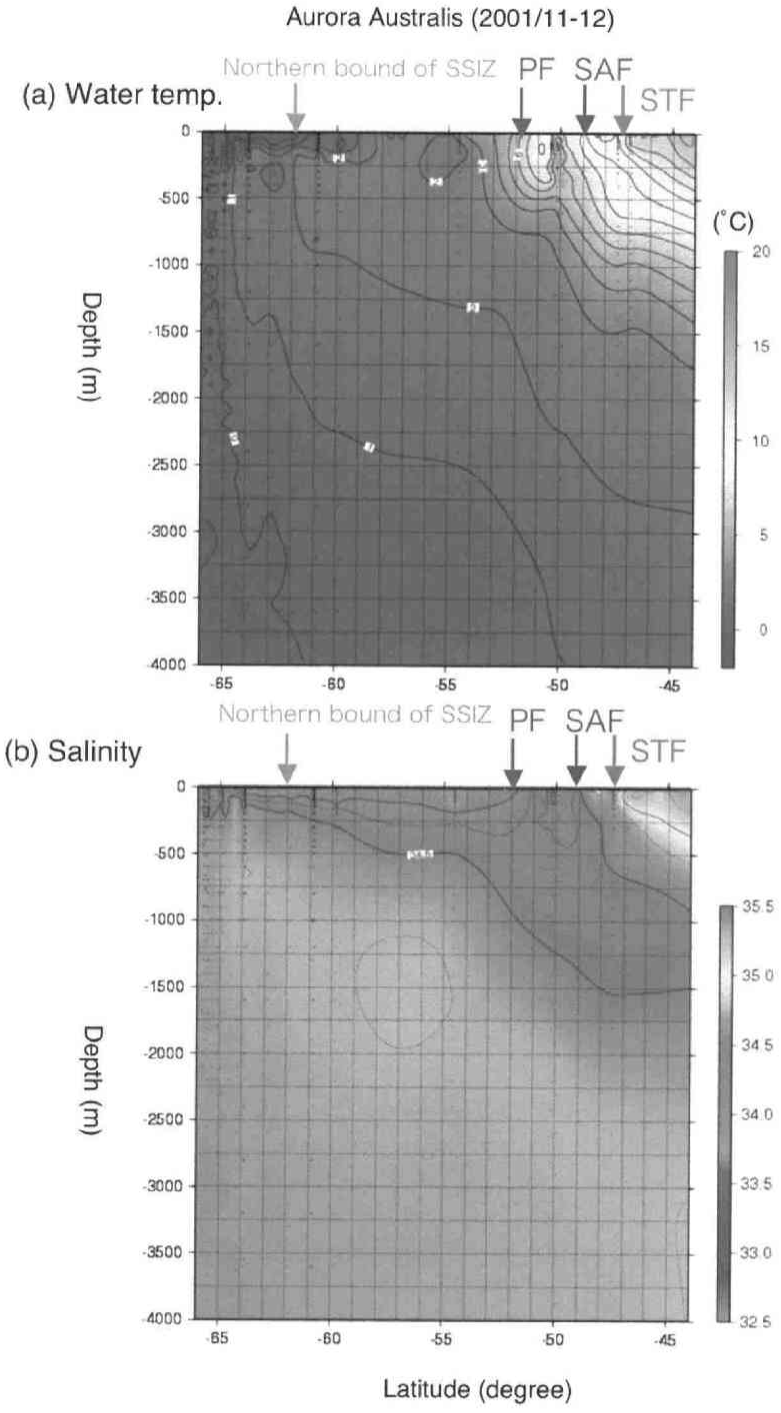

Fig. 4-20. Water temperature (a) and salinity (b) measured on the Aurora Australis cruise

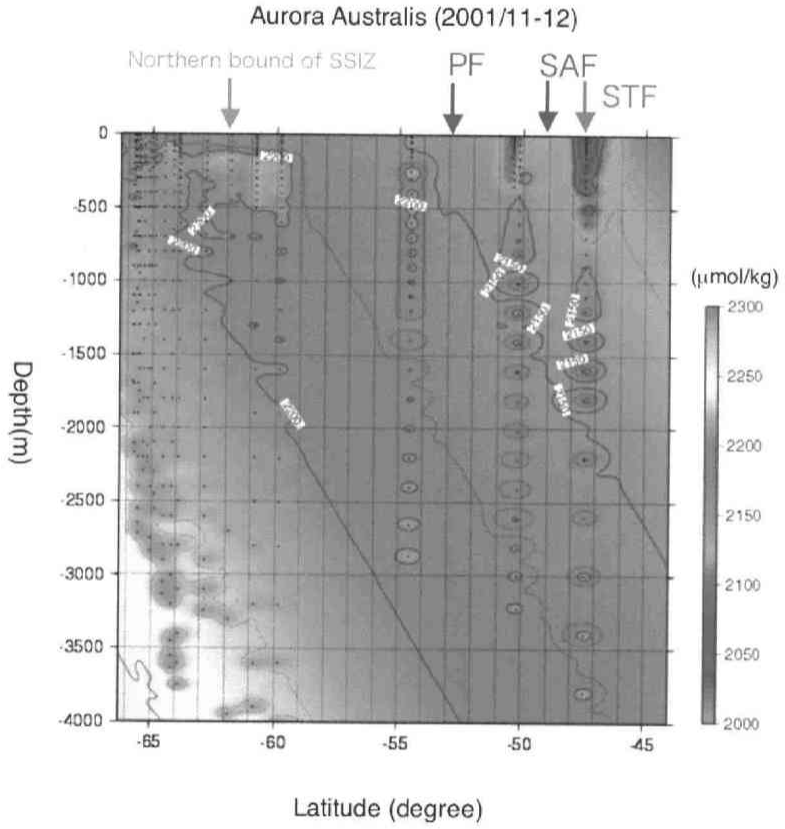

Fig. 4-21. Normalized DIC (nDIC) measured on the Aurora Australis cruise

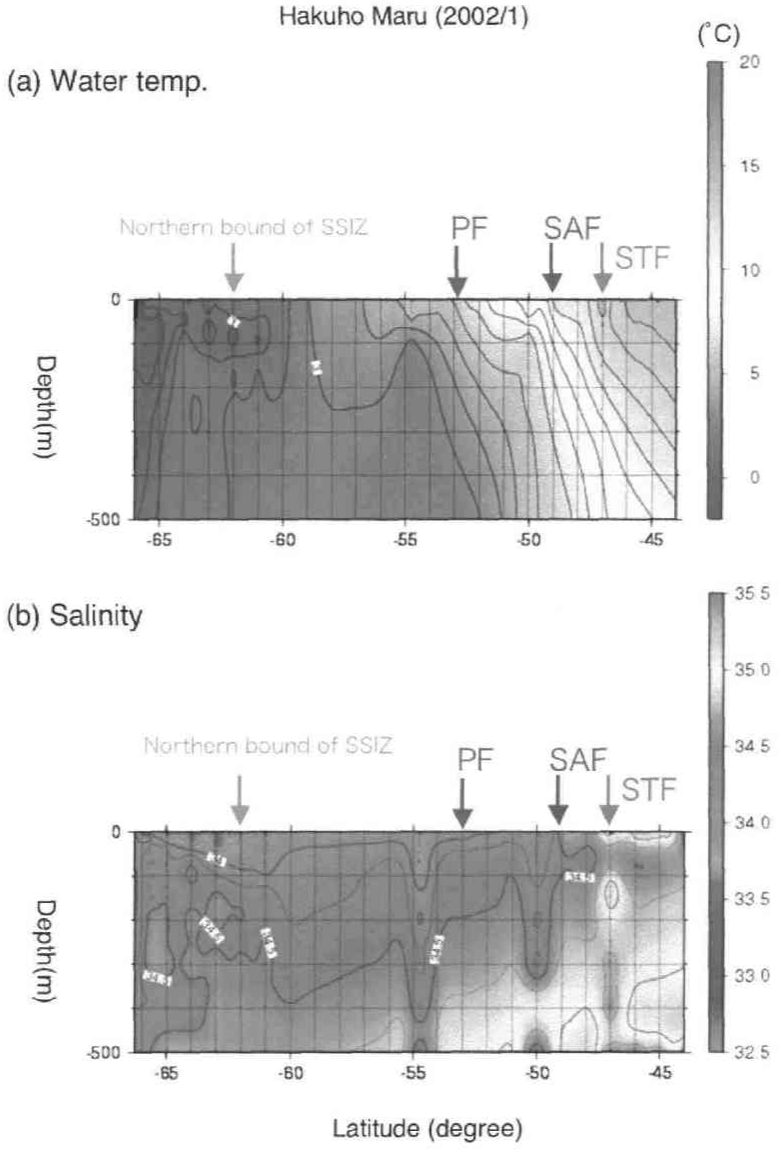

Fig. 4-22. Water temperature (a) and salinity (b) measured on the Hakuho-Maru cruise

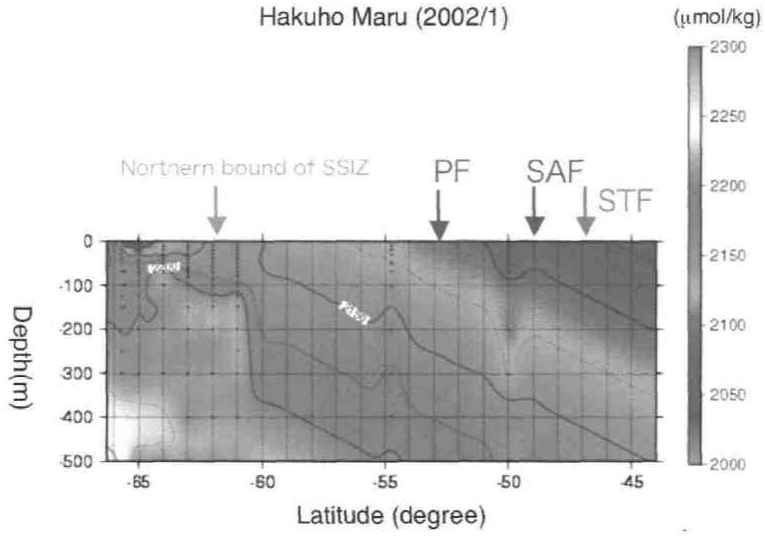

Fig. 4-23. nDIC measured on the Hakuho-Maru cruise

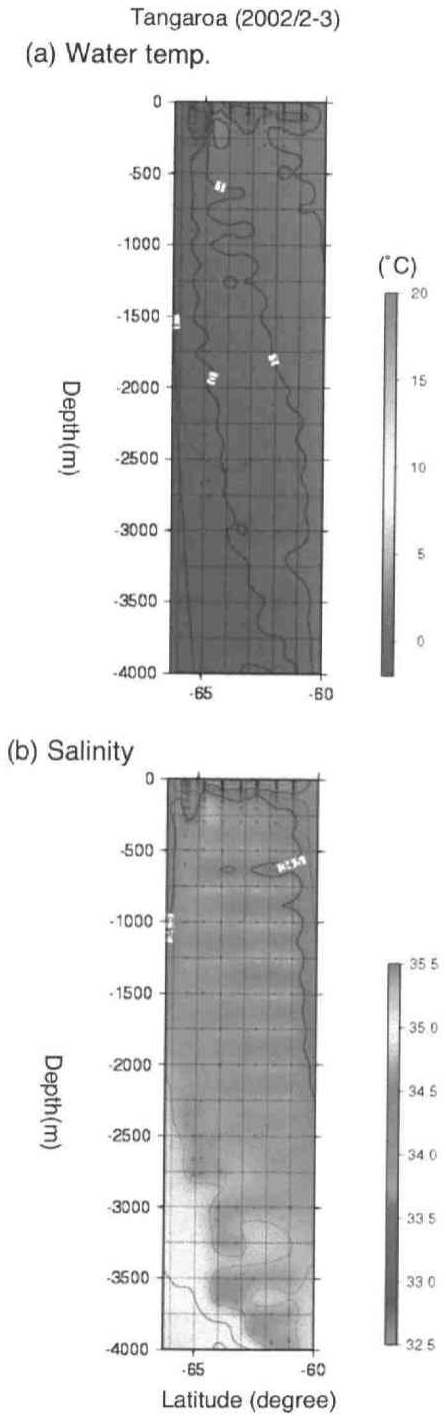

Fig. 4-24. Water temperature (a) and salinity (b) measured on the Tangaroa cruise

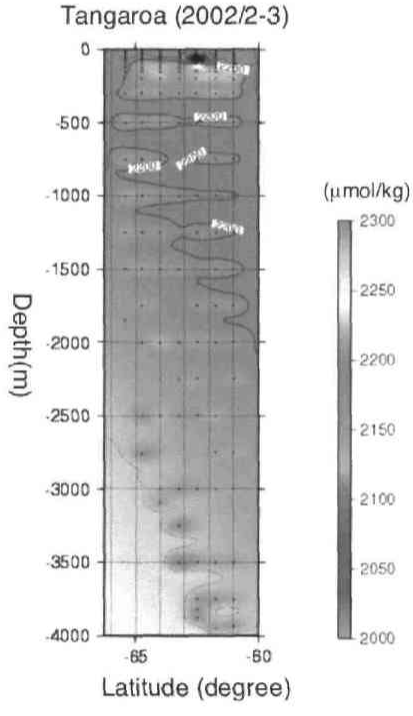

Fig. 4-25. nDIC measured on the Tangaroa cruise

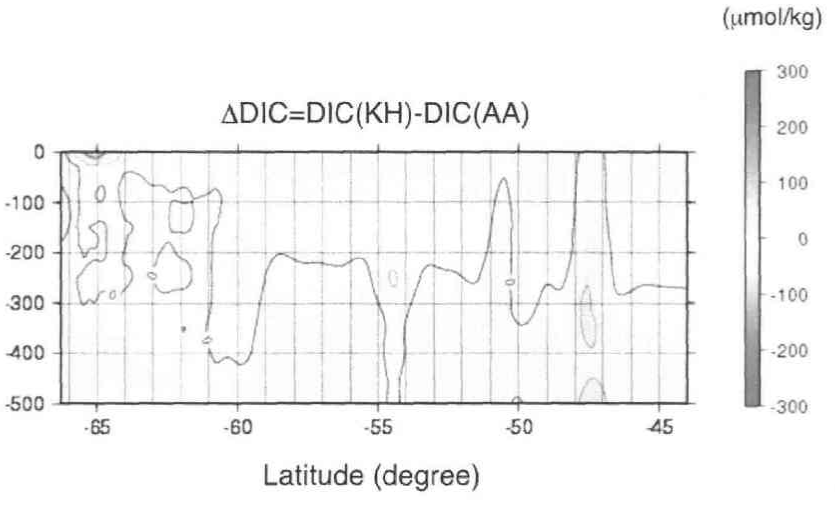

Fig. 4-26. Differences between nDIC measured on the Hakuho-Maru and Aurora Australis cruises (ΔnDIC). Green and red areas represents negative and positive values of ΔnDIC, respectively.

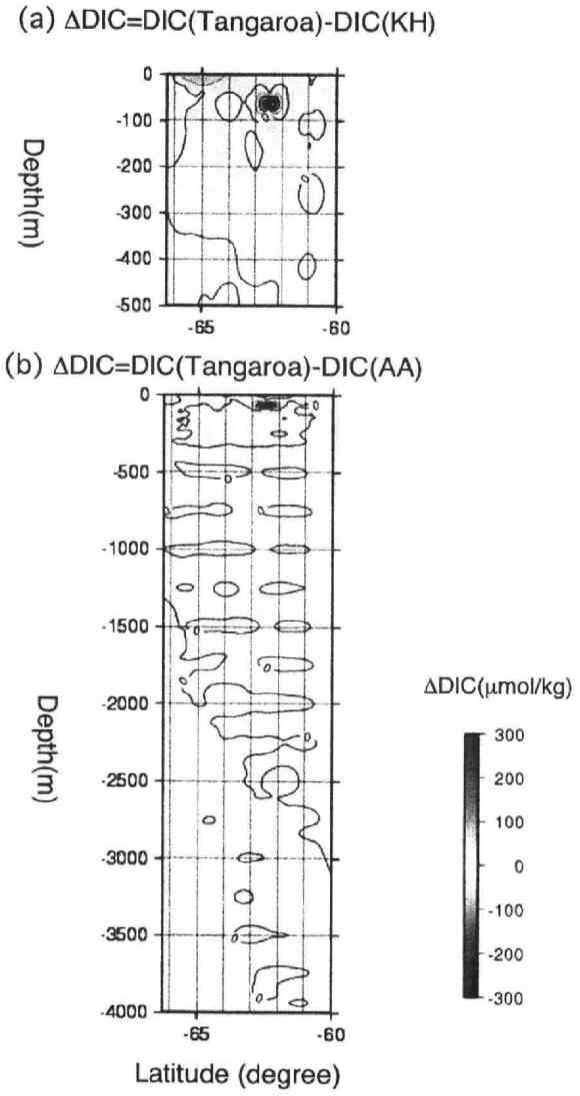

Fig. 4-27. Depth-latitude distribution of ΔnDIC derived from the Tangaroa and Aurora Australis cruises (a) and from the Tangaroa and Hakuho-Maru cruises (b). Green and red areas represent negative and positive values of ΔnDIC, respectively.

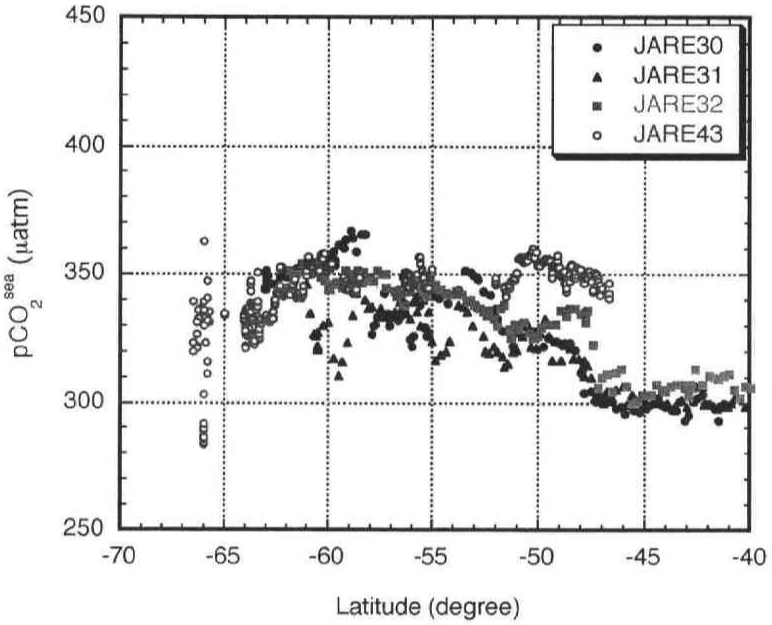

Fig. 4-28. The latitudinal pCO_2^{sea} distributions in JARE30 (purple circle), JARE31 (blue triangle), JARE32 (aqua square) and JARE43 (red circle), respectively. A part of pCO_2^{sea} in low latitude on JARE43 was not included because of trouble in position data.

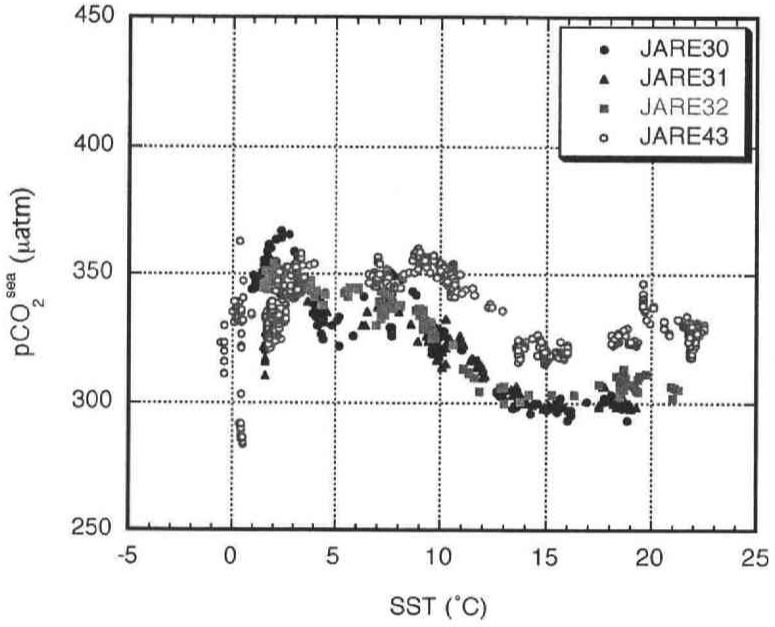

Fig. 4-29. The relationship between SST and pCO_2^{sea} in JARE30 (purple circle), JARE31 (blue triangle), JARE32 (aqua square) and JARE43 (red circle), respectively

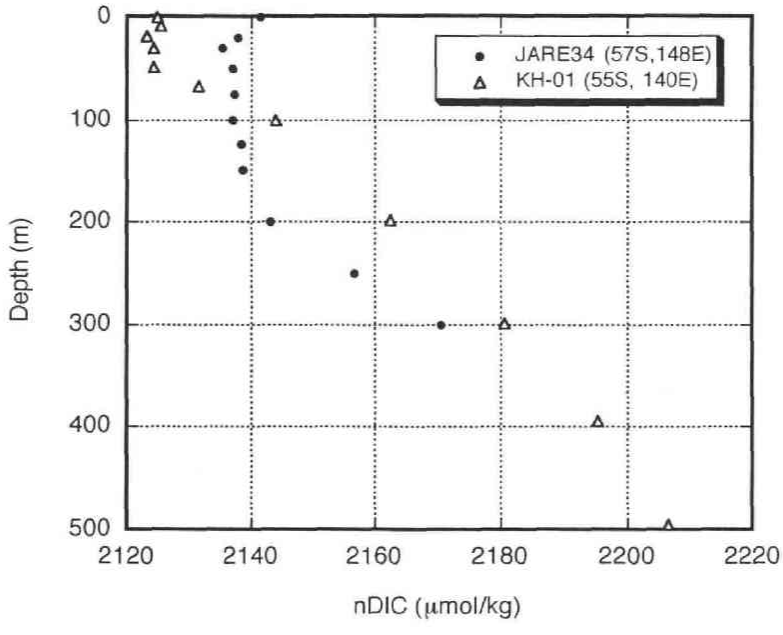

Fig.4-30. Distributions of the nDIC in JARE34 (57°S, 148°E) and in Hakuho-Maru (55°S, 140°E)

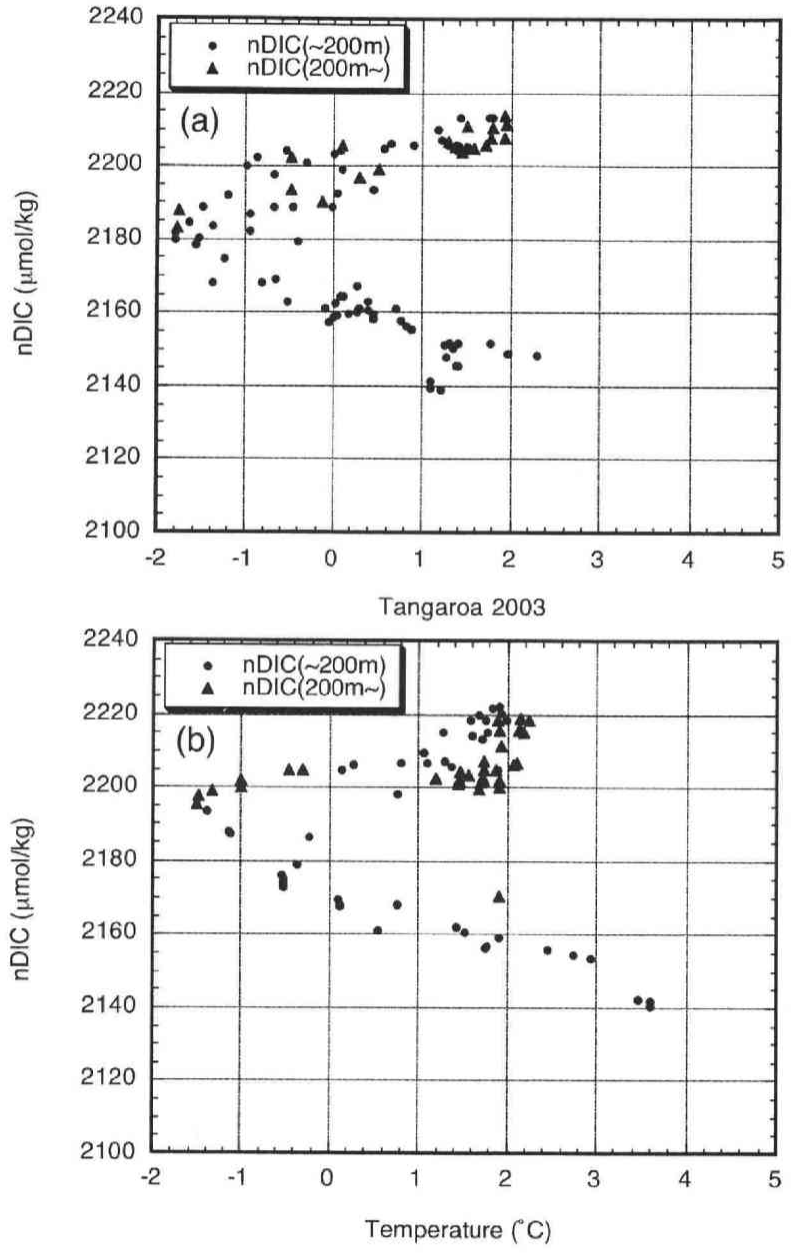

Fig. 4-31. The relationship between water temperature and nDIC in JARE34 cruise (a) and Tangaroa 2003 cruise, respectively.

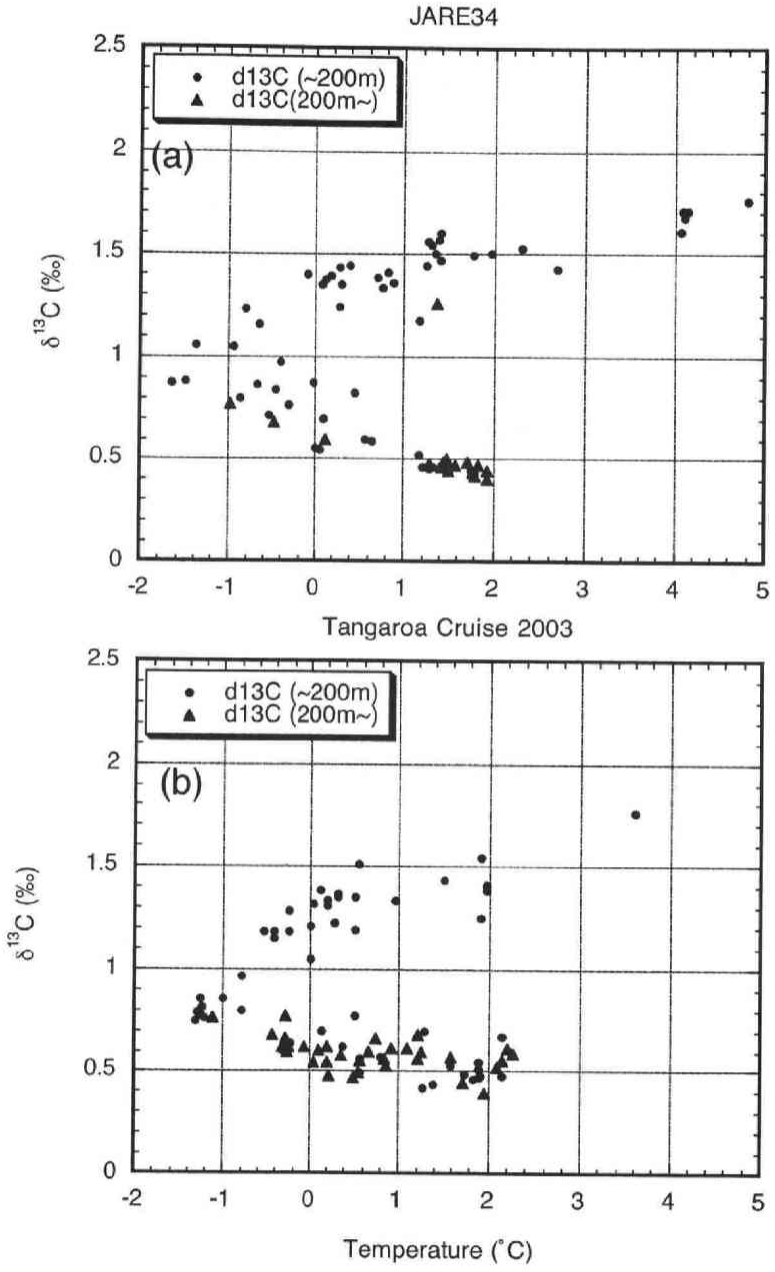

Fig. 4-32. The relationship between water temperature and nDIC in JARE34 cruise (a) and Tangaroa 2003 cruise, respective.

Chapter 5

Summary

For a better understanding of global CO_2 budget, it is important to examine variations of ocean carbon system in high latitude areas where a limited number of observations have been done due to severe weather conditions. Therefore, we measured pCO_2^{sea} in the Greenland Sea and the Barents Sea from 1992 through 2001, and pCO_2^{sea}, DIC and its $\delta^{13}C$ in the Southern Ocean from 2001 through 2003. Based on these measurements, we examined temporal and spatial variations of the respective components, as well as of air-sea CO_2 flux derived. The examination was also made for inspecting the similarity and difference of carbon system in the northern and southern polar seas. The results obtained in this study are summarized below:

The values of pCO_2^{sea} measured in the Greenland Sea and the Barents Sea ranged between 200 and 350 μatm, which are generally lower than pCO_2^{air}, supporting an effective ventilation of surface seawater to intermediate/deep layers in these seas, by which atmospheric CO_2 is taken up by the seas. The pCO_2^{sea} value showed a positive correlation with SST for every month, except for May and June when a negative pCO_2^{sea}-SST relationship was found in the western Greenland Sea due to CO_2 uptake by biological activities. Our data also suggested that pCO_2^{sea} increased secularly, as observed by Olsen et al. (2003) and Omar et al. (2003) in the North Atlantic Ocean and the Barents Sea, respectively.

By assuming that pCO_2^{sea} increased at the same rate (1.5 μatm yr^{-1}) as pCO_2^{air}, we derived a set of seasonally varying pCO_2^{sea}-SST relationships for the Greenland Sea and the Barents Sea to estimate the pCO_2^{sea} values for areas where no observation was conducted. The values of pCO_2^{sea} calculated for 1995 using those relationships and the SST data were found to be low in the northwestern Greenland Sea in July and August (< 220 μatm) and relatively high (>340 μatm) in warm water originating in the Norwegian Atlantic Current in April.

The air-sea CO_2 fluxes were calculated for 1995 using the gas transfer coefficient, wind speed, and ΔpCO_2 derived from the pCO_2^{sea}-SST relationships, SST, and pCO_2^{air} at Ny-Ålesund. The air-sea CO_2 fluxes for the Greenland Sea ranged between 37 gC m^{-2} yr^{-1} in summer and 72 gC m^{-2} yr^{-1} in winter, showing an annual average of 52 gC m^{-2} yr^{-1}. On the other hand, the CO_2 fluxes for the Barents Sea were found to be 28 gC m^{-2} yr^{-1} in spring and 63 gC m^{-2} yr^{-1} in winter, with an annual average of 46 gC m^{-2} yr^{-1}. The total CO_2 uptake in the Greenland Sea and the Barents Sea (70°-80°N, 20°W-40°E) was in a range of 0.034 GtC yr^{-1} in summer to 0.062 GtC yr^{-1} in winter, with an annual mean of 0.050 GtC yr^{-1}.

By examining the sensitivity of temporal variations of the oceanic CO_2 uptake to the gas transfer coefficient as a function of wind speed, ΔpCO_2, and sea ice area, it was found that both the wind field and ΔpCO_2 are particularly important for the seasonal variation in the CO_2 uptake. It was also found that the interannual variability of the CO_2 uptake was noticeably influenced by the wind speed (13 %, relative to the mean annual CO_2 uptake) and the sea ice area (15 %), while the contribution of ΔpCO_2 (4 %) was minor. The interannual variability of the oceanic CO_2 uptake due to anomalies of these three factors was estimated to be ±18 % of its average of 0.050 GtC yr^{-1}. The wind speed anomaly showed a positive correlation with the NAOI, while the anomalies of ΔpCO_2 and the sea ice area were negatively correlated with the index. The CO_2 uptake anomaly showed temporal variations similar to the NAOI.

In order to understand spatial variations of pCO_2^{sea} and air-sea CO_2 flux in the Southern Ocean, the measurements of pCO_2^{sea} were made by R/V Umitaka-Maru in the Indian and western Pacific sectors from January to February 2003. The measured values of pCO_2^{sea} ranged between 340 and 365 μatm, which are generally lower than pCO_2^{air}. The pCO_2^{sea} values measured in this ocean area showed a negative correlation with SST. We derived a set of pCO_2^{sea}-SST relationship using the results from this measurement, to

estimate the pCO_2^{sea} values for areas with no observations. The values of pCO_2^{sea} calculated using the relationships derived and the SST data were found to be low (< 345 μatm) in the Australian side and high (>360 μatm) in the Antarctic side. The average oceanic CO_2 uptake for the Indian and western Pacific sectors between January and February was estimated to be 0.012 GtC $month^{-1}$. By assuming that this flux is applicable to the whole Southern Ocean, the total CO_2 uptake was calculated to be 0.14 GtC $month^{-1}$.

For improving our present knowledge about summertime variations of pCO_2^{sea}, air-sea CO_2 flux and DIC, multi-ship observations with R/Vs Aurora Australis, Hakuho-Maru, Tangaroa and icebreaker Shirase were made in the western Pacific sector (140°-150°E) from October 2001 to March 2002. The values of pCO_2^{sea} off the coast of the Antarctic Continent (66°S) showed large temporal variations of 100 μatm, caused mainly by seawater upwelling from deep layers and biological activities limited by iron supply. On the other hand, pCO_2^{sea} at latitudes of 45° to 63°S showed a small variability with less than 25 μatm. The average air-sea CO_2 flux reached a minimum value of 1 mol m^{-2} yr^{-1} in December and a maximum value of 3 mol m^{-2} yr^{-1} in January, and the total CO_2 uptake by the ocean for the five summer months amounted to 0.037 GtC yr^{-1} for the present measurement area and 1.4 GtC yr^{-1} for the whole Southern Ocean. By comparing the values of air-sea CO_2 flux for the Southern Ocean with those for the Greenland Sea and the Barents Sea, we found that the physical process is much more essential than the biological process for the CO_2 uptake in the Southern Ocean even in summer, while the biological process is important for the summertime CO_2 uptake in the Greenland Sea and the Barents Sea.

It was found from the DIC measurements that large negative nDIC differences were found between the Aurora Australis and Hakuho-Maru cruises especially at 65°S where pCO_2^{sea} was remarkably low due to biological activities. On the other hand,

slightly positive differences were observed not only between the Aurora Australis and Hakuho-Maru cruises but also between the Hakuho-Maru and Tangaroa cruises below 200 m at latitudes between 44° and 60°S, as well as below 100 m south of 61°S, due to re-mineralization of organic matter.

The temporal variations of pCO_2^{sea}, DIC and $\delta^{13}C$ over 10 years were examined to detect their long-term trends in the Southern Ocean. The increase rates of pCO_2^{sea} for the area covered by this study, except for SSIZ, were estimated to be 1.5-2.2 μatm yr^{-1}, which are larger than those of earlier study. On the other hand, the pCO_2^{sea} increase rate deduced for SSIZ from the DIC increase rate (1.2 mol kg^{-1} yr^{-1} obtained by this study for SSIZ) was approximately 2.6 μatm yr^{-1}. However, a significant difference of $\delta^{13}C$ was not detected from our 10-year measurements, probably due to a very small difference which is considered to be less than -0.04 ‰ per decade.

As mentioned above, the physical process such as wind was much more essential than the biological process for the oceanic CO_2 uptake in the Southern Ocean even in summer, reflecting the fact that air-sea CO_2 exchange is greatly enhanced by strong wind, even when the value of pCO_2^{sea} is not much smaller than pCO_2^{air}. It was also found in this study that the increase rate of pCO_2^{sea} (1.5-2.6 μatm yr^{-1}) was higher than that of pCO_2^{sea} (1.4 μatm yr^{-1}). These results may suggest that the Southern Ocean acts potentially as a CO_2 source in the future. In addition, the magnitude of the Southern Ocean CO_2 sink is heavily disputed (Roy et al., 2003), and it is thought that the natural carbon cycle is responding to recent changes in climate in the Southern Ocean by ventilating deep waters rich in carbon, which reduces the capacity of the ocean to take up anthropogenic CO_2. Therefore, further measurement and analysis of carbon system are required for the Southern Ocean, by which an understanding of the global CO_2 budget will be deepened.

References

Aagaard, K., J.H. Swift and E.C. Carmack (1985) Thermohaline circulation in the arctic Mediterranean Seas, *J. Geophys. Res.* **90** 4833-4846.

Anderson, L.G (1995) Chemical Oceanography of the Arctic and its Shelf Seas. In: *Arctic Oceanography: Marginal ice Zones and Continental Sand Estuarine Studies* (eds. by W.O. Smith Jr. and J.M. Grebmeier). American Geophysical Union, Washington, DC, pp.183-202.

Anderson, L.G, H. Drange, M. Chierici, A. Fransson, T. Johannessen, I. Skjelvan and F. Rey (2000) Annual carbon fluxes in the upper Greenland Sea based on measurements and a box-model approach, *Tellus* **52B** 1013-1024.

Barnola, J.M., D. Raynaud, Y.S. Korotkevich and C. Lorius (1987) Vostok ice core provides 160000-year record of atmospheric CO_2, *Nature* **329** 408-414.

Broecker, W.S., and T.H. Peng (1982) *Tracer in the sea*, 690 pp. Eldigio Press, Palisades, New York.

Chaigneau, A. and R. Morrow (2002) Surface temperature and salinity variations between Tasmania and Antarctica, 1993-1999, *J. Geophys. Res.* **107(C12)** 8020.

Chierici, M. *"personal communication"*

Conway, T.J., P.P. Tans, L.S. Waterman, K.W. Thoning, D.R. Kitzis, K.A. Masarie and N. Zhang (1994) Evidence for Interannual Variability of the Carbon Cycle from the National Oceanic and Atmospheric Administration/Climate Monitoring and Diagnostics Laboratory Global Air Sampling Network, *J. Geophys. Res.* **99 (D11)** 22831-22855.

Cosca, C.E., R.A. Feely, J. Boutin, J. Etcheto, M. McPhaden, F.P. Chavez and P.G. Strutton (2003) Seasonal and interannual CO_2 flux for the central and eastern equatorial Pacific Ocean as determined from fCO_2-SST relationships, *J. Geophys. Res.* **108(C8)** 3278.

Dandonneau, Y (1995) Sea-surface partial pressure of carbon dioxide in the eastern equatorial Pacific (August 1991 to October 1992): A multivariate analysis of physical and biological factors, *Deep-Sea Res. II* **42** 349-364.

Enomoto, H. and A. Ohmura (1990) The influence of atmospheric half-yearly cycle on the sea ice extent in the Antarctic, *J. Geophys. Res.* **95** 9497-9511.

Etheridge, D.M., L.P. Steele, R.L. Langenfelds, R.J. Francey, J.M. Barnola and V.I. Morgan (1996) Natural and Anthropogenic Changes in Atmospheric CO_2 Over the Last 1000 Years from air in Antarctic ice and Firn, *J. Geophys. Res.* **101(D2)** 4115-4128.

Feely, R.A., J. Boutin, C.E. Cosca, Y. Dandonneau, J. Etcheto, H.Y. Inoue, M. Ishii, C. Le Quéré, D.J. Mackey, M. McPhaden, N. Metzl, A. Poisson and R. Wanninkhof (2002) Seasonal and interannual variability of CO_2 in the equatorial Pacific, *Deep-Sea Res. II* **49** 2443-2470.

Francey, R.J., P.P. Tans, C.E. Allison, I.G. Enting, J.W.C. White and M. Trolier (1995) Changes in oceanic and terrestrial carbon uptake since 1982, *Nature* **373** 326-330.

Fransson, A., M. Chierici, L.G. Anderson, I. Bussman, E.P. Jones and J.H. Swift (2001) The importance of shelf processes for the modification of chemical constituents in the waters of the eastern Arctic Ocean, *Shelf. Res.* **21** 225-242.

Furevik, T. (2001) Annual and interannual variability of Atlantic Water temperatures in the Norwegian and Barents Seas: 1980-1996, *Deep-Sea Res. I* **48** 383-404.

Gruber, N., C.D. Keeling and N. Bates (2002) Interannual variability in the North Atlantic Ocean carbon sink, *Science* **298** 2374-2378.

Hashida G. (1993) PhD thesis: *"A study on variations of greenhouse gases in the surface ocean and lower troposphere"*, Tohoku University.

Hood, E.M., M. Merlivat and T. Johannessen (1999) Variations of fCO_2 and air-sea flux of CO_2 in the Greenland Sea gyre using high-frequency time series data from CARIOCA drift buoys, *J. Geophys. Res.* **104** 20,571-20,583.

Inoue, H.Y., H. Matsueda, M. Ishii, K. Fushimi, M. Hirota, I. Asanuma and Y. Takasugi (1995) Long-term trend of the partial pressure of carbon dioxide (pCO_2) in surface waters of the western North Pacific 1984-1993, *Tellus* **47B** 391-413.

Inoue, H.Y., and M. Ishii (2005) Variations and trend of CO_2 in the surface seawater in the Southern Ocean south of Australia between 1969 and 2002, *Tellus* **57B** 58-69.

Ishidoya, S. (2003) PhD thesis: *"Development of High Precision Measurement Technique of the Atmospheric O_2/N_2 Ratio and its Application to the Global Carbon Cycle"*, Tohoku University.

Ishii, M., H.Y. Inoue, H. Matsueda and E. Tanoue (1998) Close coupling between seasonal biological production and dynamics of dissolved inorganic carbon in the Indian Ocean sector and the western Pacific Ocean sector of the Antarctic Ocean, *Deep-Sea Res. I* **45** 1187-1209.

Jabaud-Jan, A., N. Metzl, C. Brunet, A. Poisson and B. Schauer (2004) Interannual variability of the carbon dioxide system in the southern Indian Ocean (20°S-60°S): The impact of a warm anomaly in austral summer 1998, *Global Biogeochem. Cycles* **18** GB1042.

Jones, P.D., T.J. Osborn, K.R. Briffa, C.K. Folland, E.B. Horton, L.V. Alexander, D.E. Parker and N.A. Rayner (2001) Adjusting for sampling density in grid box land and ocean surface temperature time series, *J. Geophys. Res.* **106** 3371-3380.

Kalnay, E., M. Kanamitsu, R. Kistler, W. Collins, D. Deaven, L. Gandin, M. Iredell, S. Saha, G. White, J. Woollen, Y. Zhu, A. Leetmaa, B. Reynolds, M. Chelliah, W. Ebisuzaki, W. Higgins, J. Janowiak, K.C. Mo, C. Ropelewski, J. Wang, R. Jenne and D. Joseph (1996) The NCEP/NCAR 40-Year Reanalysis Project, *Bull. of Am. Meteorol. Soc.* **77** 437-472.

Kaltin, S., L.G. Anderson, K. Olsson, A. Fransson and M. Chierici (2002) Uptake of atmospheric carbon dioxide in the Barents Sea, *J. Marine Systems* **38** 31-45.

Keeling, C.D., H. Brix and N. Gruber (2004) Seasonal and Long-Term Dynamics of the Upper Ocean Carbon Cycle at Station ALOHA Near Hawaii, *Global Biogeochem. Cycles* **18** GB4006.

Kawamura, K., T. Nakazawa, T. Machida, S. Morimoto, S. Aoki, M. Ishizawa, Y. Fujii and O. Watanabe (2000) Variations of the Carbon Isotopic Ratio in Atmospheric CO_2 Over the Last 250 Years Recorded in an ice Core from H15, Antarctica, *Polar Meteorol. Glaciol* **14** 47-57.

Keeling, C.D., R.B. Bacastow, A.F. Carter, S.C. Piper, T.P. Whorf, M. Heiman, W.G. Mook and H. Roeloffzen (1989) A Three-Dimensional Model of Atmospheric CO_2 Transport Based on Observed Winds: 1. Analysis of Observational Data, *Geographycal Monograph* **55** 165-236.

Keeling, R.F., and S.R. Shertz (1992) Seasonal and interannual variations in atmospheric oxygen and implications for the global carbon cycle, *Nature* **358** 723-727.

Keeling, C.D., T.P. Whorf, M. Wahlen and J. van der Plicht (1995) Interannual Extremes in the Rate of Rise of Atmospheric Carbon Dioxide Since 1980, *Nature* **375** 666-670.

Lai, X., K. Norisuye, M. Mikata, T. Minami, A.R. Bowie and Y. Sohrin, *"personal communication"*

Lefèvre, N., A.J. Watson, A. Olsen, A.F. Ríos, F.F. Pérez and T. Johannessen (2004) A decrease in the sink for atmospheric CO_2 in the North Atlantic, *Geophys. Res. Lett.* **31** L07306.

Le Quéré, C., O. Aumont, L. Bopp, P. Bousquet, P. Ciais, R.J. Francey, M. Heimann, C.D. Keeling, R.F. Keeling, H. Kheshgi, P. Peylin, S.C. Piper, I.C. Prentice and P.J. Rayner (2003) Two decades of ocean CO_2 sink and variability, *Tellus* **55B** 649-656.

Martin, J.H., R. M. Gordon and S.E. Fitzwater (1990) Iron in Antarctic Waters, *Nature* **345** 156-158.

Metzl, N., B. Tilbrook and A. Poisson (1999) The annual fCO_2 cycle and the air-sea CO_2 flux in the sub-Antarctic Ocean, *Tellus* **51B** 849-861.

Midorikawa, T., K. Nemoto, H. Kamiya, M. Ishii and H.Y. Inoue (2005) Persistently strong oceanic CO_2 sink in the western subtropical North Pacific, *Geophys. Res. Lett.* **32** L05612.

Morimoto, S. (1993) PhD thesis: *"A Study of Carbon Cycle on the Earth's Surface from Measurement of Carbon Isotope Ratio of Atmospheric CO_2"*, Tohoku University.

Morimoto, S., S. Aoki and T. Yamanouchi (2001) Temporal variations of atmospheric CO_2 concentration and carbon isotope ratio in Ny-Ålesund, Svalbard, "Environmental Research in the Arctic 2000", *Mem. Natl. Inst. Polar Res. Spec. Issue* **54** 71-80.

Nagata, Y, Y. Michida and Y. Umimura (1988). Variations of Positions and Structures of the Ocean Fronts in the Indian Ocean Sector of the Southern Ocean in the Period from 1965 to 1987. In *Antarctic Ocean and Resources Variability*. (eds. by D. Salirhage), Springer-Verlag, New York. pp. 92-98.

Nakazawa, T., S. Morimoto, S. Aoki and M. Tanaka (1993) Time and Space Variations of the Carbon Isotopic Ratio of Tropospheric Carbon Dioxide Over Japan, *Tellus* **45B** 258-274.

Nakazawa, T., S. Morimoto, S. Aoki and M. Tanaka (1997) Temporal and spatial variations of the carbon isotopic ratio of atmospheric carbon dioxide in the western Pacific region, *J. Geophys. Res.* **102** 1271-1285.

Neftel, A., P. Jacob and D. Klockow (1986) Long-Term Record of H_2O_2 in Polar ice Cores, *Tellus* **38B** 262-270.

Noji, T.T., L.A. Miller, I. Skjelvan, E. Falck, K.Y. Børsheim, F. Rey, J. Urbam-Rich and T. Johannessen (2000) Constrains on carbon drawdown and export in the Greenland Sea. In *The Northern North Atlantic: A Changing Environment*. (eds.

by P. Schäfer, W. Ritzrau, M. Schlüter and J. Thiede). Springer. Berlin. pp. 39-52.

Olsen, A., R.G.J. Bellerby, T. Johannessen, A. Omar and I. Skjelvan (2003) Interannual variability in the wintertime air-sea flux of carbon dioxide in the northern North Atlantic, 1981-2001, *Deep-Sea Res. I* **50** 1323-1338.

Omar, A., T. Johannessen, S. Kaltin and A. Olsen (2003) Anthropogenic increase of oceanic pCO_2 in the Barents Sea surface water, *J. Geophys. Res.* **108(C12)** 3388.

Orr, J.C., V.J. Fabry, O. Aumont, L. Bopp, S.C. Doney, R.A. Feely, A. Gnanadesikan, N. Gruber, A. Ishida, F. Joos, R.M. Key, K. Lindsay, E. Maier-Reimer, R.J. Matear, P. Monfray, A. Mouchet, R.G. Najjar, G.-K. Plattner, K.B. Rodgers, C.L. Sabine, J.L. Sarmiento, R. Schlitzer, R.D. Slater, I.J. Totterdell, M.-F. Weirig, Y. Yamanaka and A. Yool (2005) Anthropogenic ocean acidification over the twenty-firstcentury and its impact on calcifying organisms, *Nature* **437** 681-686.

Orsi, A.H., T. Whitworth Iii and W.D. Nowlin (1995) On the Meridional Extent and Fronts of the Antarctic Circumpolar Current, *Deep-Sea Res. I* **42** 641-673.

Overland, J.E., and M. Wang (2005) The Arctic climate paradox: The recent decrease of the Arctic Oscillation, *Geophys. Res. Lett.* **32** L06701.

Prentice, I.C., G.D. Farquhar, N.J.R. Fasham, M.L. Goulden, M. Heimann and co-authors (2001). The carbon cycle and atmospheric CO_2. In: *Climate change: the Scientific basis, the contribution of WG1 of the IPCC to the IPCC Third Assessment Report (TAR)*, (eds. by J.T. Houghton and D. Yihui), Cambridge University Press, Cambridge, U.K, pp. 183-237.

Rayner, P.J., I.G. Enting, R.J. Francey and R.L. Langenfelds (1999) Reconstructing the recent carbon cycle from atmospheric CO_2, ^{13}C and O_2/N_2 observations, *Tellus* **51B** 213-232.

Roy, T., P.J. Rayner, R.J. Matear and R.J. Francey (2003) Southern hemisphere ocean CO_2 uptake: reconciling atmospheric and oceanic estimates, *Tellus* **55B** 701-710.

Sabine, C.L. and R.M. Key (1998) Controls on fCO_2 in the South Pacific, *Mar. Chem* **60** 95-110.

Schlosser, P., G. Bönisch, B. Kromer and K.O. Münnich (1990) Ventilation rates in the Nansen Basin of the Arctic Ocean derived from a multitracer approach, *J. Geophys. Res.* **95** 3265-3272.

Skjelvan, I., T. Johannessen and L.A. Miller (1999) Interannual variability of fCO_2 in the Greenland and Norwegian Seas, *Tellus* **51B** 477-489.

Smith, S.R., D.M. Legler and K.V. Verzone (2001) Quantifying Uncertainties in NCEP Reanalysis Using High-Quality Research Vessel Observations, *J. Climate* **14** 4062-4072.

Takahashi, T., J. Olafsson, J.G. Godard, D.W. Chipman and S.C. Sutherland (1993) Seasonal variation of CO_2 and nutrient in the high-latitude surface oceans: A comparative study, *Global Biogeochem. Cycles* **7(4)** 843-878.

Takahashi, T., R.A. Feely, R.F. Weiss, R.H. Wanninkhof, D.W. Chipman, S.C. Sutherland and T.T. Takahashi (1997) Global air-sea Flux of CO_2: An estimate based on measurements of sea-air pCO_2 difference, *Proc. Natl . Acad. Sci.* **94** 8292-8299.

Takahashi, T., C.S. Stewart, C. Sweeney, A. Poisson, N. Metzl, B. Tilbrook, N. Bates, R. Wanninkhof, R.A. Feely, C.L. Sabine, J. Olafsson and Y. Nojiri (2002) Global sea-air CO_2 flux based on climatological surface ocean pCO_2, and seasonal biological and temperature effects, *Deep-Sea Res. II* **49** 1601-1622.

Tanaka, M., T. Nakazawa and S. Aoki (1987) Time and space variations of tropospheric carbon dioxide over Japan, *Tellus* **39B** 3-12.

Tans, P.P., I.Y. Fung and T. Takahashi (1990) Observational constraints on the global atmospheric CO_2 budget, *Science* **247** 1431-1438.

Wallace, J.M. and D.S. Gutzler (1981) Teleconnections in the geopotential height field during the northern hemisphere winter, *Mon. Wea. Rev.* **109** 784-81.

Wanninkhof, R (1992) Relationship between wind speed and gas exchange over the ocean, *J. Geophys. Res.* **97** 7373-7382.

Wanninkhof, R., R.A. Feely, H. Chen, C.E. Cosca and P.P. Murphy (1996) Surface water fCO_2 in the eastern equatorial Pacific during the 1992-1993 El Niño, *J. Geophys. Res.* **101** 16,333-16,343.

Wanninkhof R. and W.R. McGills (1999) A cubic relationship between air-sea CO_2 exchange and wind speed, *Geophys. Res. Lett.* **26** 1889-1993.

Watai, T., M. Kikuchi and T. Nakazawa (1998) Temporal variations of surface oceanic and atmospheric CO_2 fugacity and total dissolved inorganic carbon in the northwestern North Pacific, *J. Oceanogr.* **54** 323-336.

Weiss R.F (1974) Carbon dioxide in water and seawater: the solubility of a non-ideal gas, *Mar. Chem.* **2** 203-215.

Weiss, R.F., F.A. Van Woy and P.K. Salameh. (1992) Surface water and atmospheric carbon dioxide and nitrous oxide observations by shipboard automated gas chromatography: Results from expeditions between 1977 and 1990, Scripps Institute of Oceanography. Carbon Dioxide Information Analysis Center Oak Ridge National Laboratory. NDP-044,